"This or That" – Light Emission from Hybrid Organic-Inorganic *vs* Coordination Cu(I) Halides

Dilruba A. Popy, Bayram Saparov

Department of Chemistry & Biochemistry, University of Oklahoma, Norman, OK 73019, USA
Email: saparov@ou.edu
ORCID ID: Dilruba A. Popy: 0000-0001-5017-3274; Bayram Saparov: 0000-0003-0190-9585.

Abstract: In recent years, multiple new families of ultra-high efficiency light emitting Cu(I) halides have been developed for various optical applications. Among the light emitting Cu(I) halides, two distinct materials classes can be recognized, *hybrid organic-inorganic Cu(I) halides* featuring structurally separated organic cations and Cu(I) halide anions, and *coordination Cu(I) halides* containing organic ligands attached to Cu(I) centers. These two materials classes have been developed in parallel, and each research field has its own set of terminologies, which has caused confusion regarding similarities and differences between them. In this review, syntheses, crystal and electronic structures, optical properties, and photoemission mechanisms of these two distinct materials classes are compared. This work is concluded with a brief review of exciting potential practical applications of both hybrid organic-inorganic and coordination Cu(I) halides.

1. Introduction

Photoluminescent materials are important in modern society because of their widespread applications in lighting and display technologies, solid-state lasers, scintillations, sensing, anticounterfeiting, information storage and bio-imaging, just to name a few.[1-13] Therefore, significant efforts have been devoted to developing efficient and environmentally friendly luminescent materials, focusing on their specific applications. Many different materials classes from quantum dots of simple binaries such as CdSe and ZnS to rare-earth element (REE)-based light emitters have been explored for optical applications.[14-19] Depending on the materials class, complex and costly synthesis methods, environmental toxicity concerns (e.g., for materials containing Cd and Pb), high cost and scarcity concerns (e.g., for REE), unsatisfactory performance parameters such as emission efficiency and strong particle size dependence (e.g., for quantum dots) may limit their practical use. Organic phosphors can be considered as a possible alternative to inorganic materials, offering vast structural diversity and tunability.[20-23] However, weak emission efficiency due to concentration quenching effect, aggregations and stability are the main obstacles of these systems.[24-27] The emergence of hybrid systems containing both organic and inorganic motifs in the same crystal lattice holds promise as this may provide an avenue to design novel materials that synergistically combine the advantageous characteristics of organic and inorganic materials, simultaneously addressing their respective drawbacks. In the past decade, novel hybrid organic-inorganic metal halides have attracted much attention due to their unusual photophysical properties, and outstanding light emission efficiencies that can rival that of the state-of-the-art inorganic and organic luminescent materials.[28, 29]

Among the hybrid organic-inorganic materials, hybrid lead (Pb) halide perovskites have been heavily explored due to their outstanding performance in optoelectronic devices such as solar cells and light-emitting diodes (LEDs).[30-33] Since the discovery of the promising semiconducting properties of lead halide perovskites, their poor air and moisture stability along with the toxicity of Pb have been well documented issues that hinder their potential practical applications.[34] To address these issues, other families of hybrid organic-inorganic metal halides containing Cu, Mn, Zn, Cd, Sn, In, Bi, Sb, etc. in place of Pb have been developed and studied.[35-44] The substitution of Pb with these metals constitutes a major change, and the resultant materials often display drastically different bonding patterns and low dimensional non-perovskite crystal structures, electronic structures, and consequently, photophysical properties.[28, 29, 45] For example, the semiconducting and photovoltaic properties of Pb-free halides can be significantly worse compared to their Pb halide perovskite counterparts.[35, 36] On the other hand, light emission is enhanced with reduction in structural dimensionality, and therefore, the typical low dimensional crystal and electronic structures of Pb-free hybrid halides can lead to enhanced exciton binding energies and efficient light emission at room temperature.[28, 37, 46, 47] Nevertheless, depending on the specific metal halide system, there are multiple challenges that need to be further addressed including comparatively lower light emission efficiency (e.g., for Zn, Cd, In, and Bi halides), stability (e.g., Sn halides), lack of emission tunability (e.g., for Mn and Sb halides), etc.[34, 45, 48] These shortcomings of the currently available material systems continue to motivate further research on the development of tunable and high emission efficiency luminescent materials that have low-cost, earth-abundant and nontoxic elemental compositions.

Among the lead-free hybrid luminescent materials, hybrid organic-inorganic Cu(I) halides have attracted tremendous attention due to the unique combination of the afore-mentioned desirable characteristics including their low cost, nontoxic and earth abundant elemental compositions and ability of Cu(I) to form variable coordination patterns and geometries.[38, 49-57] The ability of Cu(I) to form 2-, 3- and 4-coordinate polyhedral building blocks leads to a remarkable wealth of structural dimensionalities and crystal structures of hybrid Cu(I) halides, which in turn can be used as a handle to tune their optical and electronic properties.[38, 52, 54, 58] The high efficiency and tunable light emission properties of these materials signify their potential for various practical applications.[38, 50, 52, 59]

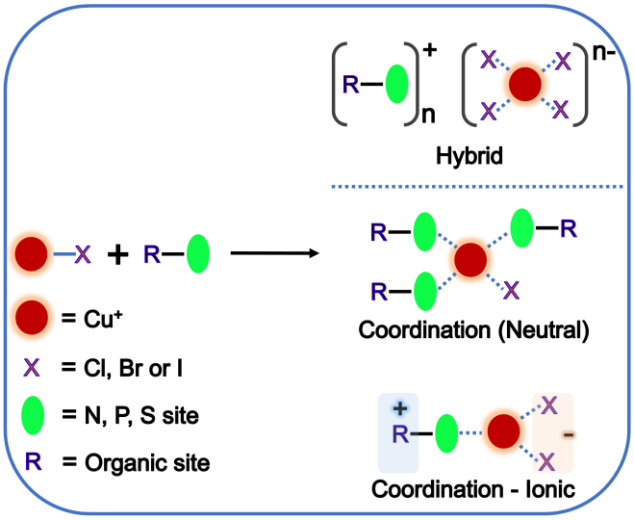

Scheme 1. Conceptual representation of luminescent organic-inorganic Cu(I) halides.

Over the past few decades, a variety of photoluminescent Cu(I) halides have been studied.[38, 60, 61] Generally, these Cu(I) halides can be divided into two categories based on the observed interactions between organic and inorganic motifs (Scheme 1). *Hybrid organic-inorganic* Cu(I) halides are formed through the electrostatic attractions between cationic organic motifs and anionic Cu(I) halide units. The study and development of hybrid organic-inorganic Cu(I) halides have accelerated after the emergence of hybrid organic-inorganic lead halide perovskites as outstanding semiconductors, as mentioned above. And just as in the case of hybrid organic-inorganic perovskites, Cu(I) halides featuring ammonium cations have been widely explored in literature with some recent reports of new compounds containing phosphonium, sulphonium, and sulfoxonium cation bearing Cu(I) halides.[58, 62-64] In contrast, direct linkages exist between the organic ligands and Cu(I) centers in Cu(I) halide *coordination compounds*. Typically, neutral organic ligands (e.g., amines) coordinate to Cu(I) centers through nitrogen and phosphorous containing functional groups in *coordination* Cu(I) halides.[59, 61] There is another subclass of coordination Cu(I) halides, *coordination-ionic* compounds, in which a cationic organic ligand forms a coordination bond with the Cu(I) core through an electron-rich donor atom and the charge

is balanced by an additional halide bonded to the Cu center.[56, 57, 65-67] This recently developed *coordination-ionic* subclass of Cu(I) halides is also known as *all-in-one* (AIO) compounds in literature, as they feature both coordination/covalent and ionic bonds.[59, 66, 68] In recent years, several literature reviews have been published covering the structures and properties of photoluminescent Cu(I) halides.[38, 49, 50, 59, 61, 69-71]

For years, hybrid organic-inorganic and coordination Cu(I) halides have been developed in parallel, and each research field has its own set of terminologies, which has caused confusion regarding similarities and differences between them. Some terminologies used in literature are outright misleading; common examples of such mistakes for hybrid organic-inorganic Cu(I) halides include the usage of "organometal", which implies the presence of metal-carbon bonds, and "perovskite", which is only accurate if the material exhibits perovskite-type crystal structure.[29, 72, 73] Importantly, the indiscriminate use of various terms not only lead to confusion but could also result in incorrect analyses of crystal and electronic structures and photophysical properties based on the comparisons of apples with oranges. Therefore, the main purpose of this work is to bring clarity to the field by reviewing recent publications on photoluminescent Cu(I) halides, explaining the usage of various terms and correcting them whenever necessary, and proposing new terms and definitions as needed. As the first step, the proposed categorization of Cu(I) halides (Scheme 1) into *hybrid organic-inorganic* Cu(I) halides (terminology following the related hybrid organic-inorganic halide perovskites) and *coordination* Cu(I) halides is very important. These two categories exhibit distinct crystal and electronic structures and hence electronic and optical properties. For example, depending on the composition and structure, the literature reported optical transition pathways for Cu(I) halides include triplet emission, self-trapped excitonic (STEs) emission, metal-centered (MC) charge transfer, cluster-centered (CC) charge transfer, metal-to-ligand charge transfer (MLCT), halide-to-ligand charge transfer (XLCT), etc.[61, 62, 74-76] For some of the recently reported compounds, open questions remain regarding the usage of accurate terms, and moreover, if the above-mentioned emission mechanisms are identical to one another (depending on the situation).

In this review, we provide a general overview of the reported commonly used synthesis methods, crystal structure types, optical and electronic properties and emission mechanisms of *hybrid organic-inorganic* and *coordination* Cu(I) halides. Rather than a comprehensive review of all recent developments in the fields of Cu(I) halides, we focus on comparative analyses of crystal and electronic structures, and light emission mechanisms. These discussions are followed by a brief overview of proposed practical applications of photoluminescent Cu(I) halides.

2. Material synthesis, crystal structures, and stability

2.1. Hybrid organic-inorganic Cu(I) halides

Although hybrid organic-inorganic Cu(I) halides have been known for decades, prior studies have primarily focused on their preparation and structural characterization. The recent discovery of interesting photoluminescence (PL) properties of all-inorganic Cu(I) halides ignited a renewed interest in Cu(I) halides as candidate optical materials.[38, 77-79] The easy accessibility via low temperature solution synthesis methods of hybrid Cu(I) halides is one of the major advantages of

this materials class that enabled rapid advancement of this field in recent years. Most common method used for the synthesis of hybrid Cu(I) halides involves dissolution of the corresponding organic salt (e.g., organoammonium halide salt) and Cu(I) halide in stoichiometric amounts in a suitable solvent followed by a slow evaporation of the solvent at room temperature over a few days; this method allows growth of sizeable single crystals of the resulting product for structural and photophysical characterizations.[80-85] The use of hydrohalic acids as solvents makes it possible to have unprotonated organics as reactants such as amines, which are then protonated in-situ.[86, 87] In either case, the organic molecules are included in the structure as cations that are packed together with the corresponding anionic Cu(I) halide motifs. To speed up the synthesis process, anti-solvent assisted diffusion method have been utilized in some cases where a suitable antisolvent is allowed to diffuse into the saturated solution of the precursors at room temperature.[88, 89] Slow-cooling of hot solutions have also been utilized in literature for the synthesis of hybrid Cu(I) halides where precursors are difficult to dissolve at room temperature. In this case, precursors are dissolved in a suitable solvent at around 100 °C to form saturated solution and then slowly cooled down to room temperature to yield crystals of the targeted compound.[76, 81, 82, 90] To prevent the oxidation of Cu(I) to Cu(II), hypophosphorous acid is typically used as a reducing agent in the aforementioned synthesis methods.[63, 76, 80, 91]

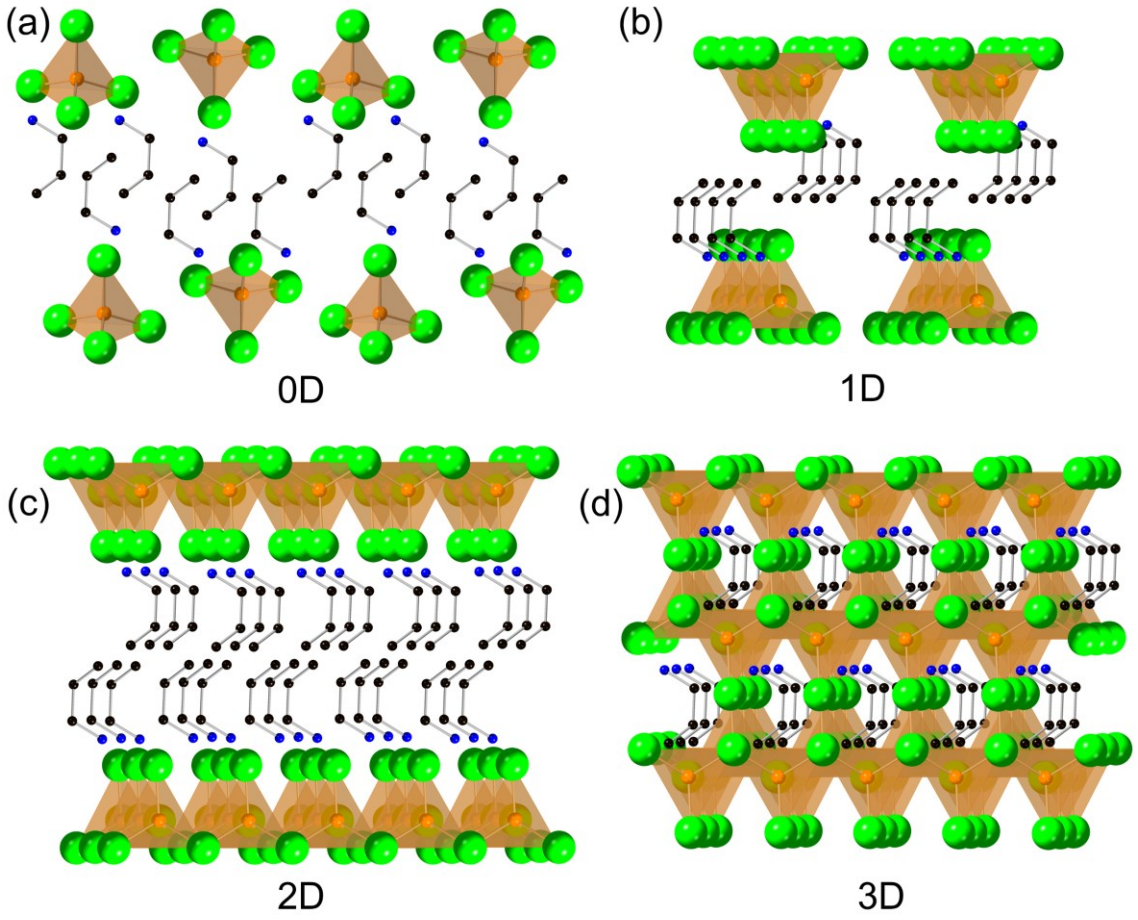

Fig. 1 Conceptual representation of hybrid compounds composed of CuX_4-tetrahedra: (a) zero-dimensional (0D), (b) one-dimensional (1D), (c) two-dimensional (2D) and (d) three-dimensional (3D) structures. Orange, green, blue, and black spheres represent copper, halide, N/P/S, and carbon atoms, respectively.

The choice of organic cations can greatly influence the coordination environment of the Cu(I) centers in the resultant hybrid materials. The ease of synthesis of Cu(I) halides combined with the wealth of the available organic cations leads to their vast structural diversity. Therefore, the structurally diverse emissive hybrid Cu(I) halides are an excellent materials group for the investigations of relationships between crystal structures and optical properties. Because of the large sizes of most organic cations, hybrid Cu(I) halides rarely exhibit high structural dimensionality (two-dimensional (2D) or three-dimensional (3D)). Instead, they usually have zero-dimensional (0D) structures where the inorganic Cu(I) halide anions are well-separated from each other by the organic cations. Note here, as there is no direct covalent connection between cations and anions, the structural dimensionality discussed refers to the connectivity modes of the inorganic structural units (Fig. 1).

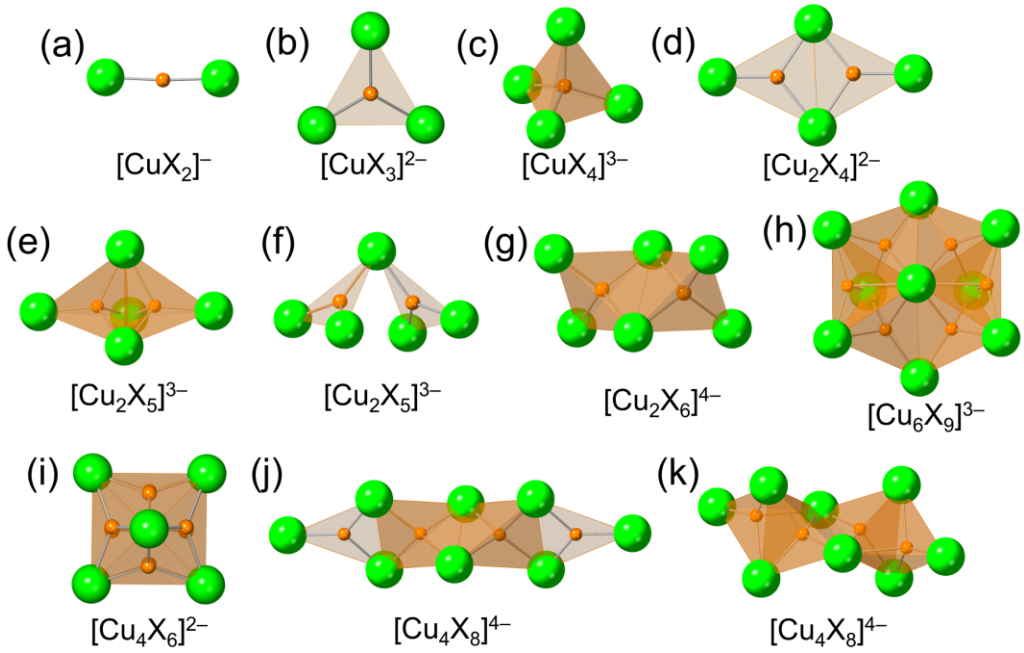

Fig. 2 Structural diversity found in hybrid Cu(I) halides showcasing 0D inorganic building blocks: (a) linear, (b) trigonal planar, (c) tetrahedra, (d) edge-sharing trigonal planar dimer, (e) face-sharing tetrahedral dimer, (f) corner-sharing trigonal planar dimer, (g) edge-sharing tetrahedral dimer, (h) face-sharing tetrahedral cluster, (i) edge-sharing trigonal planar cluster, (j) edge-sharing cluster of trigonal planar and tetrahedral units, (k) face and edge-sharing tetrahedral cluster. Orange and green spheres represent copper and halide atoms, respectively.

The 0D structures of Cu(I) halides can contain a single polyhedron, i.e., linear $[CuX_2]^-$, trigonal planar $[CuX_3]^{2-}$, tetrahedral $[CuX_4]^{3-}$,[88, 91-100] or a cluster formed by combining several polyhedra in face sharing (e.g., tetrahedral $[Cu_2X_5]^{3-}$), corner sharing (e.g., trigonal planar $[Cu_2X_5]^{3-}$), edge-sharing (e.g., trigonal planar $[Cu_2X_4]^{2-}$) fashion, or by a combination of multiple types of connections (e.g., tetrahedral $[Cu_4X_8]^{4-}$ and $[Cu_6X_9]^{3-}$) as depicted in Fig. 2.[63, 76, 80-82, 84, 85, 97, 101-124] Because of its small size, Cu(I) does not adopt coordination numbers greater than 4 in hybrid Cu(I) halides. The formation of specific coordination geometries and connectivity modes can be controlled by choosing a suitable organic cation. For instance, use of bulky organic cations like Ph_4PX (Ph_4P = TPP = tetraphenyl phosphonium) and TBAX (TBA = tetrabutyl ammonium) lead to the formation of linear $[CuX_2]^-$ units in $(Ph_4P)CuX_2$ and $(TBA)CuX_2$, respectively.[91, 99] This can be rationalized by the fact that in these examples, both cations are monovalent, Ph_4P^+ and TBA^+, only the monovalent $[CuX_2]^-$ anion can provide a stable alternating packing of anions and cations, whereas highly charged anions such as $[CuX_3]^{2-}$ and $[CuX_4]^{3-}$ would require twice and thrice the organic cation content, respectively, for charge balance. For very large organic cations, the latter would then necessitate large parts of crystal structure containing only organic cations. In contrast, comparatively smaller and structurally flexible organic cations, such as tetraethyl ammonium (TEA = $C_8H_{20}N$) and tetraethyl phosphonium (TEP) cations result in the formation of edge-sharing trigonal planar $[Cu_2Br_4]^{2-}$ units in $(TEA)_2Cu_2Br_4$ and $(TEP)_2Cu_2Br_4$.[62, 122] Moreover, flexible and adjustable organic substituents (as compared to rigid aromatic substituents such as in Ph_4P^+) may promote formation of different geometries in the inorganic structural units. For example, TEP^+ facilitates the formation of $[Cu_2Br_4]^{2-}$ and $[Cu_4Br_6]^{2-}$ clusters in $(TEP)_2Cu_2Br_4$ and $(TEP)_2Cu_4Br_6$, respectively, depending on the loading ratio of the precursor reagents.[62] Also important, different size and shapes of organic cations not only influence the coordination and geometries of the Cu(I) centers but also results in variable distances between the neighboring Cu(I) halide units and varying degrees of distortions of the inorganic polyhedra in the corresponding hybrid compounds. For example, two trigonal $CuBr_3$-units form $[Cu_2Br_4]^{2-}$ by sharing edge in both $(TEA)_2Cu_2Br_4$ and $(TEP)_2Cu_2Br_4$.[62, 122] Our careful structural analysis revealed that the $CuBr_3$-polyhrdron in the former has a lower degree of distortion (6.2207×10^{-4}) compared to the latter (1.1171×10^{-3}). Moreover, $(TEP)_2Cu_2Br_4$ has slightly higher distances (~0.8 Å) between the neighboring Cu(I) halide clusters than that in $(TEA)_2Cu_2Br_4$. Although both compounds possess similar coordination geometries around Cu-centers and similar $[Cu_2Br_4]^{2-}$ dimers, the structural differences between the two compounds have been related to their differing photophysical properties (see below).

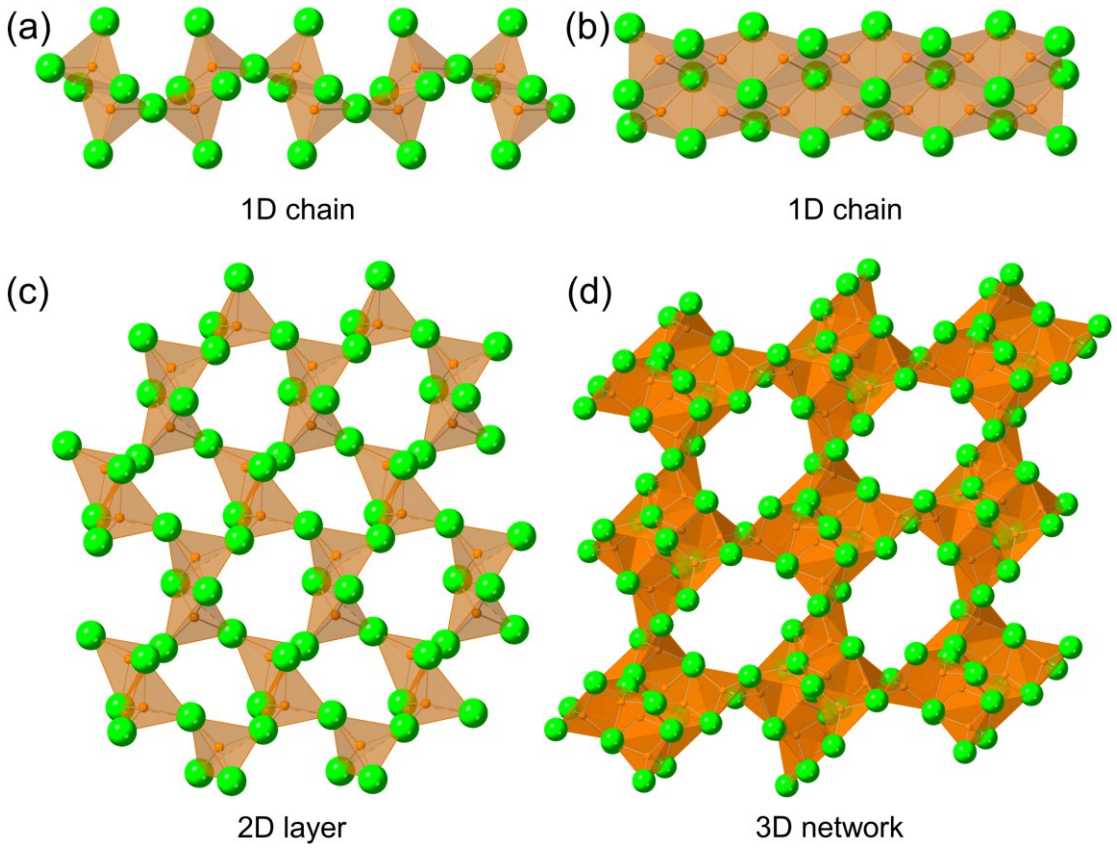

Fig. 3 Top views of the polyanionic layers in (a) $(Gua)_3Cu_2I_5$ (1D), (b) $(TMSO)Cu_2I_3$ (1D), (c) $(Bz)_2Cu_2I_4 \cdot H_2O$ (2D), and (d) $(4\text{-bzpy})_2Cu_6I_8$ (3D). Orange and green spheres represent copper and halide atoms, respectively. Gua = guanidinium; TMSO = trimethylsulfoxonium; Bz = benzylammonium; 4-bzpy = 4-benzylpyridinium.

While most reported hybrid Cu(I) halides have 0D crystal structures, the choice of nonsymmetrical organic cations can yield materials with higher structural dimensionalities. In the case of 1D-hybrids (1D = one-dimensional), organic cations separate polyanionic Cu(I) halide chains extended along a crystallographic direction .[64, 83, 89, 90, 117, 125-127] Notably, several structural variations have been observed in 1D chains depending on the mode of connectivity of the Cu(I) halide polyhedra (see Fig. 3a – b). For instance, in $(Gua)_3Cu_2I_5$ (Gua = guanidinium), CuI_4-tetrahedra are connected to each other by edge- and corner-sharing in a zigzag manner.[80] Whereas in $(TMSO)Cu_2I_3$ (TMSO = trimethylsulfoxonium), slightly distorted CuI_4-tetrahedra form 1D $[Cu_2I_3]^-$ anionic double chains by sharing common edges.[64] Subsequently, the variations in the polyhedral connectivity modes in 1D-Cu(I) chains depending on the employed organic counter cation, lead to the variations in bond distances and angles within the polyhedra, as well as within the intra- and inter-chain distances between the neighboring Cu-centers. These variations in distances and crystallographic packing patterns in turn influence the optical and electronic properties of the resultant Cu(I) halides.

There are only a few known examples of 2D Cu(I) halides in literature. Fang *et al*. and Dev *et al.* reported a unique 2D layers in the emissive Cu(I) halide hybrids $(t\text{-BA})_2Cu_2I_4\cdot H_2O$ and $(Bz)_2Cu_2I_4\cdot H_2O$ (*t*-BA = *tert*-butylammonium; Bz = benzylammonium), respectively.[128, 129] In both cases, edge-sharing tetrahedral dimeric $[Cu_2I_4]^{2-}$ units are further connected in a corner-sharing fashion to create a 2D network of $[Cu_2I_4]$-units possessing octagonal and hexagonal pores, respectively (Fig. 3c). These 2D sheets are separated by layers of organic cations, while water molecules are confined inside the pores of inorganic layers. Interestingly, the removal of water molecules from $(t\text{-BA})_2Cu_2I_4\cdot H_2O$ by heating yields another 2D network of $[Cu_6I_9]^{3-}$ building blocks in $(t\text{-BA})_3Cu_6I_9$.[128] Unlike $(t\text{-BA})_2Cu_2I_4\cdot H_2O$, $(t\text{-BA})_3Cu_6I_9$ is non-emissive upon photoexcitation, and the quenched PL of $(t\text{-BA})_3Cu_6I_9$ is not well understood.

Finally, Kong *et. al.* reported an unusual hybrid $(4\text{-bzpy})_2Cu_6I_8$, in which 4-benzylpyridinium (4-bzpy) cations facilitate the formation of 3D-networks of Cu(I) iodides.[90] To the best of our knowledge, this is the only reported example of a 3D hybrid Cu(I) halide. In this case, six CuI_4-tetrahedra form $[Cu_6I_8]^{2-}$ by sharing common edges, and in turn, $[Cu_6I_8]^{2-}$ clusters share edges with six similar clusters to form a porous 3D structure (Fig. 3d). $(4\text{-bzpy})_2Cu_6I_8$ is reported to have poor light emission properties (photoluminescence quantum yield (PLQY) <1%).

Although most of the above-mentioned hybrid Cu(I) halides are based on ammonium, phosphonium or sulphonium cations, a few luminescent Cu(I)-halides composed of cationic coordinated metal clusters have also been reported in literature (Fig. 4).[55, 130-133] In 2022, Liu *et al*. reported a novel strategy to increase the distances between the luminescent anionic Cu(I) clusters by introducing bulky crown ethers as cationic sites in the hybrid $K(18\text{-crown-6})Cu_2Br_3$.[130] The yellow emissive $K(18\text{-crown-6})Cu_2Br_3$ contains $[Cu_4Br_6]^{2-}$ anionic clusters surrounded by two layers of $[K(18\text{-crown-6})]^+$ cations (Fig. 4a) and maintain 4.436 Å distances between the neighboring anionic units. The separation between anions can be further increased to 10.288 Å by partial substitution of emissive $[Cu_4Br_6]^{2-}$ clusters with non-emissive $[InBr_4]^-$ clusters in $Na_4(18\text{-crown-6})_5In_2Cu_4Br_{14}\cdot H_2O$ (Fig. 4b).[130] As separation of the Cu(I)-halide optical centers in the crystal structure is key for a strong charge localization in the emissive anionic units, a higher light emission efficiency has been observed in the latter compound (PLQY of 97%) compared to the former (PLQY of 53%).

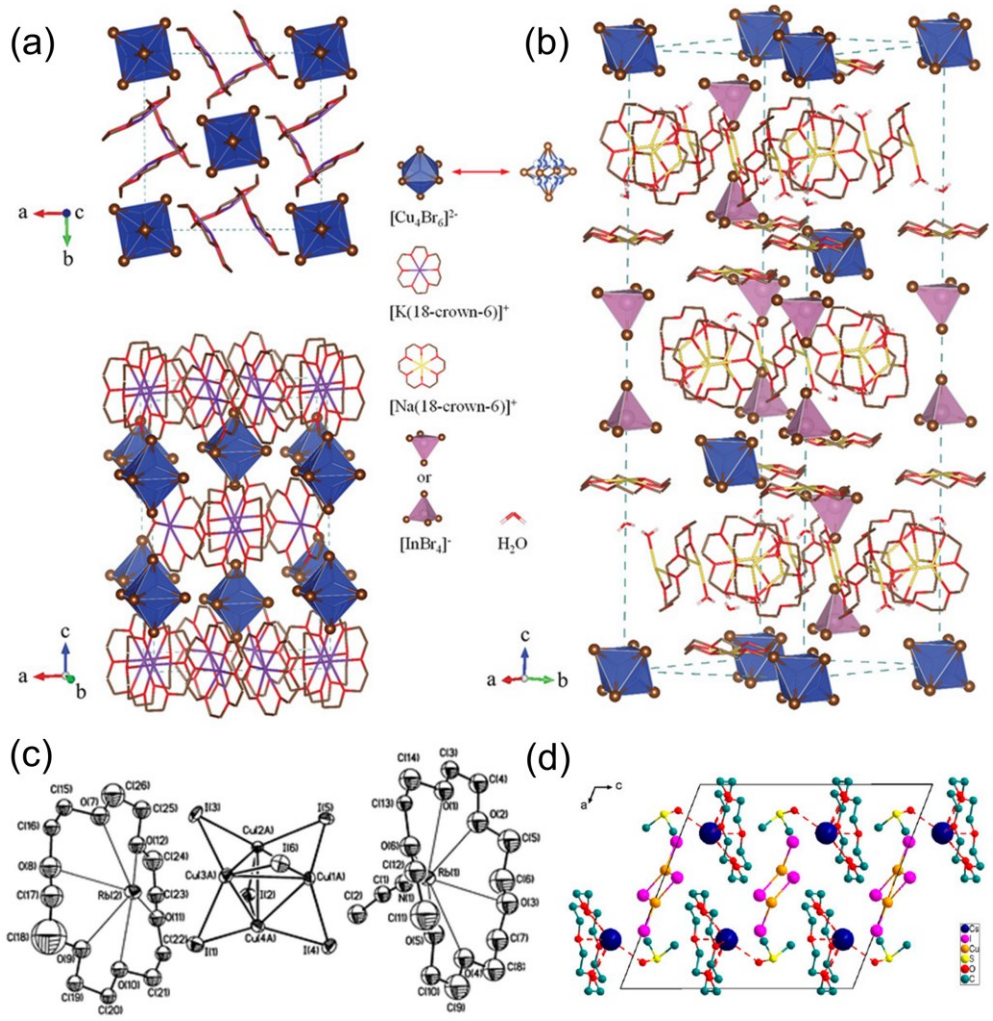

Fig. 4 (a) Crystal structure of K(18-crown-6)Cu_2Br_3 viewed along *c*-axis (top) and parallel to *a*-*b* plane (bottom). Reproduced with permission from ref 130. Copyright 2022 John Wiley and Sons. Crystal packing of (b) Na_4(18-crown-6)$_5In_2Cu_4Br_{14}\cdot H_2O$, (c) [{Rb(18c6)}$_2$MeCN][$Cu_4I_6$] and (d) $Cs_2(C_{18})_2Cu_2I_4$-DMSO. Reprinted from ref 132. Copyright 1999 Royal Society of Chemistry. Reproduced with permission from ref 131. Copyright 2023 American Chemical Society.

Besides influencing the crystal structures and photophysical properties of the hybrid Cu(I) halides, the choice of a suitable organic cation can improve the environmental stability of the resultant hybrid materials. Although all-inorganic Cu(I) halides are efficient light emitters, some exhibiting near unity PLQYs, they suffer from poor environmental stability due to the oxidation tendency of Cu^+ to Cu^{2+}. Literature survey reveals that the poor environmental stability issue of all-inorganic luminescent Cu(I) halides can be addressed by the inclusion of bulky organic cations in luminescent hybrid Cu(I) halides. This follows a hypothesis that due to their hydrophobic nature, bulky organic cations can act as a protective layer against both moisture and air for Cu(I) halide units.[88, 91, 96, 97, 99, 114, 117] For instance, (TBA)$CuBr_2$ and (TOA)$CuBr_2$ containing bulky organic cations TBA^+ and tetraoctylammonium (TOA^+), respectively, demonstrate excellent air stability

up to six months. This compares favorably to that of $(TMA)_3Cu_2Br_5$ (~four weeks; TMA = tetramethylammonium), K_2CuX_3 (~three weeks), and Rb_2CuX_3 (~one day; X = Cl, Br).[88, 96, 134, 135] $(TBA)CuBr_2$ and $(TOA)CuBr_2$ also demonstrate exceptional stability when immersed in water up to 90 days, with little to no change in PL intensity. Moreover, phosphonium-based hybrid Cu(I) halides demonstrate improved thermal stability (e.g., ~400 °C in $(TEP)_2Cu_2Br_4$) compared to the structurally similar ammonium-based Cu(I) halides (e.g., 265 °C in $(TEA)_2Cu_2Br_4$) due to the greater nucleophilicity of the phosphonium compounds.[62] These results suggest that a careful choice of organic cations not only promote different crystal structures in hybrid Cu(I) halides, but also can improve the emission efficiency, provide emission tunability, and enhance environmental and thermal stability.

2.2. Coordination compounds

Among luminescent Cu(I) halides, coordination (with general formula $L_mCu_nX_n$) compounds have been widely explored for decades.[59] Interest in this materials class predates the recent work on hybrid organic-inorganic Cu(I) halides – interesting PL properties of $L_mCu_nX_n$ have been known since 1970s.[136-138] The extensive studies conducted on $L_mCu_nX_n$ are the result of vast varieties of available organic ligands (L) and structural diversities in Cu(I) halide (CuX) modules. Many varieties of coordination modes are possible between organic and inorganic modules. For instance, the ligands can be grouped based on their denticity into mono-, di-, tri- and other multidentate ligands depending on the number of electron donor groups that can bind with the metal center.[139, 140] Moreover, some compounds contain a single type of ligand, while others contain multiple types of ligands.[69, 140-144] Organic ligands containing nitrogen (N-) and phosphorus (P-) electron donating sites are most commonly utilized due to their propensities to donate electrons to construct luminescent $L_mCu_nX_n$.[69, 145-148] Many compounds have also been reported in which sulfur (S-) acts as the electron donating site of the ligands.[71, 149-151] Due to the templating nature of the ligand structures, the preparation of the coordination compounds can range from very simple to complex depending on the synthesis procedure of the precursor ligands. One pot synthesis is often employed when the targeted ligands are easily accessible.[59, 69, 152, 153] Unlike the synthesis of hybrid compounds, neutral ligands containing lone pair electrons need to be employed for the synthesis of coordination compounds. There is a rich variation in the inorganic modules in the resultant materials depending on the ligand choice, amounts of ligands and reaction conditions. For instance, the excess amount of the ligand 3-picoline (3-*pc*) with CuI yields 0D-$CuI(3\text{-}pc)_3$ in the solution of hot pure base, while 0D-$Cu_2I_2(3\text{-}pc)_4$ forms by refluxing the precursors in acetone for 12 hours.[141, 154] Yet another product, 0D-$Cu_4I_4(3\text{-}pc)_4$ forms under ligand deficient conditions in aqueous KI solution.[155] Important to note, non-protic solvents are usually used in the reaction to avoid protonation to the N- or P-ligands, so that the lone pair electrons of N or P can be available for coordination with the Cu(I) core. The impact of solvent choice can be evidenced by considering the aforementioned reaction between CuI and 3-*pc* ligands in different conditions. While heating these precursors in hydroiodic acid and methanol at 140 °C for 5 days, 3-*pc* ligand undergoes in-situ alkylation and leading to the formation of a different compound $(Me\text{-}3\text{-}pc)Cu_2I_3$.[156] On the other hand, 1D-CuI(3-*pc*) forms immediately when an acetone solution of 3-*pc* ligands is diffused into the aqueous KI solution of CuI.[155, 157] These examples clearly demonstrate the wealth of materials that can be obtained from various combinations of 3-*pc* and CuI under different

conditions. For most studied CuI-organic ligand pseudobinary materials systems, further synthetic work could yield hitherto unknown coordination materials with outstanding optical properties.

Typically, solvent diffusion is a common method for the preparation of coordination compounds that are accessible at room temperature, where solutions of pure ligands in non-polar solvent and saturated KX solutions of CuX are allowed to diffuse into each other.[69, 157, 158] Wet chemistry methods at higher temperatures (e.g., solvothermal synthesis) are widely used to yield thermodynamically favorable coordination Cu(I) halides. This process involves heating the precursors in a suitable solvent at 100 – 200 °C for multiple hours.[59, 140, 150] Besides the solvothermal and solvent diffusion techniques, ligand exchange and mechanochemical methods have also been reported to yield coordination Cu(I) halides.[159, 160] However, the suitability of these methods are not well-explored yet and the difficulty of separation of a targeted compound from the product mixture requires further optimization of these techniques.

Unlike hybrid organic-inorganic Cu(I) halides, Cu(I) in $L_mCu_nX_n$ favors tetrahedral coordination environment in most cases with a few examples of trigonal coordination. In contrast to hybrid compounds, organic ligands are directly bonded to the Cu(I) centers in the coordination compounds. Therefore, the dimensionality in these compounds is determined by the connectivity modes of organic and inorganic modules ranging from discrete clusters (0D) to extended structures of higher dimensionality (e.g., 1D, 2D, 3D) (Fig. 5). Noteworthy, most of the reported luminescent Cu(I) halide coordination compounds contain iodide on the halide site, probably due to its larger size to balance with bulky organic ligands and to reduce the steric effects of the ligands.[61] The combination of Cu(I) with iodide is also more favorable compared to chloride and bromide following the Pearson theory of Hard and Soft Acids and Bases. Indeed, CuI-based coordination luminescent compounds tend to be more stable compared to CuCl- and CuBr-analogues.[70] Moreover, the employed ligands are typically based on aromatic rings that facilitate the electron donation of heteroatoms to form coordination bonds with Cu. In comparison, hybrid Cu(I) halides feature organic cations containing either alkyl or aryl substituents.

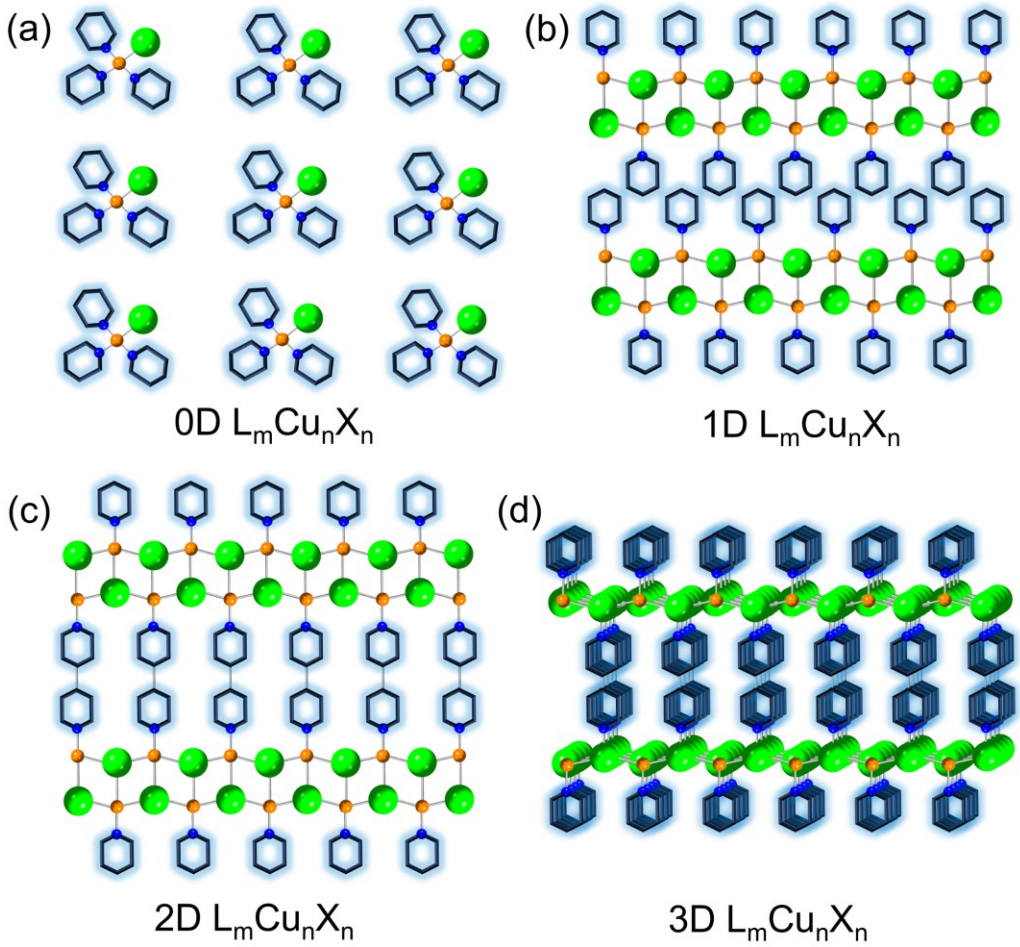

Fig. 5 Conceptual representation of coordination compounds of the general formula $L_mCu_nX_n$: (a) 0-D, (b) 1-D, (c) 2-D and (d) 3-D structures. Orange, green, blue spheres represent copper, halide, N/P/S atoms, respectively. Hexagonal black ring represents the backbone of the organic motifs.

The most common 0D structures are molecular species containing a monomer (CuX), dimer (Cu_2X_2), or a tetramer (also known as cubane-like structure) (Cu_4X_4); some less common varieties include a trimer (Cu_3X_3), hexamer (Cu_6X_6), octamer (Cu_8X_8), etc.[59] The number of ligands coordinated with the metal center depends on the steric hindrance among the ligands. For instance, three ligands bind with Cu(I) in addition to a halide to form a simple monomer L_3CuX (Fig. 6a).[143, 161-163] With increasing the steric hindrance and/or number of binding sites of the ligands, there are also examples available where each Cu(I) atom binds with two ligands and one halide to form L_2CuX (Fig. 6b).[140, 164-166] Similarly, the Cu(I) core in 0D dimeric Cu_2X_2 is tetrahedrally coordinated with two halides and two organic ligands to form $L_4Cu_2X_2$ (Fig. 6c).[141, 142, 167] Lower coordination of Cu(I) centers is also observed for bulky organic ligands like in $L_3Cu_2X_2$ and $L_2Cu_2X_2$.[69, 163] On the other hand, cubane tetramers (Cu_4X_4) are formed by four Cu(I) atoms and four halides, where each Cu(I) is usually tetrahedrally coordinated with three halide atoms and one organic ligand to form $L_nCu_4X_4$ (n = 2, 4) (Fig. 6d – e).[161, 168-170] These cubane tetramers (Cu_4X_4) or hexamers (Cu_6X_6) exhibit structural similarities with anionic Cu_4X_6- and Cu_4X_8-clusters in

hybrids Cu(I) halides, where Cu···Cu distances are less than the sum of the van der Waals radii of two Cu atoms (2.80 Å).[76, 107, 171, 172] Short Cu···Cu distances in these compounds suggest that electronic interaction may exist between neighboring Cu atoms which may influence the optical properties of these compound.[172]

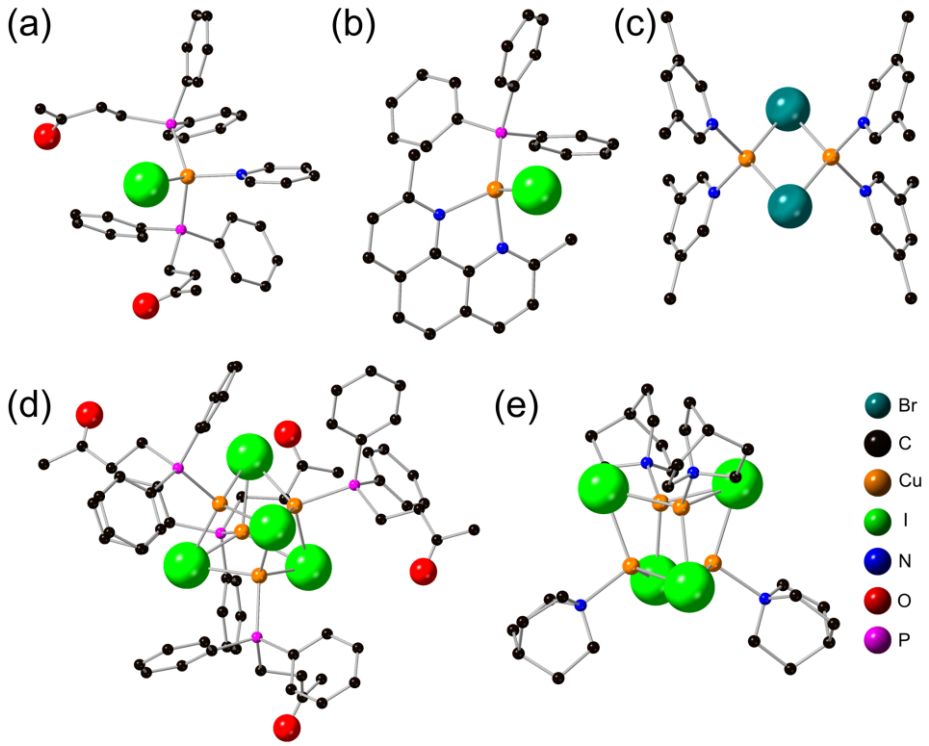

Fig. 6 Structures of selected 0D- $L_mCu_nX_n$ compounds. (a) 0D-CuI(*py*)(4-*dpp*-butane-2-one)$_2$,[161] (b) 0D-CuI(*tpp*)(2,9-*dm*-1,10-phenanthroline),[140] (c) 0D-Cu_2Br_2(3,5-*dm*-*py*)$_4$,[142] (d) 0D-Cu_4I_4(4-*dpp*-butane-2-one)$_4$,[161] (e) 0D-Cu_4I_4(quinuclidin)$_4$.[168] *py* = pyridine, *tpp* = triphenylphosphine, *dpp* = diphenylphosphine, *dm* = dimethyl. Inset shows the atomic legends. Orange, green, olive, blue, pink, red and black spheres represent copper, iodide, bromide, nitrogen, phosphorous, oxygen and carbon, respectively. Hydrogens are omitted for clarity.

Similar to hybrid Cu(I) halides, one-dimensional structures are observed in coordination Cu(I) halides. However, as a charge neutral chain, Cu and X maintain 1:1 ratio in $L_mCu_nX_n$, where each Cu is coordinated with two or three halides along the chain and two or one ligand sites in the side, respectively, such as in the case of 1D-CuI(3-Br-*py*) (*py* = pyridine) (Fig. 7a).[69, 157, 163] Moreover, organic ligands possessing multiple donating heteroatoms can also participate in forming 1D chains by acting as a bridge between the inorganic modules, such as in 1D-Cu_2I_2(*tpp*)$_2$(4,4′-*bpy*) (*tpp* = triphenylphosphine, *bpy* = bipyridine) (Fig. 7b).[173, 174] Likewise, 2D sheets or 3D extended frameworks can be obtained by bridging the inorganic modules with multidentate ligands, such as in 2D-CuI(2,5-*dm*-*pz*)$_{0.5}$ (*dm*-*pz* = dimethyl-pyrazine) (Fig. 7c) and 3D-CuI(*tz*)$_{0.5}$ (*tz* = triazine) (Fig. 7d), respectively.[158, 175, 176] Interestingly, the inorganic core in these extended networks can adopt all possible complexities available for coordination Cu(I) halides, including CuX (e.g., 1D-

CuI 5,6,11,12-tetraaza-naphthacene (*tanc*)), dimeric Cu_2X_2 (e.g., 2D-Cu_2I_2(3,3′-*bpy*)$_2$), tetrameric Cu_4X_4 (e.g., 3D-Cu_4I_4 *N*,*N*′-dimethylpiperazine (*L*21)$_2$), etc.[59, 142, 159, 166, 177-182]

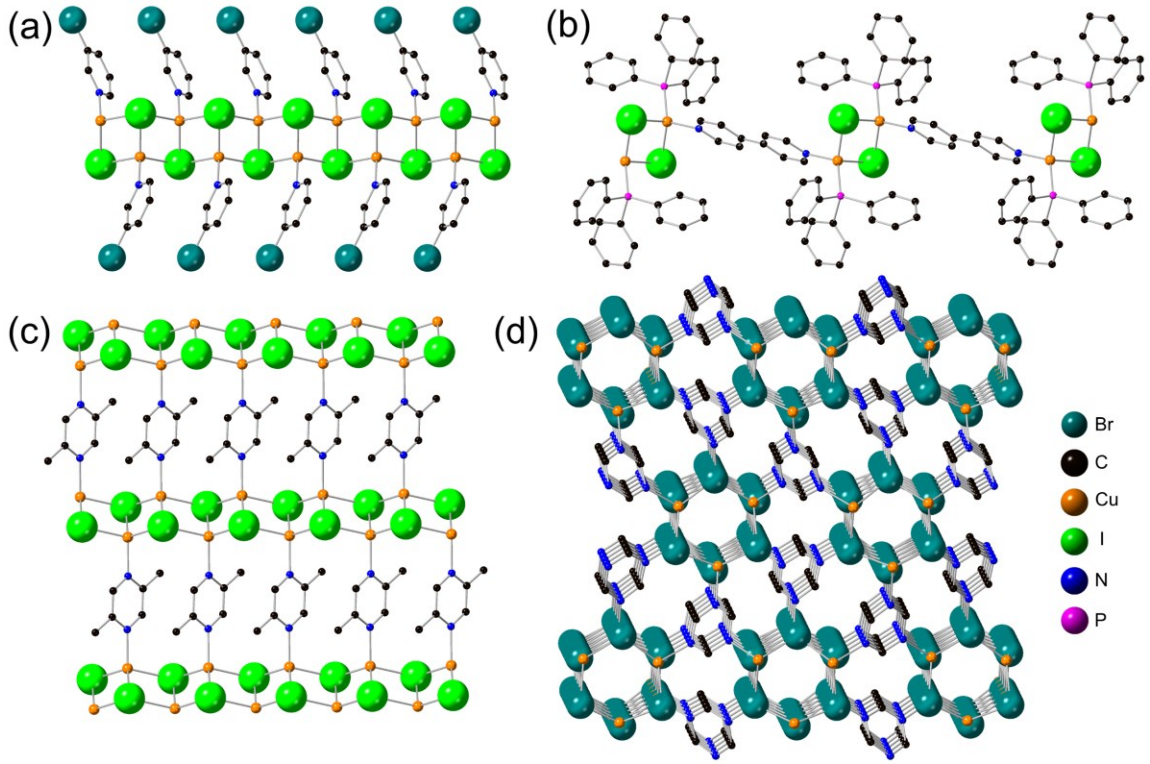

Fig. 7 Structures of select $L_mCu_nX_n$ compounds: (a) 1D-CuI(3-Br-*py*),[157] (b) 1D-Cu_2I_2(*tpp*)$_2$(4,4′-*bpy*),[173] (c) 2D-CuI(2,5-*dm*-*pz*)$_{0.5}$,[175] (d) 3D-CuI(*tz*)$_{0.5}$.[158] Inset shows the atomic legends. Orange, green, olive, blue, pink and black spheres represent copper, iodide, bromide, nitrogen, phosphorous and carbon, respectively. Hydrogens are omitted for clarity.

One of the major challenges of the coordination Cu(I) halides is their poor stability under moist air, heat and light. Due to the relatively weaker coordination bonds between Cu and ligands, these materials suffer from poor stability in harsh conditions.[59, 157, 159, 183] To address this issue, many efforts have been devoted in past decades and some progress has been made. For example, Li *et al*. showed that by constructing extended network of highly luminescent Cu(I) halide units (e.g., Cu_2I_2 and Cu_4I_4) with multidentate organic ligands, the stability of the resultant coordination compounds toward moisture, light and heat can be enhanced.[159, 183] The general trend of the stability of these compounds can be expressed as 0D < 1D < 2D < 3D. In a follow-up study, it was shown that stability can be further boosted by using a suitable organic ligand that forms comparatively stronger Cu-ligand bond; in the case of Cu_4I_4-based structures of same dimensionality, imidazole derivatives form stronger Cu-N bonds compared to the pyridine derivatives, hence are more robust compared to the coordination compounds formed by the latter ligand.[59] Therefore, just like in hybrid Cu(I) halides, the choice of suitable organic ligands plays an important role for the overall stability of coordination Cu(I) halides.

2.3. Comparisons of structure and stability of hybrid *vs* coordination Cu(I) halides

Diverse types of Cu(I) halide units such as simple linear $[CuX_2]^-$, dimeric $[Cu_2X_4]^{2-}$ and $[Cu_2X_5]^{3-}$, and anionic clusters $[Cu_4X_6]^{2-}$ and $[Cu_4X_8]^{4-}$, have been observed in the crystal structures of hybrid compounds. Although inorganic motifs are spatially isolated in 0-D compounds by the organic cations, the precise influence of the structures of organic cations, their packing patterns, rigidity and hydrogen bonding ability on the formation of these diversified Cu(I) halide units are still unclear. Therefore, systematic synthesis and structural characterization experiments are needed to get a clear understanding of their structural patterns. In contrast, monomeric CuX, dimeric Cu_2X_2 and tetrameric Cu_4X_4 are most observed inorganic motifs in coordination Cu(I) halides. While structural dimensionality in hybrid Cu(I) halides is determined by the connectivity of the inorganic units, both organic and inorganic motifs participate in forming extended networks in coordination compounds. In both materials classes, bulky organics (cations or ligands) improve their environmental stability. Coordination Cu(I) halides typically are less thermally stable (generally, decomposition temperature (T_D) is ≤200 °C) than hybrid organic-inorganic Cu(I) halides due to the presence of weaker Cu-*L* contacts in the former.[59, 159, 183] However, even hybrid Cu(I) halides are rarely stable above 300 °C.[62, 82, 114, 184] Previous studies show that the thermal behavior of both compounds can be tuned through chemical composition and crystal structure manipulations. Overall, environmental and thermal stability of both hybrid and coordination Cu(I) halides need further improvement for potential practical applications.

3. Photoluminescence (PL) properties and electronic structures

In-depth understanding of the PL emission mechanisms is fundamental for designing next-generation materials with improved functionalities for device applications. Fig. 8 shows a collection of various schematic diagrams that have been widely used in the literature to describe the light emission mechanisms in hybrid organic inorganic and coordination Cu(I) halides. *Self-trapped exciton* (STE) based emission (Fig. 8a) is the most common emission mechanism proposed for the hybrid organic inorganic Cu(I) halides.[38, 62, 82, 88, 94, 114] However, a few recent reports have also argued the possibility of *triplet* (Fig. 8b), *metal centered* (^{3}MC) (Fig. 8c) and *cluster centered* (^{3}CC) (Fig. 8d) emission mechanisms.[75, 76, 105, 185] Besides these major emission pathways, only a few publications proposed the possibility of midgap *defect-based emission* (DBE) and *through space charge transfer* (TSCT) emission pathways for hybrid Cu(I) halides,[89, 114] however, these emission pathways are not well-explained and lack sufficient supporting evidences. On the other hand, often-mentioned emission mechanisms for coordination Cu(I) halides include *metal to ligand charge transfer* (MLCT) or *halide to ligand charge transfer* (XLCT) or (M + X)LCT (Fig. 8e), with additional cases of ^{3}CC or *thermally activated delayed fluorescence* (TADF) (Fig. 8f) depending on their crystal and electronic structures.[59, 61, 181, 182, 186, 187]

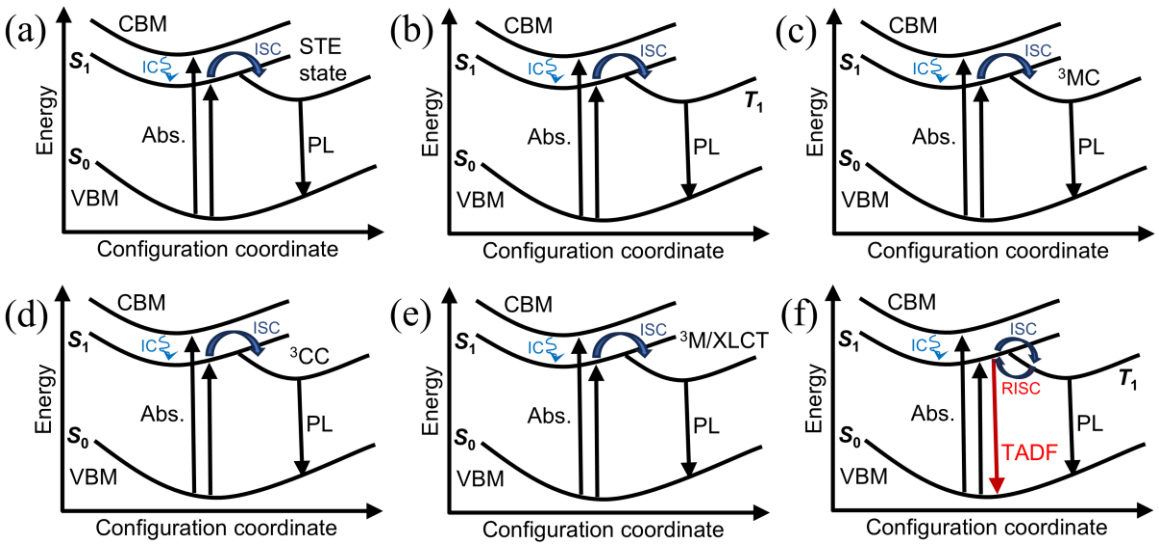

Fig. 8 Simplified configuration coordinate diagrams used to explain photoemission in hybrid organic inorganic and coordination Cu(I) halides: (a) STE, (b) triplet, (c) ^{3}MC, (d) ^{3}CC, (e) M/XLCT, and (f) TADF.

A few important observations can be made by reviewing the popular schematic diagrams of optical processes shown in Fig. 8. (1) Immediately noticeable is the fact that while some of these diagrams have appropriate labels for the states (e.g., S_0, S_1, STE state etc.), others carry labels that are not consistent with the labeling of states. For example, MLCT is a name for an optical process and not for a state in a configurational coordinate diagram. A closer analysis of the usage of this term reveals further issues (see below in 3.2) with it as typically MLCT is the process for optical absorption in most coordination Cu(I) halides, yet the emissive state is labeled as M/XLCT (Fig. 8e). (2) Another observation, most of these energy diagrams seem to represent identical or similar phenomena (especially Fig. 8a – e), which leads to questions about differences between these emission mechanisms. *Are these similar processes labeled with different names?* If so, what would be the more accurate terminology to use? To the best of our knowledge, these are yet unanswered questions. In this section, we will review the typically observed optical properties, fundamental emission mechanisms, and the luminescence modulations that have been reported for luminescent Cu(I) halides. We will also attempt to address some of the questions regarding different emission mechanisms in literature. Estimated bandgaps, excitation (λ_{ex}) and emission (λ_{em}) wavelengths, emission colors, PLQYs, decomposition temperatures (T_D) of the representative hybrid organic-inorganic and coordination Cu(I) halides have been summarized in Tables 1 and 2, respectively.

Table 1 Estimated bandgaps, excitation (λ_{ex}) and emission (λ_{em}) wavelengths, emission colors, PLQYs, decomposition temperatures (T_D) of the representative hybrid organic-inorganic Cu(I) halides.

No.	Compound	Band gap (eV)	λ_{ex} (nm)	λ_{em} (nm)	Emission Color	PLQY (%)	T_D (°C)	Ref.
1.	0D-(TBA)$CuCl_2$ (TBA = tetrabutylammonium)	4.44	286	510	Green	92.8	-	[94]
2.	0D-(2-TTPS)$CuCl_2$ (2-TTPS = triphenyl(thiophen-2-yl)phosphonium)	2.875	408	574	Yellow	34.1	280	[188]
3.	1D-$(TMA)_3Cu_2Cl_5$ (TMA = tetramethylammonium)	4.21	293	585	Yellow	53.5	100	[184]
4.	0D-(TPA)$CuBr_2$ (TPA =tetrapropylammonium)	3.7	258	504	Blue	81	245	[82]
5.	0D-(TBA)$CuBr_2$	4.23	289	498	Sky blue	80.5		[94]
6.	0D-(TOA)$CuBr_2$ (TOA = tetraoctylammonium)	5.59	280	509	Green	80.4	206 (melt at 54)	[88]
7.	0D-(ETPP)$CuBr_2$ (ETPP = (ethyl)triphenylphosphonium)	-	342	532	Green	65.2	280	[103]
8.	0D-$(PPh_4)CuBr_2$ (PPh_4 = tetraphenylphosphonium)	2.09	285	538	Yellow	1.3	419	[114]
9.	1D-$(TMA)Cu_2Br_3$	2.5	-	-	-	-	276	[84]
10.	0D-$(TEA)_2Cu_2Br_4$ (TEA = $C_8H_{20}N$ = tetraethylammonium)	2.53	280	463	Sky blue	97.1	240	[106]
11.	0D-$(TEP)_2Cu_2Br_4$ (TEP = tetraethylphosphonium)	3.97	332	503	Green	92	400 (melt at 173)	[62]
12.	0D-$(Bmpip)_2Cu_2Br_4$ (Bmpip = $C_9H_{20}N$ = BMP = 1-butyl-1-methyl-piperidinium)	3.13	320	620	Orange	48.2	290	[114]
13.	0D-$(C_9H_{20}N)_2Cu_2Br_2I_2$	-	335	464, 630	-	99.5	-	[189]
14.	1D-$(TMA)_3Cu_2Br_5$	3.98	311	535	Green	64.3	240	[184]
15.	0D-$(C_6H_{16}N_2)_3$ $[Cu_4Br_6]$ $[Cu_2Br_6]$	370 nm	-	620	-	-	230	[105]
16.	0D-$(TEP)_2Cu_4Br_6$	3.90	396	601	Orange	98	400 (melt at 126)	[62]
17.	0D-$(TPA)_2Cu_4Br_6$	3.19	360	666	Yellow-orange	95	287	[82]
18.	0D-$(ETPP)_2Cu_4Br_6$	-	365	570	Yellow	94.2	70	[103]
19.	0D-$(PTPP)_2Cu_4Br_6$ (PTPP = pentyltriphenylphosphonium)	2.82	369	610	Orange	80.2	120	[81]
20.	0D-$(2\text{-}TTPS)_2Cu_4Br_6$	2.14	395	606	Orange	11.8	390	[188]
21.	1D-$Gua_4Cu_4Br_8$ (Gua = guanidine)	2.1	330	600	-	1	300	[80]
22.	0D-(IPP)CuI_2 (IPP = *iso*-propyltriphenylphosphonium)	2.51	-	440, 550	Yellow	75	-	[190]
23.	0D-$(IPP)_2CuI_3$	-	365	500	Green	73.7	-	[190]
24.	0D-α-$(Ph_3MeP)_2CuI_3$ (Ph_3MeP = $C_{19}H_{18}P$ = MTP = methyltriphenylphosphonium)	1.18	365	475	Blue	11.8	162	[191]
25.	0D-β-$(Ph_3MeP)_2CuI_3$	1.19	375	495	Green	51.6	162	[191]

No.	Compound	Band gap (eV)	λ_{ex} (nm)	λ_{em} (nm)	Emission Color	PLQY (%)	T_D (°C)	Ref.
26.	0D-$(ETPA)_2Cu_2I_4$ (ETPA = ethyltripropylammonium)	-	325	490	Cyan	97.6	240	[84]
27.	0D-$(BzTPP)_2Cu_2I_4$ (BzTPP = benzyltriphenylphosphonium)	2.99	362	529	Yellow-green	44.2	540	[120]
28.	2D-$(Bz)_2Cu_2I_4 \cdot H_2O$ (Bz = benzyl)	-	308	470	Blue	30	99	[129]
29.	0D-α-$Gua_3Cu_2I_5$	2.54	315	472	Blue	80.8	-	[83]
30.	1D-$Gua_3Cu_2I_5$	2.44	325	575	Yellow	72	300	[80]
31.	1D-β-$Gua_3Cu_2I_5$	2.35	330	534	Yellow-green	86.9	-	[83]
32.	1D-$(4\text{-}bzpy)_3Cu_3I_6$ (4-bzpy = 4-benzylpyridine)	2.42	450	560	Yellow	0.3	277	[90]
33.	0D-α-$(MTP)_2Cu_4I_6$	-	400-500	560	Yellow-green	54	340 (melt at 126)	[97]
34.	0D-β-$(MTP)_2Cu_4I_6$	-	400-500	625	Yellow-orange	89	340 (melt at 126)	[97]
35.	0D-$(Ph_3MeP)_2Cu_4I_6$	2.99	469	633, 537	Yellow-orange	69.0	-	[121]
36.	0D-$(PTPP)_2Cu_4I_6$	2.82	370	524	Green	93.1	200	[81]
37.	1D-$(C_9H_{15}N_2)_2Cu_4I_6$ ($C_9H_{15}N_2^+$ = 4-dimethylamino-1-ethylpyridinium)	2.98	360	584	Yellow	99.5	309	[89]
38.	0D-$(C_{19}H_{18}P)_2Cu_4I_6$	2.1	470	620, 560	Yellow	87.4	350	[192]
39.	0D-$(Cy_3MeP)_2Cu_4I_6$ (Cy_3MeP = methyltricyclohexylphosphonium)	3.32	469	611, 534	Yellow-green	59.1	-	[121]
40.	0D-$(C_4H_{10}N)_4Cu_4I_8$ ($C_4H_{10}N^+$ = pyrrolidinium)	2.81	260-380	560	Green-yellow	84.7	331 (melt at 104)	[85]
41.	0D-$(C_{13}H_{28}N_2)_2Cu_4I_8$ ($C_{13}H_{28}N_2^{2+}$= biprotonated 4, 4′ -trimethylenedipiperidine)	3.11	320	530	Green	92.8	300	[76]
42.	0D-$(2\text{-}TTPS)_4Cu_4I_8$	1.87	397	590	Orange-yellow	7.2	355	[188]
43.	1D-$Gua_6Cu_4I_{10}$	2.72	340	560	Yellow	12.1	-	[80]
44.	3D-$(4\text{-}bzpy)_2Cu_6I_8$	2.36	420	540	Yellow	0.1	270	[90]
45.	0D-$(ETA)_3Cu_6I_9$ (ETA = ethyltripropylammonium)	2.47	286, 371	490, 775	Cyan, Red	18.6 (ex. at 371)	240 (melt at 138)	[123]

Table 2 Estimated bandgaps, excitation (λ_{ex}) and emission (λ_{em}) wavelengths, emission colors, PLQYs, decomposition temperatures (T_D) of the representative coordination Cu(I) halides.

No.	Compound	Band gap (eV)	λ_{ex} (nm)	λ_{em} (nm)	Emission Color	PLQY (%)	T_D (°C)	Ref.
	Coordination (Neutral)							
1.	0D-CuI(*tpp*)$_2$(4-*pc*) (*tpp* = triphenylphosphine, 4-*pc* = 4-picoline)	-	360	455	Blue	66.0	-	[162]
2.	0D-CuI(*tpp*)(2,9-*dm*-1,10-phenanthroline) (*tpp* = triphenylphosphine; *dm* = dimethyl)	2.2	360	605	Orange	25.8	190	[140]
3.	0D-CuI(*tpp*)(2,9-dichloro-1,10-phenanthroline)	2.1	360	620	Orange-red	19.3	180	[140]
4.	0D-CuI(*tpp*)(5- chloro-6-methyl-1,10-phenanthroline)	2.0	360	650	Red	3.80	180	[140]
5.	0D-CuI(*py*)(4-*dpp*-butane-2-one)$_2$ (*py* = pyridine; *dpp* = diphenylphosphine)	-	300	470	-	31.0	-	[161]
6.	1D-CuI(4,4′-*pypzpy*) (4,4′-*pypzpy* = 4-(1-(pyridin-4-yl)-1H-pyrazolyl)pyridine	-	398	575	-	-	-	[163]
7.	1D-CuI(9,10-bis(triazol-1-ylmethyl)anthracene)	-	400	486	Blue	-	300	[193]
8.	1D-CuI(4-*pc*)	3.2	365	433	Purple	35.8	100	[157]
9.	1D-CuI(3,5-*dm*-*py*)	3.1	365	490	Blue	35.3	100	[157]
10.	1D-CuI(3-*pc*)	3.0	365	469	Blue	37.2	100	[157]
11.	1D-CuI(*py*)	2.9	365	475	Blue	29.1	100	[157]
12.	1D-CuI(3-Br-*py*)	2.7	365	480	Blue	16.0	80	[157]
13.	1D-CuI(2-*et*-3-*me*-*pz*) (*et* = ethyl; *me* = methyl; *pz* = pyrazine)	2.6	365	490	Green	32.4	90	[157]
14.	1D-CuI(2,6-*dm*-*pz*)	2.4	365	525	Green	15.4	90	[157]
15.	1D-CuI(5-Br-*pm*) (*pm* = pyrimidine)	2.3	365	545	Yellow	13.1	90	[157]
16.	1D-CuI(2-*cy*-*pz*) (*cy* = cyano)	2.2	365	618	Red	10.1	80	[157]
17.	1D-CuI$(py)_{1-x}(pm)_x$	2.9	365	470, 590	White	12.5	100	[157]
18.	1D-CuI(2-(methylsulfanyl)pyridine)	3.1	375	449	Blue	0.5	90	[194]
19.	2D-CuI$(pm)_{0.5}$	2.5	360	500	Green	17.0	160	[195]
20.	2D-CuI$(pz)_{0.5}$	2.3	360	578	Yellow	12.7	170	[195]
21.	2D-CuI(4,4′-*bpy*)$_{0.5}$ (*bpy* = bipyridyl)	2.3	360	556	Yellow	2.5	290	[195]
22.	2D-CuI$(bpe)_{0.5}$ (*bpe* = 1,2-bis(4-pyridyl)ethane)	3.1	360	443	Purple	16.4	280	[195]
23.	2D-CuI$(bpee)_{0.5}$ (*bpee* = 1,2-bis(4-pyridyl)ethylene)	2.2	360	695	Red	1.00	300	[195]
24.	2D-CuI$(bbimb)_{0.5}$ (*bbimb* = 1,4-bis((1*H*-benzo[*d*]imidazol-1-yl)methyl)benzene)	2.4	360	-	-	-	310	[195]
25.	0D-$Cu_2Cl_2(Ph_2Ppy)_3$ (*Ph*$_2$*Ppy* = 2-diphenylphosphino-pyridine)	-	372	577	-	37.0	-	[187]
26.	0D-$Cu_2Cl_2(Ph_2Ppym)_3$ (*Ph*$_2$*Ppym* = 2-diphenylphosphino-pyrimidine)	-	372	616	-	9.00	-	[187]
27.	0D-$Cu_2Cl_2(Py_3P)_2$ (*Py*$_3$*P* = tris(2-pyridyl)phosphine)	-	360	550	Yellow	55.0	250	[182]
28.	0D-$Cu_2Br_2(Py_3P)_2$	-	360	530	-	53.0	250	[182]

No.	Compound	Band gap (eV)	λ_{ex} (nm)	λ_{em} (nm)	Emission Color	PLQY (%)	T_D (°C)	Ref.
29.	0D-Cu_2Br_2(*Ph_2Ppy*)$_3$	-	372	545	-	53.0	-	[187]
30.	0D-Cu_2Br_2(*Ph_2Ppym*)$_3$	-	372	583	-	33.0	-	[187]
31.	0D-Cu_2Br_2(*Ph_2Piqn*)$_3$ (*Ph_2Piqn* = 1-diphenylphosphino-isoquinoline)	-	372	660	-	11.0	-	[187]
32.	0D-Cu_2Br_2(3,5-*dm-py*)$_4$	1.5	360	520	Green	82.4	50	[142]
33.	1D-Cu_2Br_2(5-*br-pm*)$_2$ (*br* = bromo)	-	360	630	Red	2.10	110	[142]
34.	0D-Cu_2I_2(*Py_3P*)$_2$	-	360	520	-	51.0	300	[182]
35.	0D-Cu_2I_2(*Ph_2Ppy*)$_3$	-	372	539	-	81.0	-	[187]
36.	0D-Cu_2I_2(*Ph_2Ppym*)$_3$	-	372	565	-	13.0	-	[187]
37.	0D-Cu_2I_2(*Ph_2Piqn*)$_3$	-	372	636	-	38.0	-	[187]
38.	0D-Cu_2I_2(*py*)$_2$(4-*dpp*-butane-2-one)$_2$	-	300	485	-	42.0	-	[161]
39.	0D-Cu_2I_2(*tpp*)$_2$(4-*pc*)$_2$	-	360	470	-	33.0	-	[69]
40.	0D-Cu_2I_2(*tpp*)$_2$ (4-*ph-py*)$_2$ (4-*ph-py* = 4-phenyl-pyridine)	-	360	480	-	62.0	-	[69]
41.	0D-Cu_2I_2(3-*pc*)$_4$	2.6	360	496	Blue-green	95.2	60	[159]
42.	0D-Cu_2I_2(3,5-*dm-py*)$_4$	2.8	360	479	Blue	81.5	60	[159]
43.	0D-Cu_2I_2(3-Cl-*py*)$_4$	2.5	360	530	Green	85.6	50	[159]
44.	0D-Cu_2I_2(*tpp*)$_2$(3-*pc*)$_2$	3.0	360	455	Blue	90.3	135	[159]
45.	0D-Cu_2I_2(*tpp*)$_2$(4,6-*dm-pm*)$_2$	2.9	360	465	Blue	72.3	120	[159]
46.	1D-Cu_2I_2(*tpp*)$_2$(*bpp*) (*bpp* = 1,3-bis(4-pyridyl)propane)	2.8	360	458	Blue	91.7	180	[159]
47.	1D-Cu_2I_2(*tpp*)$_2$(4,4′-*dps*) (*4,4′-dps* = 4,4′-dipyridyl sulfide)	2.6	360	532	Green-yellow	80.0	150	[159]
48.	1D-Cu_2I_2(*tpp*)$_2$(4,4′-*bpy*)	2.4	360	540	Yellow	76.2	160	[159]
49.	1D-Cu_2I_2(*tpp*)$_2$(*pz*)	2.1	360	631	Red	26.1	120	[159]
50.	1D-Cu_2I_2(5-*me-pm*)$_2$	2.3	360	570	Orange	30.8	130	[159]
51.	1D-Cu_2I_2(*biprbt*)$_2$ (*biprbt* = 1-(3-(1*H*-benzo[*d*]imidazol-1-yl)propyl)-1*H*-benzo[*d*][1,2,3]triazole)	2.3	360	572	Yellow	56.0	260	[196]
52.	1D-Cu_2I_2(*bbtbu*)$_2$ (*bbtbu* = 1,4-bis(1*H*-benzo[*d*][1,2,3]triazol-1-yl)butane)	2.4	360	562	Yellow	66.0	250	[196]
53.	1D-Cu_2I_2(*bihebt*)$_2$ (*bihebt* = 1-(6-(1*H*-benzo[*d*]imidazol-1-yl)hexyl)-1*H*-benzo[*d*][1,2,3]triazole)	2.6	360	542	Yellow	63.0	250	[196]
54.	1D-Cu_2I_2(*bbtpe*)$_2$ (*bbtpe* = 1,5-bis(1*H*-benzo[*d*][1,2,3]triazol-1-yl)pentane)	2.7	360	508	Blue-green	83.0	250	[196]
55.	1D-Cu_2I_2(*bpoe*)$_2$ (*bpoe* = 1,2-bis(pyridin-3-yloxy)ethane)	2.5	360	560	Yellow	45.0	200	[174]
56.	1D-Cu_2I_2(*bbtpe-m*)$_2$ (*bbtpe-m* = 1,1′-(3-methylpentane-1,5-diyl)bis(1*H*-benzo[1,2,3]triazole))	2.7	360	510	Cyan	25.0	260	[174]
57.	1D-Cu_2I_2(2-(methylsulfanyl)pyridine)	3.1	375	451	Blue	45	90	[194]
58.	1D-Cu_2I_2(2-methyl-6-(methylsulfanyl)pyridine)	3.0	420	562, 638	Orange	20	70	[194]
59.	1D-Cu_2I_2(2-(methylsulfanyl)-3-phenylpyridine)	2.9	375	520	Green	1	90	[194]

No.	Compound	Band gap (eV)	λ_{ex} (nm)	λ_{em} (nm)	Emission Color	PLQY (%)	T_D (°C)	Ref.
60.	1D-Cu_2I_2(3-butoxy-2-(methylsulfanyl)pyridine)	3.0	375	477	Cyan	44	90	[194]
61.	1D-Cu_2I_2(3-ethoxy-2-(methylsulfanyl)pyridine)	2.9	375	470	Cyan	16	90	[194]
62.	1D-Cu_2I_2(6-hydroxymethyl-2-(methylsulfanyl)pyridine)	3.0	375	470	Cyan	14	90	[194]
63.	2D-Cu_2I_2(*bpe*)$_2$	2.8	360	494	Blue-green	82.3	170	[159]
64.	2D-Cu_2I_2(3,3′-*bpy*)$_2$	2.6	360	515	Green	77.3	210	[159]
65.	2D-Cu_2I_2(4,4′-*dps*)$_2$	2.5	360	547	Yellow	70.8	160	[159]
66.	1D-Cu_3I_3(2-(butylsulfany)-6-methylpyridine)$_2$	3.1	375	440	Blue	13	90	[194]
67.	0D-Cu_4Cl_4(6-Me)$_2$ (6-Me = 2-(diphenylphosphino)pyridine)	-	350	501	Green	33.0	-	[186]
68.	1D-Cu_4Cl_4(L1)$_2$ (L1= ris[2-(pyridin-2-yl)ethyl]phosphine)	-	350	520	Green	62.0	280	[180]
69.	0D-Cu_4Br_4(6-Me)$_2$	-	350	605	Yellow	65.0	-	[186]
70.	1D-Cu_4Br_4(L1)$_2$	-	350	490	Cyan	54.0	280	[180]
71.	0D-Cu_4I_4(6-Me)$_2$	-	350	593	Orange	93.0	-	[186]
72.	0D-[Cu_4I_4(*Ph_3As*)$_3$] (*Ph_3As* = triphenylarsine)	3.07	350	565	Yellow	100	210	[197]
73.	0D-[Cu_4I_4(*An_3As*)$_3$(*Et*CN)] (*An_3As* = tris(*p*-anisyl)arsine; *Et* = ethyl)	3.11	350	555	Yellow	60.0	92	[197]
74.	0D-[Cu_4I_4(*An_3As*)$_3$(^{i}*Pr*CN)] (^{i}*Pr* = *iso*-propyl)	3.09	350	562	Yellow	63.0	76	[197]
75.	0D-[Cu_4I_4(*Ph_3As*)$_3$(*Ph*CN)] (*Ph* = phenyl)	3.05	380	560	Yellow	96.0	155	[197]
76.	0D-Cu_4I_4(*N*-methylpiperidine)$_4$	-	330	560	-	44.0	80	[168]
77.	0D-Cu_4I_4(quinuclidine)$_4$	-	330	540	-	50.0	160	[168]
78.	0D-Cu_4I_4(3-quinuclidinol)$_4$	-	350	550	-	48.0	180	[168]
79.	0D-Cu_4I_4(4-*dpp*-butane-2-one)$_4$	-	300	425, 605	-	28.0	-	[161]
80.	0D-Cu_4I_4(*py*)$_4$	2.7	360	560	Yellow	92.3	60	[183]
81.	0D-Cu_4I_4(*3-bzo-py*)$_4$ (*bzo* = benzyloxy)	2.9	360	590	Yellow	85.6	130	[183]
82.	0D-Cu_4I_4(*3-pc*)$_4$	2.8	360	560	Yellow	94.3	60	[183]
83.	0D-Cu_4I_4(*4-bz-py*)$_4$ (*bz* = benzyl)	2.7	360	560	Yellow	95.7	120	[183]
84.	0D-Cu_4I_4(*4-ph-py*)$_4$	2.6	360	545	Yellow	93.2	110	[183]
85.	0D-Cu_4I_4(*prbi*)$_4$ (*prbi* = 1-propyl-1H-benzo[d]imidazole)	2.7	360	600	Orange	96.1	160	[183]
86.	1D-Cu_4I_4(*bbipe*)$_2$ (*bbipe* = 1,5-bis(1H-benzo[d]imidazol-1-yl)pentane)	2.7	360	560	Yellow	71.8	320	[183]
87.	1D-Cu_4I_4(*msmbi*)$_2$ (*msmbi* = 1-((methylthio)methyl)-1H-benzo[d]imidazole)	3.2	360	550	Yellow	70.2	170	[183]
88.	1D-Cu_4I_4(L1)$_2$	-	350	448	Blue	45.0	280	[180]
89.	1D-Cu_4I_4(*bbtpe*)$_2$	2.4	360	560	Yellow	82.0	250	[196]
90.	1D-Cu_4I_4(*N*-methylpiperazine)$_2$	-	336	593	-	-	-	[177]
91.	2D-Cu_4I_4(*pda*)$_2$ (*pda* = 1,3-propandiamine)	3.0	360	616	Orange	65.3	200	[183]
92.	2D-Cu_4I_4(*dipe*)$_2$ (*dipe* = 1,5-di(1H-imidazol-1-yl)pentane)	2.8	360	620	Orange	64.4	290	[183]

No.	Compound	Band gap (eV)	λ_{ex} (nm)	λ_{em} (nm)	Emission Color	PLQY (%)	T_D (°C)	Ref.
93.	2D-Cu_4I_4(*bmbipe*)$_2$ (*bmbipe* = 1,5-bis(5-methyl-1H-benzo[d]imidazol-1-yl)pentane)	2.7	360	550	Yellow	67.1	350	[183]
94.	2D-Cu_4I_4(*bpp*)$_2$	2.6	360	613	Orange	56.2	240	[183]
95.	2D-Cu_4I_4(*4,4'-dps*)$_2$	2.4	360	577	Yellow	60.6	220	[183]
96.	2D-Cu_4I_4(*dmimpr*)$_2$ (*dmimpr* = 1,3-di(2-methyl-imidazol-1-yl)propane)	-	365	555	Yellow	20	300	[198]
97.	2D-Cu_4I_4(1,10-dithia-18-crown-6)$_2$	-	340	546	Yellow-green	-	-	[199]
98.	2D-Cu_4I_4(*bix*)$_2$ (*bix* = 1,4-bis(imidazole-1-ylmethyl)benzene)	-	396	604	-	-	339	[200]
99.	3D-Cu_4I_4(*1,4-bda*)$_2$ (*1,4-bda* = 1,4-butanediamine)	3.1	360	585	Yellow	60.7	230	[183]
100.	3D-Cu_4I_4(*en*)$_2$ (*en* = ethylene diamine)	3.0	360	590	Yellow	70.1	160	[183]
101.	3D-Cu_4I_4(*dipe*)$_2$	2.9	360	580	Yellow	65.6	300	[183]
102.	3D-Cu_4I_4(*N,N'*-dimethylpiperazine)$_2$	-	321	525	Yellow	-	-	[177]
103.	3D-Cu_4I_4(dimethyl-2,2′-biimidazole)$_2$	-	347	572	Yellow	-	230	[201]
104.	1D-Cu_6I_6(*bmibu*)$_3$ (*bmibu* = 1,4-bis(2-methyl-1*H*-imidazol-1-yl)butane)	2.5	360	554	Yellow	50.0	280	[196]
105.	0D-Cu_6I_6(*ppda*)$_2$ (*ppda* = 2-[2-(dimethylamino)phenyl(phenyl)phosphino]-N,N-dimethylaniline)	-	372	476	Blue	0.30	248	[181]
	Coordination - Ionic							
106.	1D-Cu_4Br_6(*bttme*)$_2$ (*bttme* = 2-(1*H*-benzo[d][1,2,3]triazol-1-yl)-*N,N,N*-trimethylethan-1-aminium)	2.5	360	615	Orange-red	56	220	[202]
107.	1D-Cu_4Br_6(*bttmpe*)$_2$ (*bttmpe* = 5-(1*H*-Benzo[*d*][1,2,3]triazol-1-yl)-*N,N,N*-trimethylpentan-1-aminium)	2.5	360	600	Orange-red	69	250	[202]
108.	0D-Cu_2I_4(*mtp*)$_2$ (*mtp* = 4-mercaptopyridine)	2.3	360	555	Yellow	61	210	[203]
109.	0D-Cu_3I_5(*bz-ted*)$_2$	3.0	360	560	Yellow	75	270	[203]
110.	0D-Cu_4I_6(*3-Cl-pr-ted*)$_2$ (*pr* = propyl)	3.1	360	540	Green-yellow	92	270	[203]
111.	0D-Cu_4I_6(*pr-ted*)$_2$	3.1	360	535	Green	92	280	[203]
112.	0D-Cu_4I_6(*2-Br-et-ted*)$_2$	2.9	360	535	Green	75	280	[203]
113.	0D-Cu_4I_6(*Pr-tpp*)$_2$	2.0	440	640	Red	1.1	250	[204]
114.	0D-Cu_4I_6(*Bu-tpp*)$_2$	2.0	440	623	Orange-red	1.0	230	[204]
115.	0D-Cu_4I_6(*Bn-tpp*)$_2$ (*Bn* = benzyl)	2.0	440	649	Red	3.5	225	[204]
116.	0D-Cu_4I_6(*tpp*)$_2$(*bttmm*)$_2$ (*bttmm* = 1-(1*H*-Benzo[*d*][1,2,3]triazol-1-yl)-*N,N,N*-trimethylmethanaminium)	2.5	360	540	Green-yellow	90	200	[203]
117.	0D-Cu_4I_6(*tpp*)$_2$(*btmdme*)$_2$ (*btmdme* = *N*-((1*H*-Benzo[*d*][1,2,3]triazol-1-yl)methyl)-*N,N*-dimethyl ethanaminium)	2.4	360	545	Green-yellow	64	180	[203]
118.	0D-Cu_4I_6(*L5*)$_2$ (*L5* = 1,3-bis((5,6-dimethyl-1H-benzo[d][1,2,3]triazol-1-yl)methyl)-1H-imidazol-3-ium)	2.4	360	590	Orange	64	210	[56]

No.	Compound	Band gap (eV)	λ_{ex} (nm)	λ_{em} (nm)	Emission Color	PLQY (%)	T_D (°C)	Ref.
119.	1D-Cu_4I_6(*L4*)$_2$ (*L4* = 1,3-bis((1*H*-benzo[*d*][1,2,3]triazol-1-yl)methyl)-4ethyl-1*H*-imidazol-3-ium)	2.3	360	625	Red	38	220	[56]
120.	1D-Cu_4I_6(*Pr-hmta*)$_2$ (*hmta* = hexamethylenetetramine)	3.5	300	510	Yellow	16	160	[205]
121.	1D-Cu_4I_6(*Ppg-hmta*)$_2$ (*Ppg* = propargyl)	3.0	300	470	Cyan	50	180	[205]
122.	1D-Cu_4I_6(*btdmem*)$_2$ (*btdmem* = *N*-((1*H*-Benzo[*d*][1,2,3]triazol-1-yl)methyl)-*N*,*N*-dimethylethanaminium)	2.6	360	550	Green-yellow	25	190	[206]
123.	1D-Cu_4I_6(*bttmp*)$_2$ (*bttmp* = 3-(1H-benzo[d][1,2,3]triazol-1-yl)-*N*,*N*,*N*-trimethylpropan-1-aminium)	2.5	360	562	Yellow	91	240	[67]
124.	1D-Cu_4I_6(*bttmpe*)$_2$	2.45	360	552	Green-yellow	70	235	[206]
125.	1D-Cu_4I_6(*bttme*)$_2$	2.45	360	585	Orange	69	210	[202]
126.	1D-Cu_4I_6(*5-F-bttmp*)$_2$ (*5-F-bttmp* = 3-(5-Fluoro-1*H*-benzo[*d*][1,2,3]triazol-1-yl)-*N*,*N*,*N*-trimethylpropan-1-aminium)	2.2	360	615	Orange-red	53	225	[206]
127.	1D-Cu_4I_6(*5-m-bttmp*)$_2$ (*5-m-bttmp* = 3-(5-Methyl-1*H*-benzo[*d*][1,2,3]triazol-1-yl)-*N*,*N*,*N*-trimethylpropan-1-aminium)	2.45	360	596	Orange-red	85	225	[206]
128.	1D-Cu_4I_6(*5,6-dm-bttmp*)$_2$ (*5,6-dm-bttmp* = 3-(5,6-Dimethyl-1*H*-benzo[*d*][1,2,3]triazol-1-yl)-*N*,*N*,*N*-trimethylpropan-1-aminium)	2.5	360	570	Yellow-orange	68	235	[206]
129.	1D-Cu_4I_6(*bttmmp*)$_2$ (*bttmmp* = 3-(1*H*-Benzo[*d*][1,2,3]triazol-1-yl)-*N*,*N*,*N*,2-tetramethylpropan-1-aminium)	2.4	360	553	Green-yellow	53	211	[206]
130.	2D-Cu_4I_6(*Me-hmta*)$_2$	3.4	300	430	Blue	26	230	[205]
131.	2D-[*Et-hmta*][Cu_4I_6(*Et-hmta*)] · *MeCN* (*MeCN* = methyl cyanide)	2.3	300	570	Yellow	78	105	[205]
132.	0D-Cu_5I_7(^{i}*pr-ted*)$_2$	3.1	360	575	Orange	70	310	[203]
133.	0D-Cu_6I_8(*bu-ted*)$_2$ (*bu* = butyl))	3.0	360	530	Green	90	300	[203]
134.	0D-Cu_6I_8(*btmdb*)$_2$ (*btmdb* = *N*-((1*H*-Benzo[*d*][1,2,3]triazol-1-yl)methyl)-*N*,*N*-dibutylbutan-1-aminium)	2.4	360	540	Green-yellow	70	200	[203]
135.	0D-Cu_6I_8(*L3*)$_2$ (*L3* = 1,3-bis((1*H*-benzo[*d*][1,2,3]triazol-1-yl)methyl)-2-methyl-1*H*-imidazol-3-ium)	2.9	360	550	Yellow	34	230	[56]
136.	1D-Cu_6I_8(*btdmpm*)$_2$ (*btdmpm* = *N*-((1*H*-Benzo[*d*][1,2,3]triazol-1-yl)methyl)-*N*,*N*-dimethylpropan-2-aminium)	2.5	360	650	Red	29	193	[206]
137.	2D-Cu_6I_8(*Pr-hmta*)$_2$(*MeCN*)$_2$	3.5	300	630	Orange-red	56	145	[205]
138.	2D-Cu_6I_8(*L2*)$_2$ (*L2* = 1,3-bis((1*H*-benzo[*d*][1,2,3]triazol-1-yl)methyl)-1*H*-imidazol-3-ium)	2.4	360	610	Orange	21	220	[56]
139.	2D-Cu_6I_8(*L3*)$_2$	2.7	360	560	Yellow	15	240	[56]
140.	1D-Cu_8I_{10}(*bttmb*)$_2$ (*bttmb* = 4-(1*H*-Benzo[*d*][1,2,3]triazol-1-yl)-*N*,*N*,*N*-trimethylbutan-1-aminium)	2.65	360	528	Green	80	245	[206]
141.	2D-Cu_8I_{10}(*Me-hmta*)2(*MeCN*)$_2$	3.3	300	497	Cyan	10	140	[205]

3.1. Hybrid compounds

Self-Trapped Excitonic (STE) Emission: In addition to the low-cost, non-toxic and earth abundant elemental compositions, one of the major advantages of Cu(I) halide hybrids is that the incorporation of organic cations typically result in the formation of low dimensional connectivity of the inorganic anionic structural units.[38] It has been previously shown (e.g., in lead halide

perovskites) that progressive lowering of the structural dimensionality promotes increased charge localization in the structurally isolated metal halide units in low dimensional hybrid organic-inorganic metal halides.[28, 29, 46, 207, 208] In the case of hybrid Cu(I) halides, this increased charge localization results in high exciton binding energies and strong quantum confinement effect in the Cu(I) halide anionic units.[29, 38, 209, 210] In turn, these facilitate the formation of stable excitons and efficient excitonic photoemission at or near room temperature. Hybrid Cu(I) halides are characterized by strong electron-phonon coupling, which is the origin for the commonly documented structural reorganization in their photoexcited states. This reorganization or distortion of the crystal lattice in the excited state trap excitons, eventually leading to their below band gap emission. In literature, this phenomenon has been most commonly referred to as STE-based light emission, which conveniently explains the observed large Stokes shifted low energy broadband emission in hybrid Cu(I) halides (see Fig. 9a and d).[38, 50, 54, 58] Here, the Stokes shift is determined by the energy difference between the maxima of the photoluminescence excitation (PLE) and emission (PL) spectra.[211] Along with the high exciton binding energy values and strong quantum confinement effect, minimal self-absorbance due to the large Stokes shift values are important contributors to the very high PLQYs up to 100% reported for low-dimensional hybrid Cu(I) halides.

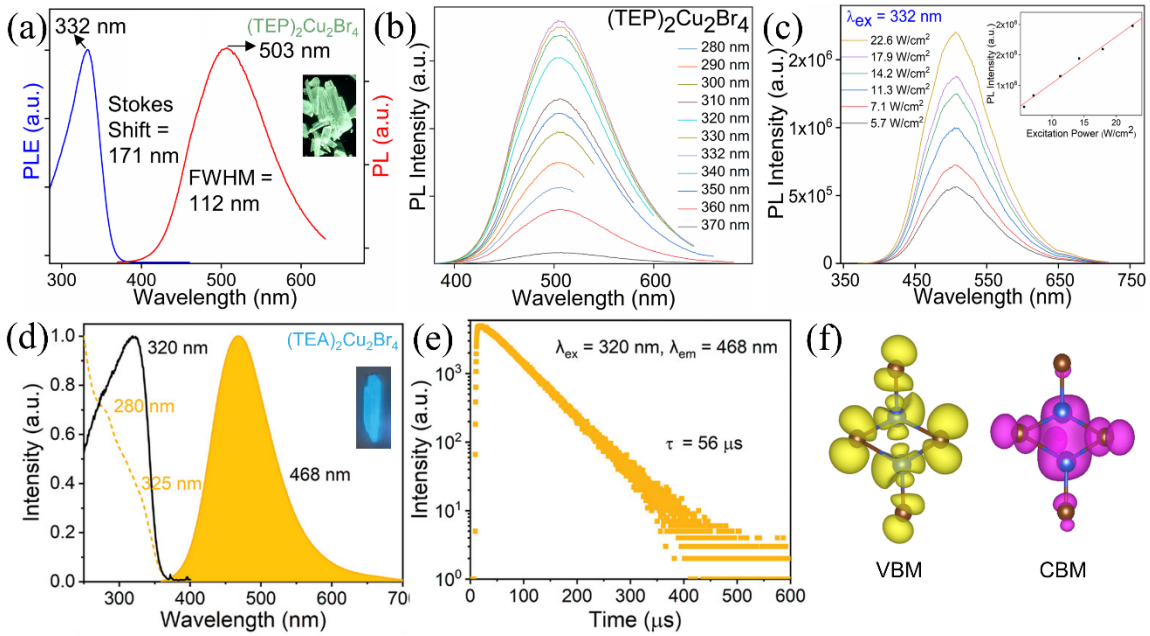

Fig. 9 PL and PLE spectra of (a) $(TEP)_2Cu_2Br_4$ and (d) $(TEA)_2Cu_2Br_4$ at room temperature. Insets show the single crystals of the corresponding compounds under UV irradiation. (b) Excitation-dependent PL spectra of $(TEP)_2Cu_2Br_4$. (c) Power-dependent PL spectra of $(TEP)_2Cu_2Br_4$. Inset shows the corresponding plot of the excitation power vs PL intensity. Reproduced from ref 62. Copyright 2024 John Wiley and Sons. (e) Time-resolved PL spectrum of $(TEA)_2Cu_2Br_4$ crystals at room temperature. Reproduced with permission from ref 75. Copyright 2022 John Wiley and Sons. (f) Partial charge density contours of the hole (yellow) and electron (purple) in the exciton of

$(TEP)_2Cu_2Br_4$. Blue and brown spheres represent copper and bromide, respectively. Reproduced from ref 62. Copyright 2024 John Wiley and Sons.

Multiple strategies have been reported in the literature to ascertain the origin of down-converted low energy emission as STE emission in hybrid Cu(I) halides (see Fig. 9).[38, 58, 75] Firstly, the large Stokes shift values suggest that the emission in these compounds are due to intrinsic trap states below their band gaps. Secondly, the invariable shapes and positions of the PL spectra with different excitation wavelengths in hybrid Cu(I) halides suggest that the emission in these compounds originates from the same excited states (see Fig. 9b for example). As hybrid compounds consist of both organic cationic and inorganic anionic structural motifs, the PL peak position and/or shape would change with different excitation wavelength if the emission were not from the same excited states. Moreover, hybrid compounds where emission originates from organic motifs, multiple peaks and hump features are typically observed in the PL emission spectra just as in the case of the corresponding to the organic components.[44, 212] This behavior is yet to be reported in hybrid Cu(I) halides. Third, if the emission is due to the excitons trapped into permanent defects in the crystal lattice, population of the defect states gradually by increasing the excitation power should lead to a saturation point of the emission intensity. However, in luminescent hybrid Cu(I) halides, the PL intensity demonstrates linear dependency with the excitation power, ruling out the possibility of emission due to permanent defects in these compounds (see Fig. 9c for example). Another supportive evidence of triplet STE-based emission is the observed long PL decay times (usually, tenths or hundreds of microseconds) due to excited state structural reorganization and subsequent phosphorescence in hybrid Cu(I) halides.[38, 213] Finally, transient absorption (TA) spectroscopy studies suggest the formation of a transient midgap state. Altogether, these experimental results complemented with computational studies (see below) are in agreement with the STE-based emission in hybrid Cu(I) halides due to the intrinsic structural deformation of the Cu(I) halide units upon photoexcitation.

The excited state distortion of the Cu(I) halide structural units depends on multiple factors, including the coordination number and geometry of Cu(I) center, crystal packing and rigidity, size and relative orientations of the organic cationic units, etc. Consequently, all these factors influence the trapping depth of STEs, providing handles for a chemist to tune the emission colors of hybrid Cu(I) halides. As a result, the emission color of the hybrid compounds with similar Cu(I) halide clusters can be different primarily depending on the degree of distortions in the photoexcited states and other above-mentioned factors. For example, both $(TEA)_2Cu_2Br_4$ and $(TEP)_2Cu_2Br_4$ consist of dimeric $[Cu_2Br_4]^{2-}$ inorganic structural units and their organic counter-cations possess almost identical structures with four ethyl-substituents on ammonium or phosphonium cationic centers. $(TEA)_2Cu_2Br_4$ and $(TEP)_2Cu_2Br_4$ are efficient light emitters with >90% PLQYs and the origin of emission in both was assigned to STEs localized in the Cu(I) halide units.[62, 75, 122] However, these compounds demonstrate different emission colors with PL at 468 nm (sky-blue emission) for the former and 503 nm (greenish-white emission) for the latter (see Fig. 9a and d).[62, 75] The variation in the emission colors in these two compounds are likely related to the differing trapping depth of excitons and the differing degrees of distortions of the same $[Cu_2Br_4]^{2-}$ anions (see Section 2.1). The difference in the organic cations may result in differing crystal packing and structural

rigidity/softness, which have impact on the distortions of Cu(I) bromide polyhedral units. The differing distortions in turn lead to the energy difference between the STE states of these compounds, resulting in different emission colors.

The above example compares hybrids containing similar size organoammonium and organophosphonium cations. However, even the same class of organic cations, such as quaternary ammonium cations with different sizes and shapes may lead to the formation of identical inorganic anionic structural units. Chen *et al*. reported two hybrid Cu(I) bromides possessing 0D $[Cu_4Br_6]^{2-}$ anions isolated by tetrapropylammonium (TPA) and methyltributylammonium (MTBA) cations in $(TPA)_2Cu_4Br_6$ and $(MTBA)_2Cu_4Br_6$, respectively.[101] $(TPA)_2Cu_4Br_6$ and $(MTBA)_2Cu_4Br_6$ demonstrate orange-red and yellow emissions, respectively, with a PL shift of 39 nm. Besides the degrees of distortions of Cu(I) bromide polyhedra discussed above, the influence of crystal packing and structural rigidity on this PL shift cannot be completely ignored in this case. In this work, the authors provided a comprehensive study of the effect of coordination environment and geometries of Cu(I) centers on the photoemission behavior of the corresponding compounds by gradually changing the chain lengths of the alkyl substituents in six tetraalkylammonium Cu(I) bromides. In addition to the above mentioned two compounds, the utilization of tetramethylammonium (TMA), tetraethylammonium (TEA), tetrapropylammonium (TPA), tetrabutylammonium (TBA) yielded zero-dimensional $(TMA)_3Cu_2Br_5$, $(TEA)_2Cu_2Br_4$, $(TPA)CuBr_2$ and $(TBA)CuBr_2$, respectively (see Fig. 10). High efficiency broadband emission (PLQYs up to 97%) in all six compounds have been attributed to STEs localized on Cu(I) bromide structural motifs (Table 3). The main take away from this study is that emission color tunability within a broad range from blue to orange red can be achieved by engineering the structures of Cu(I) halide units using appropriate organic cations. In addition, another promising finding is that hybrid Cu(I) bromides with similar anionic units may exhibit emission color in very close proximity to each other. This is demonstrated by cyan/green emission in $(TPA)CuBr_2$ and $(TBA)CuBr_2$ containing $[CuBr_2]^-$ units and orange/yellow in $(TPA)_2Cu_4Br_6$ and $(MTBA)_2Cu_4Br_6$ containing $[Cu_4Br_6]^{2-}$ units (Fig. 10). Besides the inclusion of structurally diverse organic cations, substitutions on the halide sites can also bring emission tunability in hybrid Cu(I) halides. Li *et al*. reported almost similar orange-red emission colors with PL_{max} 610 nm and 620 nm for $(PTPP)_2Cu_4Br_6$ (PTPP = pentyltriphenylphosphonium) and $(TPA)_2Cu_4Br_6$, respectively, possessing identical $[Cu_4Br_6]^{2-}$ inorganic units.[81] The substitution of bromide with iodide leads to the formation of similar $[Cu_4I_6]^{2-}$ anions, but the corresponding hybrid $(PTPP)_2Cu_4I_6$ demonstrates unique green emission with PL_{max} of 524 nm. Note that such a strong blue-shift of PL going from a bromide to iodide can be viewed as counter-intuitive if one assumes dominant halide contributions to the states around the band gap (i.e., the top of the valence band) and band-to-band transitions. However, as mentioned above, hybrid Cu(I) halides are midgap STE-based emitters and their electronic structures significantly differ (see electronic structure discussions below) from that of other hybrid metal halides (e.g., hybrid organic-inorganic lead halide perovskites). Another example to support these conclusions, Liang *et al*. showed that by halide alloying in $(TMA)_3Cu_2Br_{5-x}Cl_x$, materials with emission wavelengths from 535 nm (for $(TMA)_3Cu_2Br_5$) to 587 nm (for $(TMA)_3Cu_2Cl_5$) can be obtained, tuning the emission color from green to yellow.[184] Notice that the heavier halide (i.e., bromide) has a more blue-shifted emission in this family as well, which again is unlike the emission trends in halide perovskites but is consistent with the STE emission proposed for hybrid Cu(I) halides. Overall, these reports suggest

the tunability of the STE emission wavelengths in hybrid Cu(I) halides by substitutions on halide sites, as opposed to the all-inorganic Cu(I) halides, where changing halide ions typically results in little to no change to the emission wavelengths within the same crystal structure family.[134, 135]

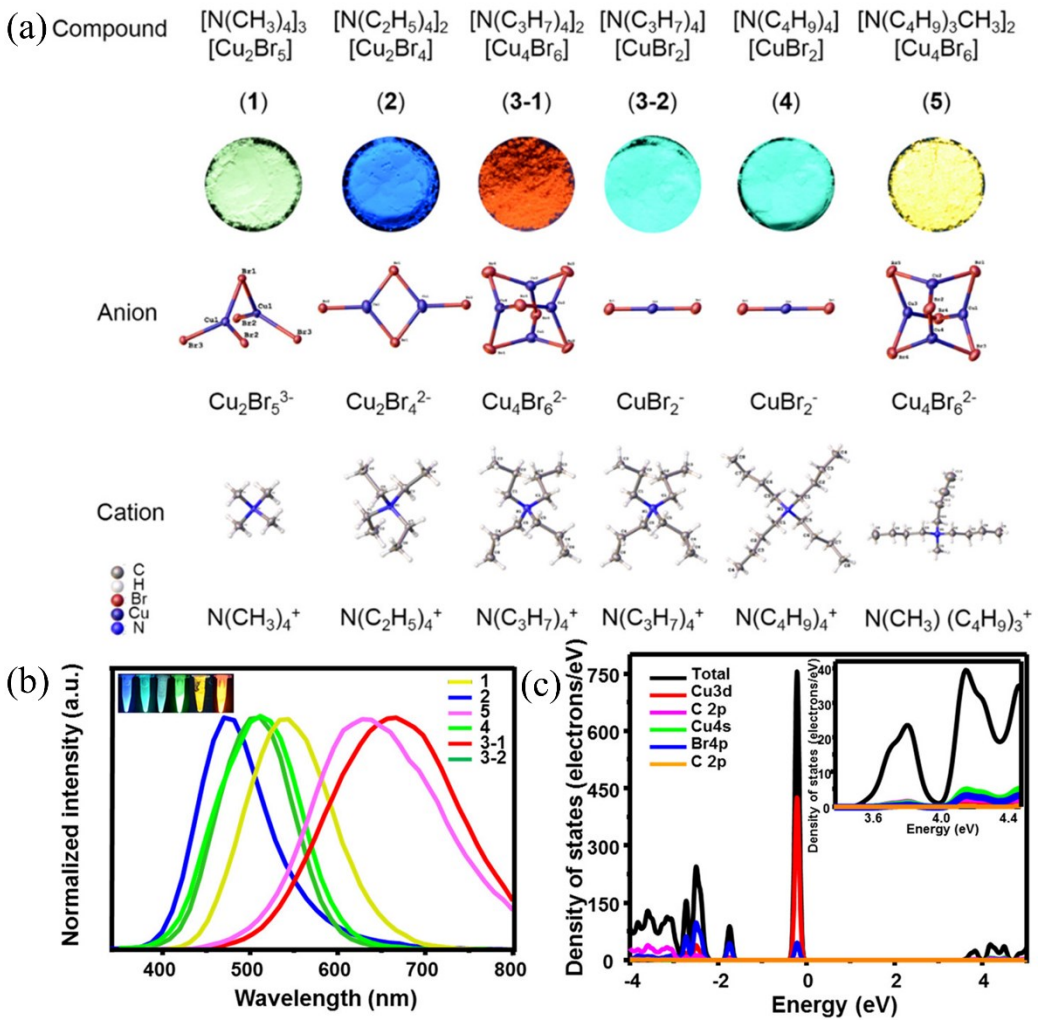

Fig. 10 (a) Powder samples of $(TMA)_3Cu_2Br_5$ (**1**), $(TEA)_2Cu_2Br_4$ (**2**), $(TPA)_2Cu_4Br_6$ (**3-1**), $(TPA)CuBr_2$ (**3-2**), $(TBA)CuBr_2$ (**4**) and $(MTBA)_2Cu_4Br_6$ (**5**) under 254 nm UV light and the anionic and cationic structural motifs of these six compounds. (b) PL spectra of these six tetraalkylammonium compounds cover a broad range of the visible region (blue to orange red). Insets show the powder samples of these compounds under 254 nm UV light. (c) Density of states plot for compound **3-1**. Reproduced with permission from ref 101. Copyright 2019 American Chemical Society.

Table 3 Optical properties of tetraalkylammonium Cu(I) bromides.[101]

Compound	Band gap (eV)	PLE_{max} (nm)	PL_{max} (nm)	Emission color	CIE	QY (%)
$(TMA)_3Cu_2Br_5$ (1)	3.08	315	542	Yellow	0.35, 0.51	91
$(TEA)_2Cu_2Br_4$ (2)	3.09	317	476	Blue	0.18, 0.25	91
$(TPA)_2Cu_4Br_6$ (3-1)	3.01	386	664	Orange-red	0.53, 0.43	97
$(TPA)CuBr_2$ (3-2)	3.13	254	507	Green	0.20, 0.40	83
$(TBA)CuBr_2$ (4)	3.52	254	504	Green	0.22, 0.40	97
$(MTBA)_2Cu_4Br_6$ (5)	2.96	365	623	Yellow	0.50, 0.45	2

The electronic transitions are localized within the Cu(I) halide structural units in hybrid Cu(I) halides as evident from their electronic structures in which dominant contribution of Cu-3*d* and halide *p* orbitals to the top of valence band maxima (VBM) and Cu-4*s* orbitals to conduction band minima (CBM).[38, 75] Occasionally, some halide *p* orbital contributions are mentioned, but the halide influence in hybrid Cu(I) halides is significantly less than hybrid lead halide perovskites, where halogen substitution has a major impact on optoelectronic properties such as their band gaps. Such uniformity of the electronic structures of hybrid Cu(I) halides result in similar optical absorption profiles of these compounds, most of which absorb in the UV range irrespective of the halide used. In fact, the weak tunability of PLE is a recognized challenge in hybrid Cu(I) halides.[38] On the other hand, as mentioned above, their PL emission spectra can be tuned by chemical composition and crystal structure manipulations. In terms of their structures, the highest charge localization is expected for lower dimensional compounds, specifically in 0D and 1D structures. Furthermore, 0D and 1D structures are also more prone to a high degree of structural distortions in the excited states. For these reasons, many families of high efficiency light emitting 0D and 1D Cu(I) halides have been discovered. In comparison, there are very few known 2D and 3D hybrid Cu(I) halides, and their emission efficiencies are typically weaker. For example,$(t\text{-BA})_2Cu_2I_4{\cdot}H_2O$ and $(Bz)_2Cu_2I_4{\cdot}H_2O$ contain 2D networks of Cu(I) iodides, and they exhibit reasonably high PLQYs of 59.4% and 30%, respectively, but these fall short of some hybrid 0-1D Cu(I) halides with PLQYs of 90-100%.[62, 75, 80, 128, 129] Even a more striking example, $(4\text{-bzpy})_2Cu_6I_8$ contains a 3D inorganic network structure composed of CuI_4-tetrahedra, and it is a poor light emitter with PLQY less than 1%. Although photoemission has been assigned to STEs in all these cases, the observed emission efficiencies clearly indicate the importance of crystal structure dimensionality when designing hybrid Cu(I) halide light emitters. The structural dimensionality directly relates to charge localization, concentration quenching effects (i.e., the proximity of optical centers in a crystal lattice) and structural rigidity/deformability. As a rule of thumb, compared to 0-1D structures, 3D structures have higher charge delocalization, close packing of Cu(I) halide emission

centers leading to concentration quenching, and rigid extended Cu(I) halide networks that are less likely to allow structural distortions in the photoexcited states.[90]

The experimental and theoretical results discussed above validate the STE-originated emission in hybrid Cu(I) halides.[38, 62, 81, 82, 84, 106, 107] According to the most commonly cited configurational coordinate diagram model (Fig. 11a), electrons are photoexcited from the ground state of inorganic Cu(I) halide structural units, leaving holes in the ground state. Very large electron-phonon coupling in hybrid Cu(I) halides as evidenced by high Huang-Rhys coupling parameters leads to structural distortions in the excited states,[81, 82, 103, 106] which is accompanied by the relaxation of excited electrons from the initial singlet excited state to a triplet state via intersystem crossing (ISC). Finally, light emission occurs via a radiative recombination of STEs; such broadband emission is characterized by long decay times up to hundreds of microseconds, large Stokes shifts up to 300 nm, and full width at half maximum (FWHM) values up to 125 nm.[82, 94, 103, 184] Although some earlier studies described luminescent Cu(I) halides with singlet STE emission, most hybrid Cu(I) halides show triplet STE emission with long PL decay times.[76, 84, 105, 106, 214]

Triplet Emission: The formation of triplet excited state was further demonstrated by Lenzer and Oum from the excited state dynamics studies on the thin films of $(TEA)_2Cu_2Br_4$ and $(MA)_4Cu_2Br_6$ (MA = methylammonium).[74, 185] However, these researchers make a distinction between "structurally relaxed triplet species" and "STEs", arguing the presence of latter in Cu(I) halides with extended structures such as 1D-$CsCu_2I_3$ but not in 0D hybrid Cu(I) halides. These arguments are not well-justified, and therefore, are not accepted by the larger community; on the contrary, both experimental and computational results for hybrid 0D and 1D halides can be perfectly explained either by arguing the presence of "structurally relaxed triplet species" or STEs, indicating that they are one and the same mechanism. In our view, this is a clear example of confusion in literature when describing the same phenomenon using different terms.

In the studies of Lenzer and Oum, the formation of a long-lived triplet species through ISC has been observed from the femto- to microsecond UV-Vis-NIR transient absorption experiments. In the case of $(TEA)_2Cu_2Br_4$ thin films, after the initial light absorption, the system undergoes vibrational relaxation (1.8 ps) within the S_1 excited state, followed by the ISC (184 ps) from S_1 state to a broadly absorbing triplet state (T_1). This further undergoes slower cooling process in the T_1 state that corresponds to the acoustic phonon relaxation (8.3 ns and 465 ns). Finally, the residuals very slowly decay from T_1 state to S_0, resulting in a microsecond long lifetime (57 μs) (Fig. 11b). This long decay time observed in transient absorption profile is consistent with the 56.5 μs lifetime obtained from the transient PL experiment for the same compound. In fact, these excited state dynamics could have been explained by referring to triplet STEs instead of triplet T_1 state, as the configurational coordinate diagram models for the two match perfectly (Fig. 11). Interestingly, a separate study on $(TEA)_2Cu_2Br_4$ by Liu *et al*. showed only a small difference in lifetime at room temperature and low temperature (52 μs at 300 K and 35 μs at 77K),[106] which safely excludes the possibility of *thermally activated delayed fluorescence* (TADF) processes in these compounds. This is because an increase in temperature should lead to a reduction in the lifetime as the reverse intersystem crossing (RISC) step from T_1 to S_1 should become faster at a higher temperature.[185]

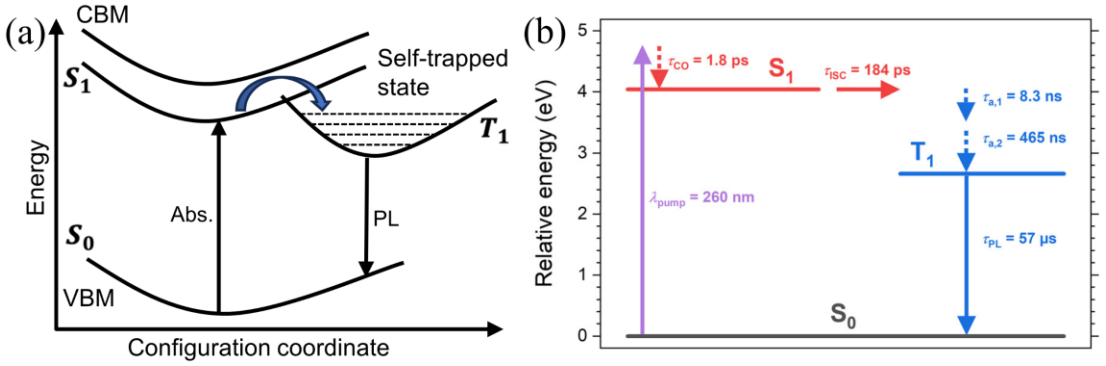

Fig. 11 (a) Simplified configuration coordinate diagram for the formation of STEs. (b) Schematic illustration of the electronic states, relaxation processes, and their respective time constants obtained from the transient absorption measurements on the thin film of $(TEA)_2Cu_2Br_4$ on quartz substrate. Reproduced from ref 185. Copyright 2023 MDPI.

Metal-Centered (MC) and Cluster-Centered (CC) transitions: A few previous reports discussed other possible emission pathways in hybrid Cu(I) halides, including MC and CC transitions. Su *et al*. attributed the room temperature blue emission of $(C_8H_{20}N)_2Cu_2Br_4$ (can also be written as $(TEA)_2Cu_2Br_4$) to an MC transition considering the dominant contribution of Cu(I) 3*d* and 4*s* atomic orbitals in VBM and CBM, respectively.[75] On the other hand, CC transition is mostly proposed for compounds containing multinuclear Cu(I)-halide clusters, in which the Cu···Cu distances are less than the sum of the van der Waals radii of two Cu atoms (2.8 Å). For instance, this applies to hybrid compounds containing $[Cu_4X_6]^{2-}$ and $[Cu_4X_8]^{4-}$ clusters with Cu···Cu distances below 2.8 Å.[62, 76, 81, 82, 107, 171, 215] These shorter Cu···Cu distances indicate the presence of strong metal-metal interactions in these compounds, which is argued to result in CC transitions. One of the characteristic features of PL emission based on MC or CC transition is that PL peak positions shifts slightly lower wavelength with decreasing temperature due to the shrinkage of atomic orbitals in VBM and CBM.[76, 81, 82, 84] Further, this feature is accompanied by the reduction of electron-phonon coupling, resulting in the reduction of full width half maxima (FWHM) of the emission peak at lower temperature compared to room temperature.

However, the proposed MC and CC transitions are in contrast with other publications on similar compounds with STE emission. A recent computational study on luminescent all-inorganic Cu(I) halide $CsCu_2X_3$ suggests that adjacent Cu atoms undergo displacement upon photoexcitation to minimize the energy of the excited electrons; these displacements shorten the Cu···Cu distances due to enhanced mixing between the Cu-4*s* orbitals of close-lying Cu atoms.[216] Consequently, this deformation of the adjacent Cu atoms affects not only the Cu···Cu distances but also the nearby Cu-X bond lengths. Since there are multiple close Cu···Cu distances in the structures of $CsCu_2X_3$, the study suggested the formation of different STEs corresponding to different structural deformations. In the case of $CsCu_2X_3$, the stability of various structural deformations (and hence STE states) depends on the halogen. Similar conclusions were made in a study focused on $Cs_3Cu_2X_5$,[217] which showed a significant decrease in Cu···Cu distances (e.g., 8.6% decrease in $Cs_3Cu_2Cl_5$) in 0D-$Cu_2X_5^{3-}$ anions in their photoexcited states. Corroborating these findings on all-

inorganic Cu(I) halides, another computational study on hybrid Cu(I) halide $(TEP)_2Cu_2Br_4$ revealed that electron clouds are mostly localized around Cu atoms in the excited state (see Fig. 9f).[62] In this case, the Cu···Cu distances in the excited state of $(TEP)_2Cu_2Br_4$ have been shortened by 12% compared to the ground state. This prompts the formation of highly stable STEs at room temperature and midgap emission with near unity PLQY in $(TEP)_2Cu_2Br_4$. Adding to the credibility of these results, the calculated emission energies of high-efficiency light emitting Cu(I) halides are typically in a reasonable agreement with the experimental determined PL peak positions. Altogether, these computational results along with the afore-mentioned spectroscopic evidence support the formation of different energy STEs in hybrid Cu(I) halides. Yet another important conclusion is that in structures with close Cu···Cu distances, the distortions that trap STEs invariably involve the shortening of these distances. Therefore, the optical properties of these types of Cu(I) halides can be influenced by the immediate crystallographic environment of the Cu atoms.

The above examples clearly demonstrate that both MC and CC transitions and STE based emission mechanisms have been proposed for Cu(I) halides with similar structures (e.g., containing close Cu···Cu distances).[76] This raises an important question if these terms all describe the same phenomenon. Since Cu-orbitals dominate the band-edge of the high efficiency luminescent hybrid Cu(I) halides, it is suggested that electron promotes from Cu-3*d* to Cu-4*s* upon photoexcitation, leaving a hole behind.[38] Therefore, the optical transitions are very much localized around Cu(I) centers, i.e., one could say that STEs are localized around metal centers, and as such, there is no difference between the described MC and STE transitions. Yet, we favor the use of STE terminology because embedded in this term are the excited state structural distortion and the subsequent formation of transient midgap state, which naturally has PL characteristics observed in hybrid Cu(I) halides (e.g., large Stokes shift, broad PL due to electron-phonon coupling, etc.). Similarly, CC transition terminology suggests the localization of optical transitions in Cu(I) halide clusters, yet another description, STE localization in the same Cu(I) halide clusters carries more relevant information (e.g., the STE formation involving the shortening of Cu···Cu distances, longer expected lifetimes due to STE formation etc.). Furthermore, the use of MC and CC transition labels for the excited states in the respective configuration coordinate diagrams (Fig. 8) is non-descriptive (consider labeling a state as "cluster-centered" or "metal-centered"), whereas the STE label of the emissive excited state suggests that this transient state is a trapped excitonic state and this is a valid description from a physics perspective.

Energy band alignment and Through-Space Charge-Transfer (TSCT): Besides the above-mentioned factors, energy band alignment plays an important role in the emission efficiency and PL mechanism of hybrid Cu(I) halides. Usually, a high PLQY has been observed in hybrid compounds when they possess Type-I band alignment, where VBM and CBM have major contribution from the same structural units (inorganic units in the case of emissive hybrid Cu(I) halides) (Fig. 12). For instance, the utilization of bulky organic cations TBA^+ and Ph_4P^+ result in the formation of 0D crystal structures in $(Ph_4P)CuX_2$ and $(TBA)CuX_2$, featuring isolated linear $[CuX_2]^-$ units (X = Cl, Br).[91, 94] $(TBA)CuCl_2$ and $(TBA)CuBr_2$ demonstrate bright green and sky-blue emission with high PLQY values (92% and 80%, respectively). Despite having similar anionic structural units, $(Ph_4P)CuCl_2$ and $(Ph_4P)CuBr_2$ exhibit yellowish emission with quenched PL (PLQYs < 1%). This marked difference between the PLQY values of these two families of

compounds cannot be simply explained by the crystal structural differences, rather their electronic structures play an important role in this case. (TBA)CuX_2 possess large bandgaps of >4.0 eV corresponding to the inorganic band gaps.[94] Due to even larger band gaps of the corresponding organic cations containing saturated substituents, organic orbitals do not appear within the inorganic gap. Instead, their VBM are composed of Cu-3*d* orbitals hybridized with X *p* orbitals, while CBM has predominant contribution from Cu-4*s* and X *p* orbitals. On the other hand, states belonging to the aromatic organic Ph_4P^+ cations in (Ph_4P)CuX_2 appear as midgap states within the inorganic gap.[91] This results in a Type-II band alignment in which the organic orbitals are in CBM, while the VBM is primarily originating from the Cu-3*d* and X *p* orbitals. The Type-II band alignment has important consequences for both optical absorption and emission properties of (Ph_4P)CuX_2. Computational work shows that optical transitions between separated organic and inorganic parts yields very small optical matrix elements, which explains the very weak absorption in the lower energy region (~2.6 eV) observed for these materials. The strong optical absorption only occurs at ~4 eV, which corresponds to the inorganic band gaps. To observe any measurable PL, (Ph_4P)CuX_2 must be excited above their respective inorganic band gaps (>4 eV). Upon photoexcitation, the spatial separation of excited electrons and holes in different structural units occurs as the electrons relax to the midgap organic state, which eventually results in quenched PL in (Ph_4P)CuX_2. Another example, $PyCs_3Cu_2Br_6$, which contains pyridinium as the organic cation and isolated trigonal planar $CuBr_3$ inorganic building blocks, is reported to be non-emissive due to the spatial separation of electrons and holes in different structural units.[92]

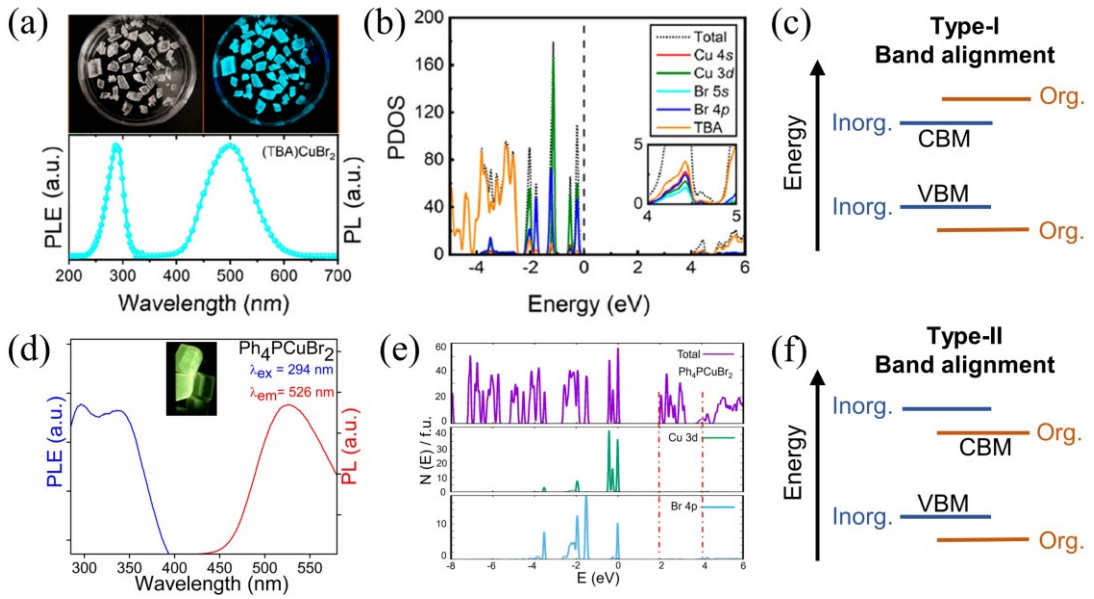

Fig. 12 Photoluminescence excitation (PLE) and emission (PL) spectra of (a) (TBA)$CuBr_2$ and (d) (Ph_4P)$CuBr_2$. Insets show the crystals and emission color under UV excitation. Partial density of states (PDOS) plots for (b) (TBA)$CuBr_2$ and (e) (Ph_4P)$CuBr_2$. Reproduced with permission from ref 94. Copyright 2021 American Chemical Society. Reproduced with permission from ref 91. Copyright 2022 Elsevier. Schematic representations of (c) Type-I and (f) Type-II band alignments.

There are also reports suggesting the possibility of high-efficiency light emission for materials with Type-II band alignment. Lian *et al*. reported that $(C_{16}H_{36}N)CuI_2$ (can be written as $(TBA)CuI_2$ or $(TBA)_2Cu_2I_4$ to provide more structural information), which contains structurally isolated $[Cu_2I_4]^{2-}$ inorganic units, exhibits white emission with PLQY of 54.3%.[115] Although authors assigned the origin of the high efficiency emission in this compound to STEs, they reported that the VBM of this compound is constructed by hybridized Cu-3*d* and I-5*p* orbitals, while CBM has main contribution from the organic orbitals. Considering the energy band alignment patterns of most of the hybrid Cu(I) halide hybrids available in literature, type II band alignment should not lead to high efficiency light emission. Interestingly, two separate works by Zhang *et al*. and Peng *et al*. on the same material report different band structures in which Cu-4*s* and I-5*p* orbitals contribute to the bottom of the conduction band of $(TBA)_2Cu_2I_4$.[111, 116] These results suggesting optical transitions localized on inorganic units are in agreement with the vast majority of publications. These discrepancies in the reported band structures of hybrid Cu(I) halides point to an important issue – the observation of Cu-4*s* orbitals in PDOS plots can be difficult.[80] This is because of multiple factors including the dispersive nature of Cu-4*s* orbitals and their low relative content, e.g., one Cu-4*s* vs five Cu-3*d* orbitals may be shown together in a single plot. The issue is further amplified if one considers the relative ratios of all elements; in the case of $(TBA)_2Cu_2I_4$, one formula unit of this material with the C_{16}:H_{36}:N_1:Cu_1:I_2 formula contains only one Cu-4*s* orbital as compared to much higher orbital contributions from the organic structural part, halogen and even other Cu orbitals (i.e., Cu-3*d*). Therefore, special attention must be given to localization of Cu-4*s* orbitals in the electronic structures of hybrid Cu(I) halides for the accurate description of their photophysical properties.

$(TBA)_2Cu_2I_4$ is not the only compound for which conflicting band structures have been reported. A similar example is the case of $Gua_3Cu_2I_5$ (or β-$Gua_3Cu_2I_5$), which has a yellowish emission with high PLQY of ~80%.[80, 83] Wu *et al*. proposed the involvement of metal-to-ligand charge transfer (M/XLCT) from inorganic anions to the organic cations based on their computational results showing a Type-II band alignment, i.e., dominant contributions of halide and organic cations in CBM of this compound with VBM originating from the inorganic structural unit.[83] In contrast, Song *et al*. reported that the main contributors to CBM of $Gua_3Cu_2I_5$ are the Cu-4*s* orbitals overlapped with the atomic orbitals of iodide, which then suggests a charge transfer within the inorganic units.[80] Based on the reviewed literature, the description of the electronic structure of $Gua_3Cu_2I_5$ by Song *et al*. is more likely to be accurate. Nevertheless, this example once again shows that extra attention is needed to correctly assign the atomic orbital contributions in VBM and CBM in hybrid Cu(I) halides.

As a thought experiment, if we were to accept that high-efficiency light emission can also occur in materials with Type-II band alignments where the charges are on separate structural units, an important question arises – what would be the photoemission mechanism in this case? This important question is not satisfactorily answered even in the publications claiming efficient optical processes in materials with Type-II band alignments. One other such example concerns $(C_9H_{15}N_2)_2Cu_4I_6$ ($C_9H_{15}N_2^+$ = 4-dimethylamino-1-ethylpyridinium) containing 1D-$[Cu_4I_6]^{2-}$ chains; this material possesses a Type-II energy band alignment with sole contribution of organic atomic orbitals in CBM. This compound is reported to demonstrate bright yellow emission with a high PLQY value of 99%.[89] Considering the fact that there is no direct bonding between the anionic inorganic units and cationic organic motifs, the authors suggested *Through-Space Charge-Transfer* (TSCT) as a possible mechanism of electronic transitions in this compound. In literature, typical TSCT materials require π-conjugated organic molecules allowing donor and acceptor to be placed

in close proximity.[218-221] In this case, direct orbital overlaps through space, not electrons moving in empty space, promote electronic transitions. However, the applicability of TSCT in Cu(I) halide hybrids is quite unlikely for structurally isolated ionic structural parts. On the contrary, almost every example of a high-efficiency light emitting Cu(I) halide with a Type-II band alignment, upon a closer inspection (see the examples above), shows a Type-I band alignment with inorganic structural parts dominating VBM and CBM. While follow-up studies on $(C_9H_{15}N_2)_2Cu_4I_6$ have not yet been reported, the claim of efficient TSCT process that results in high PLQY value of 99% demands further evidence.

3.2. Coordination compounds

Metal-to-Ligand Charge Transfer (MLCT) and Halide-to-Ligand Charge Transfer (XLCT): Generally, luminescent coordination Cu(I) halides are strong absorbers demonstrating broad absorption spectra.[59, 182, 222] Computational studies of these compounds reveal that the VBM of these compounds are usually composed of inorganic orbitals (i.e., Cu-3*d* and X-*p*), while the CBM comes from the ligand's lowest unoccupied molecular orbitals (LUMO) (Fig. 13a). Note that this kind of electronic structure should not be described as an example of a Type-II band alignment, because such classification of the energy band alignments was originally developed for semiconductor heterojunctions (e.g., two layers of interfacing semiconductors).[29, 223] In the case of coordination Cu(I) halides, the organic ligands are not spatially separated from the inorganic Cu(I) halide modules, and electronic transitions can occur within the same molecular unit that contains both. The described electronic structure above suggests MLCT and XLCT as dominant absorption pathways in the compounds where metal halide core is directly bonded to ligands.[59, 61, 69, 142] Therefore, in addition to the modifications of the inorganic structural motifs, the choice of suitable ligands directly influences the optical properties of this class of compounds. This is in stark contrast to optical transitions centered around Cu(I) metal in light emitting hybrid organic-inorganic compounds. As a result, significant research efforts in the field of coordination Cu(I) halides have focused on the exploration of organic ligands of varying shapes and energy band alignments. For instance, Lv *et al*. reported orange-to-red broadband emissions in three 0D monomeric Cu(I) iodides coordinated with *tpp* and phenanthroline derivative ligands having electron withdrawing and donating groups in the latter.[140] Although the substituents on the ligands have negligible impact on the structures of the resultant Cu(I) iodides, the compounds containing electron donating groups exhibit comparatively higher bandgap and subsequently, high energy emission in contrast to the compounds with electron withdrawing substituents. In a separate study directed by theoretical calculations, it was shown that a series of ligands with different LUMO energies indeed yield 1D-CuI(*L*) compounds with bandgaps corresponding to the calculated LUMO energies (see Table 4 and Fig. 13b – c).[157] Although emission color can be tuned by the choice of ligands, PLQY values of the resulting coordination Cu(I) iodides are limited to 3% – 37% under UV excitation (365 nm). This study suggests that the rational design of ligands can precisely modulate and tune the emission energies and color (from blue to orange red) of the luminescent coordination Cu(I) halides possessing the same inorganic modules. Such a wide range emission color tunability is very unlikely in the case of luminescent hybrid Cu(I) halides, where emission color is mostly regulated by the structurally isolated inorganic units and their

deformations in the excited states (i.e., the same inorganic unit is unlikely to produce tunability across the visible spectrum). Indeed, while the choice of the organic cation used for the construction of a hybrid Cu(I) halide has an indirect influence (e.g., via the structural rigidity of the resultant crystal lattice), comparable systematic shifts of emission spectra has not been reported to date. Furthermore, even in the case of hybrid Cu(I) halides possessing Type-II band alignment, the structural separation of the inorganic anions and organic cations renders optical transitions ineffective, resulting in quenched PL but not MLCT, LMCT or XLCT.

Table 4 Optical properties of selected 1D-CuI(*L*) compounds.[157]

Compound	Band gap (eV)	PL_{max} (nm)	Emission color	CIE	QY (%)	LUMO (eV)
1D-CuI(4-*pc*) (**1**)	3.2	433	Blue	0.20, 0.15	35.8	-0.96
1D-CuI(3-*pc*) (**3**)	3.0	469	Blue	0.19, 0.22	37.2	-1.07
1D-CuI(*py*) (**4**)	2.9	475	Sky-blue	0.20, 0.29	29.1	-1.12
1D-CuI(2-*et*-3-*me*-*pz*) (**6**)	2.6	490	Cyan	0.23, 0.40	32.4	-1.49
1D-CuI(2,6-*dm*-*pz*) (**7**)	2.4	525	Green	0.35, 0.55	15.4	-1.61
1D-CuI(5-Br-*pm*) (**8**)	2.3	545	Yellow	0.46, 0.52	13.1	-1.97
1D-CuI(2-*cy*-*pz*) (**9**)	2.2	618	Orange	0.55, 0.38	10.1	-2.80
1D-CuI(4-*ac*-*py*) (**10**)	2.0	680	Orange	-	-	-

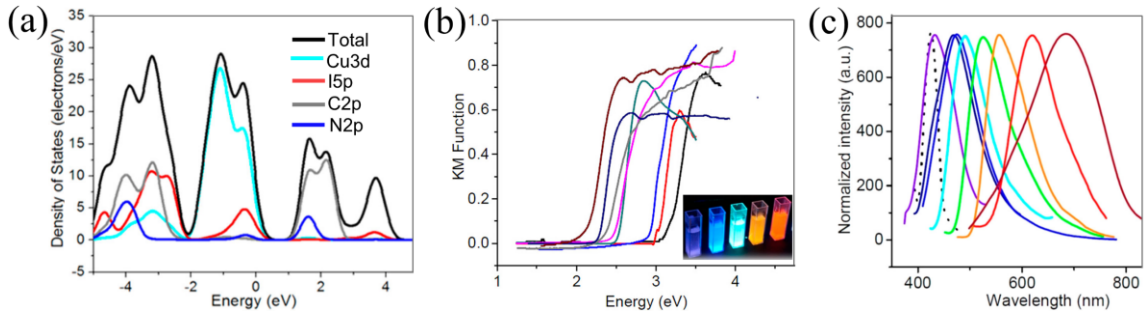

Fig. 13 (a) Density of states (DOS) of 1D-CuI(*py*) (**4**). (b) Optical absorption spectra of selected 1D-CuI(*L*) compounds: (black) **1**; (red) **3**; (blue) **4**; (green) **6**; (pink) **7**; (gray) **8**; (dark blue) **9**; (brown) **10**. Inset shows the solution of selected 1D-CuI(*L*) compounds under 365 nm UV light (from left to right: **1**, **3**, **6**, **8**, **9**). (c) Emission spectra of CuI and selected 1D-CuI(*L*) compounds excited at 365 nm: (dotted black) bulk CuI, (purple) **1**; (dark blue) **3**; (blue) **4**; (cyan) **6**; (green) **7**;

(orange) **8**; (red) **9**; (brown) **10**. Reproduced with permission from ref 157. Copyright 2014 American Chemical Society.

Interestingly, similar trends in the electronic properties and band structures have been observed in the case of coordination compounds containing dimeric Cu_2X_2 core coordinated with select ligands of targeted LUMO energies.[69] Full visible spectrum tunability of the emission color (from blue to red) in these compounds can be achieved by utilizing suitable ligands. MLCT and/or XLCT have been used to explain the excited state dynamics and dominant emission pathways in these compounds.[224, 225] These further support the influence of organic ligands on the emission properties of coordination Cu(I) halides irrespective of the types of inorganic cores. The μs range lifetimes indicate phosphorescence in these compounds. Moreover, PL quantum yield exceeds over 70% in these dimeric Cu_2X_2-based compounds. In general, higher PLQYs have been observed in 0D molecular clusters such as in monomeric, dimeric and tetrameric Cu(I) compounds compared to the coordination Cu(I) halides with extended structures like 1D chains and 2D sheets. The higher charge localizations in the 0D cluster structures and reduced non-radiative recombination pathways result in high PLQYs in these compounds. Therefore, observed emission efficiency trend can be expressed as $CuX < Cu_2X_2 < Cu_4X_4$ for compounds containing these respective structural units (see section 2.2).[59]

Table 5 Optical properties of selected $Cu_4I_4(L)_4$ compounds.[183]

Compound	Band gap (eV)	PL_{max} (nm)	Emission color	QY (%)
0D-Cu_4I_4(3-*pc*)$_4$	2.8	560	Yellow	94.3
1D-Cu_4I_4(*bbipe*)$_2$	2.7	560	Yellow	71.8
2D-Cu_4I_4(*dipe*)$_2$	2.8	620	Orange	64.4
2D-Cu_4I_4(*bmbipe*)$_2$	2.7	550	Yellow	67.1
3D-Cu_4I_4(1,4-*bda*)$_2$	3.1	585	Yellow	60.7
3D-Cu_4I_4(*dipe*)$_2$	2.9	580	Yellow	65.6

Cluster-Centered (CC) emission: Among the luminescent coordination Cu(I) halides, Cu_4I_4-compounds have been extensively studied in literature due to their rich photophysical properties. These compounds generally exhibit high PLQY values which was attributed to the high charge localizations in these clusters and suppressed thermal quenching effect.[70, 226, 227] Previous studies reported the origin of the high efficiency low-energy emission in these compounds as the CC

emission. In such compounds, the excited state involves electronic delocalization over the metal (Cu_4) core and the term "cluster-centered" was originally coined to highlight this fact.[70] We will discuss more experimental evidence from literature that supports the existence of CC-type emissions in coordination multinuclear Cu(I) halides with short Cu···Cu distances in the following section. As mentioned in the structural discussion section, the Cu_4I_4-cubane structures usually maintain a Cu···Cu distance below the sum of the van der Waals radii of two Cu-atoms (2.8 Å). These shorter Cu···Cu distances suggest the existence of metal-metal interactions in these compounds. In comparison, Cu_4Cl_4-cubane analogues possessing higher Cu···Cu distances than 2.8 Å demonstrate moderate to little emission.[228] Moreover, the room temperature emission energies in the Cu_4I_4-cubane structures are determined by the inorganic core and they exhibit characteristic yellow-orange emissions (see Table 5 and Fig. 14c) (under 360 nm excitation).[183] These observations further support the existence of CC-type emission in different types of Cu_4I_4-cubane containing compounds. Notable examples include CC emissions in Cu_4I_4-cubane compounds possessing aliphatic ligands (e.g., 3D-Cu_4I_4(1,4-*bda*)$_2$, 3D-Cu_4I_4(*en*)$_2$; *bda* = butanediamine, *en* = ethylenediamine).[183] Ligands in these compounds have negligible influence on PL as the VBM and CBM are found to be predominantly arising from the inorganic cores (Fig. 14b).

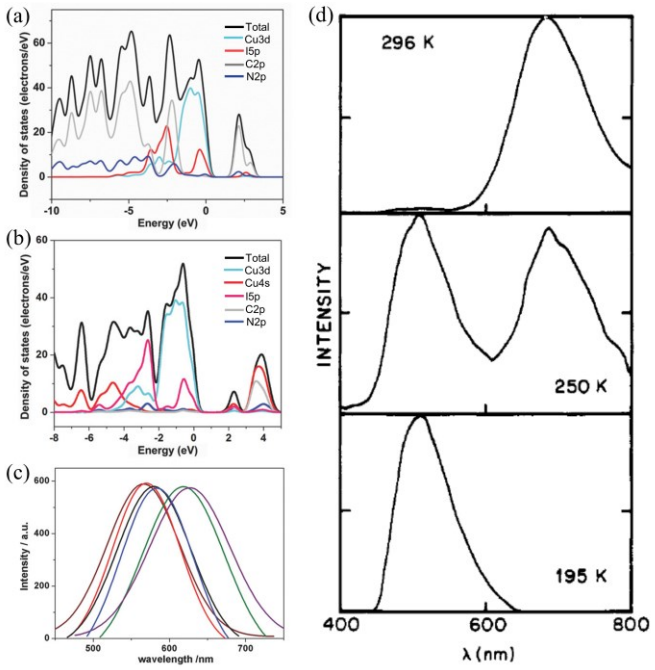

Fig. 14 (a) Density of states (DOS) of 1D-Cu_4I_4(*bbipe*)$_2$. (b) DOS of 3D-Cu_4I_4(1,4-*bda*)$_2$. (c) Room temperature photoluminescence emission spectra of selected compounds excited at 360 nm: 0D-Cu_4I_4(3-*pc*)$_4$ (wine), 1D-Cu_4I_4(*bbipe*)$_2$ (red), 2D-Cu_4I_4(*dipe*)$_2$ (green), 2D-Cu_4I_4(*bmbipe*)$_2$ (black), 3D-Cu_4I_4(1,4-*bda*)$_2$ (purple), 3D-Cu_4I_4(*dipe*)$_2$ (blue). *dipe* = 1,5-di(1H-imidazol-1-yl)pentane, *bbipe* = 1,5-bis(1H-benzo[d]imidazol-1-yl)pentane, *ph-py* = phenyl pyridine. Reproduced with permission from ref 183. Copyright 2016 John Wiley and Sons. (d) Photoluminescence spectra of 0D-Cu_4I_4(4-*ph-py*)$_4$ in toluene solution at 296 K (top), 250 K (middle), 195 K (bottom). Reproduced with permission from ref 172. Copyright 1991 American Chemical Society.

The electronic structures of Cu_4I_4-cubane containing compounds can be adjusted by using appropriate ligands. For instance, compounds containing Cu_4I_4-cubane cores and aromatic ligands (e.g., 3D-Cu_4I_4(*dipe*)$_2$, 2D-Cu_4I_4(*dipe*)$_2$, 1D-Cu_4I_4(*bbipe*)$_2$, 0D-Cu_4I_4(4-*ph-py*)$_4$; *dipe* = 1,5-di(1H-imidazol-1-yl)pentane, *bbipe* = 1,5-bis(1H-benzo[d]imidazol-1-yl)pentane, *ph-py* = phenyl pyridine) have electronic structures, PDOS and emission characteristics that resemble that of coordination compounds for which MLCT/XLCT was proposed.[183] Several important conclusions can be made for this series: first, 0D-Cu_4I_4(L)$_4$ exhibits the highest PLQY, which can be attributed to a higher charge localization in this compound. Second, Cu_4I_4(L)$_4$ compounds containing 2D sheets and 3D networks exhibit higher emission efficiency (~ 60% – 95%) (see Table 5 and Fig. 15a – c) compared to those with extended networks of CuI (e.g., Table 4 and Fig. 7a). The latter compounds contain extended pure inorganic Cu-I bonded networks in which charges can be delocalized, whereas Cu_4I_4(L)$_4$ compounds exhibit 2D and 3D connectivity via Cu_4I_4–L bonds. Importantly, these observations support the idea that although the cluster and ligand connectivity can be extended (2D or 3D), there is a strong charge localization in the Cu_4I_4 cores leading to a CC-type bright emission in Cu_4I_4(L)$_4$ at room temperature. Such high efficiency emission is unlikely to occur if there was a charge transfer between organic and inorganic motifs and delocalization of charges over the extended networks of Cu_4I_4(L)$_4$ compounds. Finally, Cu_4I_4-cubane compounds containing both aromatic and aliphatic ligands emit in a narrow yellow-orange range irrespective of the change in their electronic structure. This further supports the assignment of photoemission to the inorganic Cu_4I_4 cores.

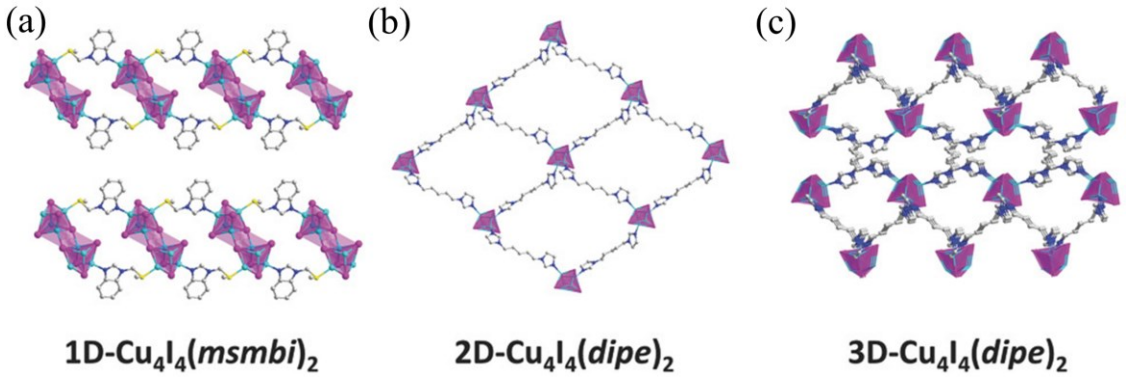

Fig. 15 Structures of select Cu_4I_4(L)$_4$ compounds: (a) 1D-Cu_4I_4(msmbi)$_2$, (b) 2D-Cu_4I_4(dipe)$_2$, and (c) 3D-Cu_4I_4(dipe)$_2$. msmbi = 1-((methylthio)methyl)-1H-benzo[d]imidazole. Cyan, purple, blue, yellow and grey spheres represent copper, iodide, nitrogen, sulfur, and carbon, respectively. Reproduced with permission from ref 183. Copyright 2016 John Wiley and Sons.

To get a deeper understanding of the literature reported results, we carefully compared the DOS plots of 1D-Cu_4I_4(*bbipe*)$_2$ and 3D-Cu_4I_4(1,4-*bda*)$_2$. According to our observations, the orbital contributions of organic and inorganic structural motifs are very close in energy in the lower conduction band (Fig. 14a), while they are further apart in the 1D-CuI compounds (Table 4) exhibiting lower emission efficiency (Fig. 13a). This is likely because a larger overlap of Cu-I orbitals in the Cu_4I_4-clusters lowers the band gap of the inorganic core sufficiently to appear in

CBM. Consequently, while VBMs are dominated by the inorganic orbitals, CBMs have contributions from both inorganic and organic structural parts of $Cu_4I_4(L)_4$ compounds.[183] In this scenario, although some charge transfer between the organic and inorganic motifs is possible due to their direct coordination/covalent bonding and strong presence of organic states in CBM, CC transition within the Cu_4I_4 core is the prominent pathway due to proximity. The proximity of inorganic states to the top of VBM and the bottom of CBM, and proximity of Cu and I atoms to each other within the Cu_4I_4 cluster makes the electronic transitions within the same structural units more favorable. Moreover, the preferred localization of charges inside the inorganic clusters explains the very high efficiency of $Cu_4I_4(L)_4$ compounds with 2D and 3D structural networks, i.e., metal halide cores can act like 0D molecular clusters even in an extended network structure.[59, 183] In comparison, hybrid Cu(I) halides possessing extended networks (e.g., pure inorganic 2D and 3D frameworks) suffer from poor emission efficiency most likely due to charge delocalization, and high structural rigidity and lack of structural deformability that prevent the effective formation of STEs (see section 3.1).

The $Cu_4I_4(L)_4$ compounds often exhibit two distinct emission peaks at room temperature with different emission lifetimes. The reported μs lifetimes of both emission bands suggest phosphorescence involving triplet excited state dynamics in these compounds. The strong room temperature low-energy (LE) emission band is assigned to a CC emission, while the weaker high-energy (HE) emission band is assigned to MLCT and/or XLCT.[224, 225, 229-234] The CC transition prompts structural distortions lowering the energy of the excited states, hence generate low energy emission.[235] In support of this hypothesis, several studies on luminescent $Cu_4I_4(L)_4$ compounds by Hardt and Holt and their co-workers demonstrated that the compounds possessing longer Cu···Cu distances than the sum of the van der Waals radii of two Cu-atoms demonstrate little to no emission in the low energy region.[236-238] Considering these results, the assignment of LE emission as CC-type seems to be reasonable. Furthermore, the relative intensities of these two emission bands vary depending on the temperature, such as in the case of $Cu_4I_4(L)_4$ containing pyridine derivatives as ligands (Fig. 14d).[70, 172] The changing relative intensities of two emission bands at different temperatures appear as variable emission colors to naked eyes. Therefore, luminescence thermochromism is a common feature in these compounds. The HE band becomes prominent at low temperatures and the LE is shifted to lower wavelength. At temperatures below 80 K, the HE often becomes the prominent emission band and demonstrates longer lifetime. This effect also depend on the excitation energy, specifically at low temperatures.[239] For instance, in two consecutive studies by Vogler and Kyle, both LE and HE emission bands have been observed in $Cu_4I_4(py)_4$ containing an aromatic amine cluster, with the LE band being more prominent at low temperatures.[172, 235] However, only an LE band was observed at all temperatures in the PL emission spectra of Cu_4I_4(morpholine)$_4$ containing an aliphatic amine cluster. The LE band for Cu_4I_4(morpholine)$_4$ appears in the similar region to that of $Cu_4I_4(py)_4$ under same experimental conditions. Based on these results, Vogler *et al*. proposed CC transitions as the origin of the LE band, because the electronic structure of saturated aliphatic ligand containing compounds is dominated by the states arising from the inorganic Cu_4I_4 core and this excludes the possibility of MLCT/XLCT.[172, 235] The fact that the intensity of LE band becomes weaker at low temperatures can be explained by the lack of sufficient thermal energy for the excited state distortions of the clusters. On the other hand, the high sensitivity of the HE bands on the choice of ligands among aromatic amine clusters was observed in the study by Kyle *et al*.; this indicates that the HE band is associated with the charge transfer between the organic and inorganic motifs.[172] In a separate study by Radjaipour *et al*., the HE bands at 15 K demonstrates some vibronic features similar to

that of the ligands.[239] This finding further confirms that the HE band is associated to the electronic transitions related to ligands. It can be argued whether this transition is MLCT, LMCT, XLCT or (M + X)LCT, or in fact transitions purely localized on the organic ligands.

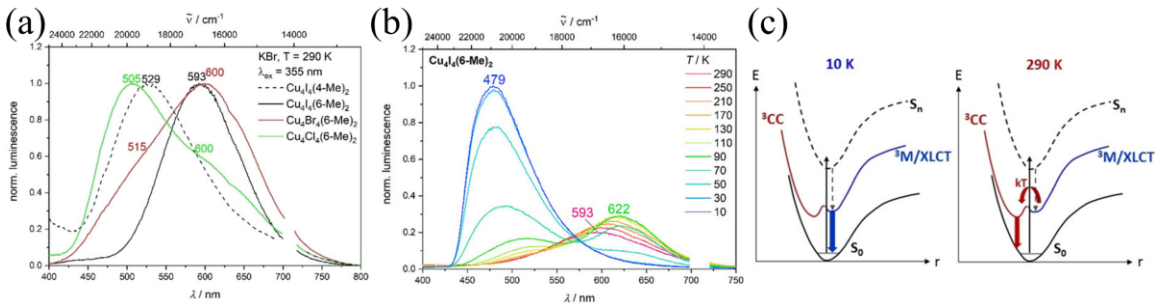

Fig. 16 (a) Photoluminescence emission spectra of Cu_4I_4(**4-Me**)$_2$, Cu_4I_4(**6-Me**)$_2$, Cu_4Br_4(**6-Me**)$_2$, Cu_4Cl_4(**6-Me**)$_2$ at 290 K excited at 355 nm (where **6-Me** = 2-(diphenylphosphino)pyridine). (b) Temperature dependent emission spectra of Cu_4I_4(**6-Me**)$_2$ recorded in the temperature range 10 K – 290 K. (C) Simplified energy diagram of the complex Cu_4X_4(**6-Me**)$_2$, where blue emission associated with M/XLCT at 10 K (left) and red emission associated with CC at 290 K (right) are represented. Reproduced with permission from ref 186. Copyright 2020 John Wiley and Sons.

A recent study by Boden *et al*. can also be discussed in this context. The authors carried out a detailed study on the optical and electronic properties of a series of Cu_4X_4 (X = Cl, Br, I) cluster compounds possessing 2-(diphenylphosphino)pyridine (**6-Me**) as a bridging ligand, where the pyridine ring contains a methyl substituent in *ortho*-position.[186] Interestingly, Cu_4I_4(**6-Me**)$_2$ exhibits LE emission band around 600 nm at 290 K, while the HE band (479 nm) appears at low temperatures (Fig. 16a – b). The bromide analog demonstrates a prominent LE band with an HE shoulder band at 290 K. On the other hand, the chloride analog shows opposite trend, a prominent HE band with an LE shoulder band at 290 K. At 10 K, only the HE band observed for all three compounds. Notably, Cu···Cu distances in Cu_4I_4(**6-Me**)$_2$ ranges from 2.66 – 2.78 Å and for Cu_4Cl_4(**6-Me**)$_2$ ranges from 2.77 – 2.92 Å with bromide analogous in between these values. These values align well with the required distances for metal-metal interactions (below 2.8 Å). Moreover, the expected stronger Cu···Cu interactions in Cu_4I_4(**6-Me**)$_2$ can be the origin of the prominent LE emission band at 290 K and the intensity of LE band is reduced with decreasing metal-metal interactions in Cu_4Cl_4(**6-Me**)$_2$. In agreement with these observations, the investigation of the structures of excited triplet states by time dependent (TD) DFT calculations revealed that the lowest energy triplet state has charge localization in the inorganic core, whereas charge carriers are concentrated on the organic motifs in the second lowest energy triplet state. These observations agreed well with literature confirming the existence of two separate emissive states, low energy CC and higher energy M/XLCT triplet states in this series of coordination Cu(I) halides. As shown in Fig. 16c, the high energy M/XLCT triplet state of Cu_4X_4(**6-Me**)$_2$ is populated initially followed by its thermal depopulation, and conversely, thermal population of the low energy CC triplet state .[186] The energy barrier between these two excited triplet states increases from iodide to bromide to chloride. High energy band is exclusively observed for all three compounds at 10 K due to insufficient thermal energy to overcome this barrier at this temperature. To summarize, the CC based emission involves excited state deformations of the Cu-halide clusters; probably due to the

lack of sufficient energy for structural deformation and weak electron-phonon coupling at low temperature results in the quenched CC emission (the LE band). Finally, the observed trends in PLQY values, 33%, 65%, 93% recorded for Cu_4Cl_4(**6-Me**)$_2$, Cu_4Br_4(**6-Me**)$_2$ and Cu_4I_4(**6-Me**)$_2$, respectively, suggest that the highest PLQY values can be achieved when charge transfer occurs within the same inorganic Cu_4X_4 cores.

As is clear from this depiction and the schematic diagram provided in Fig. 16c, the photophysics of Cu_4X_4(**6-Me**)$_2$ could have also been explained by referring to STEs localized on the Cu_4X_4 cores (i.e., CC transitions) leading to LE emission, and a higher energy MLCT-type transitions leading to HE emission. However, further evidence is needed to confirm this conclusion. Although similar dual or multi-band emissions have been observed in some hybrid Cu(I) halides (e.g., those containing $[Cu_4X_6]^{2-}$ anionic clusters) at low temperatures, these multiple peaks are typically assigned to multiple STE states within inorganic units that are stabilized by different structural distortions at different temperatures or phase transitions stabilizing different STEs at low temperatures.[76, 82, 95, 111] Photoemission in hybrid compounds at all temperatures largely relies on the inorganic structural units and is insensitive to aliphatic or aromatic organic cations. For instance, Li *et al*. reported that two hybrid compounds containing aliphatic TPA and aromatic PTPP cations and $[Cu_4Br_6]^{2-}$ anions demonstrate similar orange red emissions within the temperature range 80 K to 300 K.[81] These results confirm little to no impact of the organic cations on the emission behavior of the hybrid Cu(I) halides possessing same inorganic anionic units. On the other hand, the sensitivity of the HE band on the choice of ligands in $Cu_4I_4(L)_4$ is a clear indication of the direct contributions of organic ligands in the photoemission properties of these materials. Nevertheless, further research is warranted to probe the possibility of emission in $Cu_4I_4(L)_4$ compounds due to free excitons (akin to band-to-band transitions), defect-bound excitons (DBEs), multiple kinds of STEs that are stabilized by different structural distortions at different temperatures etc.[38, 76, 82, 95, 111] To date, these possible scenarios have not been seriously considered for coordination Cu(I) halides.

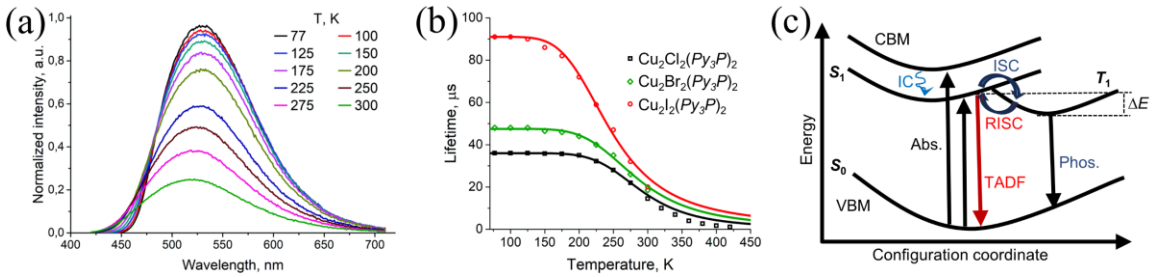

Fig. 17 (a) Temperature dependent photoluminescence emission spectra of $Cu_2I_2(Py_3P)_2$ excited at 360 nm. (b) Comparison of temperature dependent lifetimes of $Cu_2Cl_2(Py_3P)_2$, $Cu_2Br_2(Py_3P)_2$ and $Cu_2I_2(Py_3P)_2$. Reproduced from ref 182. Copyright 2020 Royal Society of Chemistry. (c) A simplified energy diagram of TADF accompanied by phosphorescence process.

Thermally Activated Delayed Fluorescence (TADF): There are dedicated review articles covering TADF in Cu(I) complexes.[240, 241] Here, we will briefly cover the materials parameters that enable TADF as an emission pathway with a few examples of reported cases. The Cu(I) halides with MLCT transitions can exhibit a configuration coordinate diagram (Fig. 8f) in which there is

only a small energy difference between the lowest singlet S_1 and triplet T_1 state. In these circumstances, TADF can be another radiative decay pathway. Upon photoexcitation ($S_0 \rightarrow S_1$) at very low temperatures, such systems may undergo ISC to the T_1 state and show long-lived phosphorescence ($T_1 \rightarrow S_0$); however, at elevated temperatures, the singlet excited S_1 state can be re-populated via reverse inter system crossing (RISC) to prompt eventual emission from the higher energy singlet state ($S_1 \rightarrow S_0$). The preceding ISC and RISC steps, which add to the long lifetime of this radiative process, and the thermal activation of this emission are the reasons for the name of this mechanism, *thermally activated delayed fluorescence* (TADF). The temperature at which the transition to TADF occurs will depend on the energy separation between the lowest singlet S_1 and triplet T_1 states, $\Delta E(S_1–T_1)$. Although, detection of TADF has been reported for materials with $\Delta E(S_1–T_1)$ as large as 10 kcal/mol (≈3500 cm^{-1}; ≈0.43 eV), this separation should be as small as possible for optimized TADF emissions. For reference, $\Delta E(S_1–T_1)$ value below 10^3 cm^{-1} (120 meV) is cited for efficient TADF. Coordination Cu(I) halides with small spatial HOMO–LUMO overlap, which ensures the spatial separation of holes and electrons, can achieve much lower $\Delta E(S_1–T_1)$ values below 300 cm^{-1} (≈37 meV), leading to relative short TADF lifetimes (<5 μs).

As an example, Cu(I) halides containing 0D-Cu_2X_2 (X = Cl, Br, I) complexes and tris(2-pyridyl)phosphine (Py_3P) ligands are reported to exhibit TADF emissions. TDDFT calculations on these compounds revealed only one triplet state.[182] In this case, the metallophilic interactions can simply be ignored as the Cu···Cu distances are more than 3.6 Å for all three compounds. Baranov *et al*. reported that both triplet T_1 and lowest singlet S_1 excited states in these compounds possess charge density in the organic motifs, while the VBM still has dominant contribution from the inorganic core.[182] Therefore, the authors of the study suggested (M + X)LCT as the emission pathways in these compounds. The energy differences (ΔE) between S_1 and T_1 for all three compounds are obtained below 1500 cm^{-1}, which is within the required thermal activation energy barrier for reverse inter system crossing (RISC) to prompt TADF.[240, 241] Notably, the ΔE value follows a trend in the order of $Cu_2Cl_2(Py_3P)_2$ > $Cu_2Br_2(Py_3P)_2$ > $Cu_2I_2(Py_3P)_2$. At room temperature, all three compounds demonstrate broad emission peaks with PLQYs around 53% and lifetimes of 14.5, 18.3, and 20.0 μs for chloride, bromide and iodide analogs, respectively (Fig. 17). The PL intensity increases in this series of compounds with decreasing temperature, reaching close to 100% at 77 K. According to the calculated values of $\Delta E(S_1 – T_1)$, if TADF is favored at room temperature, the lifetime should increase at low temperatures because RISC process slows down due to the lack of required thermal energy. Indeed, the longer lifetimes of 36, 48 and 91 μs were observed at 77 K for chloride over bromide to iodide analogs, confirming the existence of TADF process at room temperature in $Cu_2X_2(Py_3P)_2$. In general, lifetime at 77 K is more than double of the value observed at room temperature. The authors reported that TADF is completely suppressed below 100 K due to the lack of sufficient thermal energy and pure phosphorescence starts to dominate. Therefore, at these temperatures, the peak maxima should shift towards the higher wavelength ($T_1 \rightarrow S_0$) and emission bandwidth should decrease due to the absence of high energy TADF ($S_1 \rightarrow S_0$). Indeed, in all three compounds, the emission peak maxima shifted ~10 nm towards the higher wavelength at 77 K accompanied by narrowing of the peak bandwidth. Noteworthy, although there are several studies in literature reporting TADF in coordination Cu(I) halides, careful ligand choice is important to satisfy the requirements (e.g., small ΔE ($S_1 – T_1$) value (< 120 meV)) to observe TADF.[187, 242-249] Moreover, some reports claim that TADF may allow achieving high PLQYs from (M + X) LCT compounds at room temperature by harvesting up to 100% singlet excitons through faster RISC.[250] Interested readers are referred to the available in-

depth reviews on the topic, which also cover materials design ideas and strategies for efficient Cu(I)-based TADF emitters.[240, 241]

Noteworthy, TADF is unlikely to occur in hybrid Cu(I) halides, because the triplet state is typically a deep midgap state and it relies on the deformation of the inorganic core in the excited states (i.e., is not heavily impacted by the organic cation choice). Indeed, TADF as an emission pathway has been excluded by considering the reported temperature dependence of lifetimes in hybrid compounds (see the discussion in Section 3.1).

3.3. Hybrid *vs* coordination Cu(I) halides (optical properties and emission mechanisms)

Despite the wealth of chemical compositions and crystal structures of high-efficiency light emitting hybrid organic-inorganic Cu(I) halides, they are reported to demonstrate the same emission pathways – recombination of triplet STEs localized on inorganic units. There have been other alternative terms used in reference to this emission including MC and CC type transitions, however, they all refer to the same phenomenon – largely Stokes shifted and broad emission from a transient midgap state localized on the inorganic structural units. In our view, these characteristics are best captured by the STE emission terminology and the dominant use of this terminology to explain PL in the hybrid Cu(I) halides literature is well justified. Furthermore, STE terminology has also been heavily used for the parent all-inorganic compounds such as A_2CuX_3, $A_3Cu_2X_5$ (A = alkali cation; X = halide anion) etc.,[38] and the use of STE terminology signifies that the replacement of alkali cations with organic cations does not change the emission mechanism in hybrid Cu(I) halides as STEs are localized on copper(I) halide structural units.

The localization of STEs on the inorganic anions is evidenced by the electronic structures of hybrid Cu(I) halides showing dominant contributions of Cu-3*d* and Cu-4*s* orbitals to VBM and CBM, respectively. In comparison to all-inorganic Cu(I) halides, halogen-*p* orbitals also have greater contributions to both CBM and especially VBM in hybrid Cu(I) halides. Nevertheless, emission color tunability in this class is typically achieved by varying the coordination environment and geometries around Cu(I) metal centers, and to a lesser degree, halogen substitutions. Although organic cations do not directly contribute to optical transitions, they can play important roles by templating the inorganic structures. Furthermore, organic cations can influence the structural rigidity and structural deformations in the excited states, thereby having important indirect influences on the optical properties of hybrid Cu(I) halides. Finally, H-bonding of the organic cation to the specific halide used may also be an important factor that impacts the structural distortions of the Cu-halide units; however, dedicated experimental and computational studies are needed to ascertain the impact of H-bonding on the structures and properties of hybrid Cu(I) halides.

In contrast, coordination Cu(I) halides show a greater variety of photoemission mechanisms including MLCT and/or XLCT, CC emissions and TADF. Of these, CC-type emissions closely mirror the reported STE emissions in hybrid Cu(I) halides. Cluster-centered emissions are observed in compounds containing Cu_4X_4 clusters featuring Cu···Cu distances smaller than 2.8 Å. In such cases, irrespective of the broader connectivity of the Cu_4X_4-*L* framework, strong charge localization in Cu_4X_4 clusters prompts deformations of these clusters upon photoexcitation, resulting in high efficiency low energy emission localized on the inorganic Cu_4X_4 cores. This description mirrors the described STE-based photoemission in hybrid Cu(I) halides containing

multinuclear $[Cu_4X_6]^{2-}$ and $[Cu_4X_8]^{4-}$ clusters with Cu···Cu distances below 2.8 Å. The work on hybrid compounds shows that photoexcitation in such cases leads to a drastic shortening of Cu···Cu distances within the clusters, and the strong distortions of the clusters explains the large Stokes shifts and low energy emission observed. In this regard, here too, the use of STE terminology is more descriptive of the photophysical processes, however, this terminology is typically not used for coordination Cu(I) halides.

Yet another common emission pathway in coordination Cu(I) halides is MLCT and/or XLCT, and it produces higher energy emission closer to absorption edge compared to the low energy CC emissions. Here, MLCT and/or XLCT refer to the fact that in most coordination Cu(I) halides, VBM has dominant contributions from the inorganic structural part, whereas CBM is dominated by the organic ligand orbitals. In strict terms, the use of this terminology can be questioned because MLCT and/or XLCT perhaps accurately describe the optical absorption that takes an electron from a metal or halide orbital to a ligand orbital. However, the radiative recombination of the excited electron with the hole it left behind must then be more accurately described as *ligand-to-metal charge transfer* (LMCT), yet this term is hardly used in literature. In addition, MLCT and/or XLCT labels, which are the names for optical absorption processes, are inappropriately used to label the excited states in the configurational coordinate diagrams (Fig. 8). From a perspective of scientists working on hybrid Cu(I) halides, there is no justification for the usage of MLCT and/or XLCT to describe either photoemission processes or label the excited states in schematic diagrams.

Notwithstanding the issues with the accurate use of terms, the direct bonding between Cu(I) halide units and organic ligands enables efficient charge transfer between them. This is in stark contrast to the observations made for hybrid Cu(I) halides for which charge transfer between the organic cations and inorganic anions is notoriously inefficient. Therefore, hybrid compounds possessing Type-II band alignment (i.e., VBM and CBM are dominated by the inorganic and organic states, respectively) have quenched PL due to the separation of charges on structurally isolated organic and inorganic units. Yet another difference, because CBM of coordination Cu(I) halides are typically dominated by the organic motifs, organic ligands have direct contributions to their optical absorption and emission properties. In fact, unlike hybrid Cu(I) halides in which the position of midgap STE state is hard to predict *a priori*, photoemissions in coordination compounds can be tuned by using organic ligands of suitable LUMO energies. However, compared to the compounds exhibiting localized CC emissions, higher energy MLCT and/or XLCT transitions typically lead to poorer emission efficiencies. The emission efficiency can be improved by enabling TADF process through a careful design of the organic ligands that can provide very small energy gap between the singlet S_1 and triplet T_1 excited states. Invariably, TADF also leads to higher energy emissions close to the absorption edge. TADF has not been reported for hybrid Cu(I) halides and is very unlikely given the very large distortions and large Stokes shifts typical for midgap STE emissions in these compounds.

Similar to the neutral coordination Cu(I) halides, the VBMs of coordination-ionic (or AIO) Cu(I) halides also have dominant contributions from the inorganic motifs, while the CBMs are primarily composed of the ligand orbitals.[56, 57, 65-67] Thus, the bandgaps and emission wavelengths of these compounds can be effectively tuned by using suitable organic structural motifs,[59, 66] and light emissions in these compounds are typically assigned to (M+X)LCT transitions.[66] An

exception to the described electronic structures and optical transition pathways is the case of the AIO compounds containing inorganic structural units featuring Cu···Cu distances below 2.8 Å. These, just like the hybrid and neutral coordination Cu(I) halides featuring inorganic clusters with short Cu···Cu distances, exhibit strong CC-based emission; in certain cases, the CC-based emission in these compounds can be accompanied with (M+X)LCT emission.[205] The relative intensity of these two types of emission can often vary in response to temperature and excitation wavelengths. Moreover, like the neutral coordination Cu(I) halides, AIO compounds with a small ΔE ($S_1 - T_1$) value between the triplet (T_1) and lowest singlet (S_1) excited states often exhibit TADF, facilitating the harvesting of both singlet and triplet excitons.[55, 66]

4. Potential practical applications

Luminescent Cu(I) halides demonstrate strong potential for a variety of applications including solid state lighting, photodetectors, ionizing radiation detection, coating materials, luminescent ratiometric thermometers, sensing, anticounterfeiting, etc.[64, 91, 140, 251-254] Below, we provide a concise review of a few of the most common applications of these materials discussed in literature.

4.1. Solid state lighting

One of the potential applications of luminescent materials is their use as phosphors in lighting technologies, including light emitting diodes and displays. The low-cost, low toxicity, and earth-abundant elemental compositions, along with the high emission efficiency of luminescent Cu(I) halides, make them advantageous over toxic and/or rare-earth element based traditional phosphors used for lighting applications. The traditional methods to construct white light emitting diodes (WLEDs) require the use of multiple of phosphors (e.g., red, green, and blue) on top of a UV LED chip to cover the full spectral range of visible light with balanced emissions, or the use of a yellow phosphor on top of a blue LED chip (Fig. 18a). The ultrabright emission of hybrid Cu(I) halides have been utilized by different research groups to fabricate WLEDs. Solution processability of these Cu(I) halide-based phosphors provides additional advantages for coating these materials on different types of surfaces, including on top of commercial LEDs. For instance, Su *et al*. achieved a warm white light by fabricating a phosphor converted (pc-) WLED mixing yellow-emissive (1,3-dppH$_2$)$_2$Cu$_4$I$_8$·H$_2$O (1,3-dppH$_2$ = protonated 1,3-di(pyridin-4-yl)propane) and commercial green emitting phosphor (LuAG:Ce^{3+}) (LuAG = lutetium aluminum garnet) onto a commercial blue LED (440 nm).[215] The corresponding pc-WLED demonstrate Commission Internationale de l'Eclairage (CIE) of (0.4452, 0.3989), a high color rendering index (CRI) value of 91.4 and color correlated temperature (CCT) of 2823 K. In contrast, a rare-earth metal free two-component WLED has been fabricated by Liang *et al*. using a 300 nm commercial LED chip as an excitation light source, (TMA)$_3$Cu$_2$Br$_2$Cl$_3$ as a yellow phosphor and Cs$_3$Cu$_2$I$_5$ as a blue phosphor.[184] This pc-WLED exhibits a CIE value of (0.324, 0.333), CRI of 84 and CCT of 5893 K. Authors reported that the PL intensity of the hybrid (TMA)$_3$Cu$_2$Br$_2$Cl$_3$ decreases over time compared to that of the all-inorganic phosphor Cs$_3$Cu$_2$I$_5$. This increases the CCT of the corresponding device over time, although the device performance is promising in the initial stage considering CIE, CRI and CCT values. Separately, Liu *et al*. demonstrate that the CIE coordinate values of (0.16, 0.13) to (0.34, 0.44) can be achieved by mixing yellow emissive (DTA)$_2$Cu$_2$I$_4$ (DTA = dodecyl trimethyl ammonium) and blue emissive Cs$_3$Cu$_2$I$_5$ in different ratios.[113]

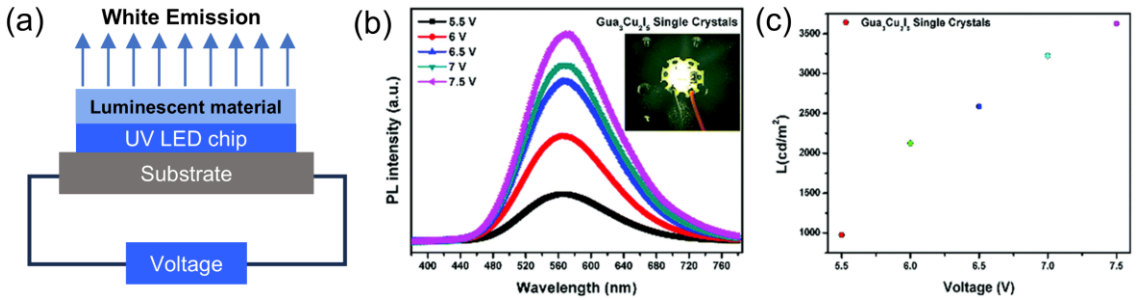

Fig. 18 (a) Schematic illustration of phosphor converted (pc) UV-pumped LEDs. (b) PL spectra of $Gua_3Cu_2I_5$ based pc-WLED device employing a 255 nm LED chip at different working voltages. Inset: Photograph of $Gua_3Cu_2I_5$ based pc-WLED at a working voltage of 7.5 V. (c) Luminance–voltage diagram of $Gua_3Cu_2I_5$ based pc-WLED. Reproduced from ref 80. Copyright 2022 Royal Society of Chemistry.

The issues of color changes over operation time, variable excitation energy requirements to achieve maximum emission efficiency of individual phosphors and complex device configuration could be minimized by fabricating single-component pc-WLED. To achieve this, several pc-WLEDs have been reported in literature using yellow-emissive hybrid Cu(I) halides that cover a wide spectral range of visible light. A single-component pc-WLED using yellow-emissive $Gua_3Cu_2I_5$ (emission covers 430 nm to 750 nm of visible light) on top of a commercial 255 nm LED chip demonstrate warm white light with CIE of (0.44, 0.51).[80] In this work, Song *et al*. also demonstrates that the luminance of the fabricated WLED increased with increasing the working voltage of the device from 5.5 V to 7.5 V and reached up to 3600 cd m^2 (Fig. 18b – c). Another pc-WLED fabricated by positioning a $(C_4H_{10}N)_4Cu_4I_8$ single crystal onto a 360 nm LED chip demonstrates CIE of (0.39, 0.54) and CCT of 4519 K.[85] Moreover, Banerjee *et al*. fabricated a prototype pc-WLED by coating 365 nm LED with yellow emitting $(TMS)_3Cu_2I_5$ based luminescent ink. The resultant warm WLED demonstrates a CRI value of 82 with CCT of 3248 K and CIE of (0.44, 0.45).[63] These results are comparable to the commercial rare-earth phosphor YAG:Ce (YAG = yttrium aluminum garnet) based commercial WLED with CRI of ~80 and CCT value of 3000 K.[255]

Notice that these pc-WLED require high energy LED light source to achieve bright emission from the employed phosphors. This is because most of the hybrid Cu(I) halides demonstrate maximum absorption in the UV region (generally, below 360 nm).[38] This hinders the usability of commercial blue LED excitation light source (390 nm – 450 nm).[54, 256] Moreover, CIE color rendering index of these pc-WLEDs mostly remains in the yellow region of the visible light. Which limits the high-end lighting applications of these single-component pc-WLEDs. Therefore, the development of blue light excitable yellow-emissive hybrid Cu(I) halides exhibiting high emission efficiency is crucial for the fabrication of single-component pc-WLED for desired applications. Some work has been done on this front; Zhou *et al*. fabricated a single-component WLED utilizing the broad absorption (up to 460 nm) characteristic of yellow-emissive $DPCu_4I_6$ (DP = $(C_6H_{10}N_2)_4(H_2PO_2)_6$) onto a commercial blue LED chip (450 nm).[257] Notably, this high-performance WLED demonstrates a CIE color coordinate of (0.36, 0.35) with CCT 4415 K, CRI 85.1 and luminous efficiency of 18.41 lm W^{-1} (Fig. 19a – b).

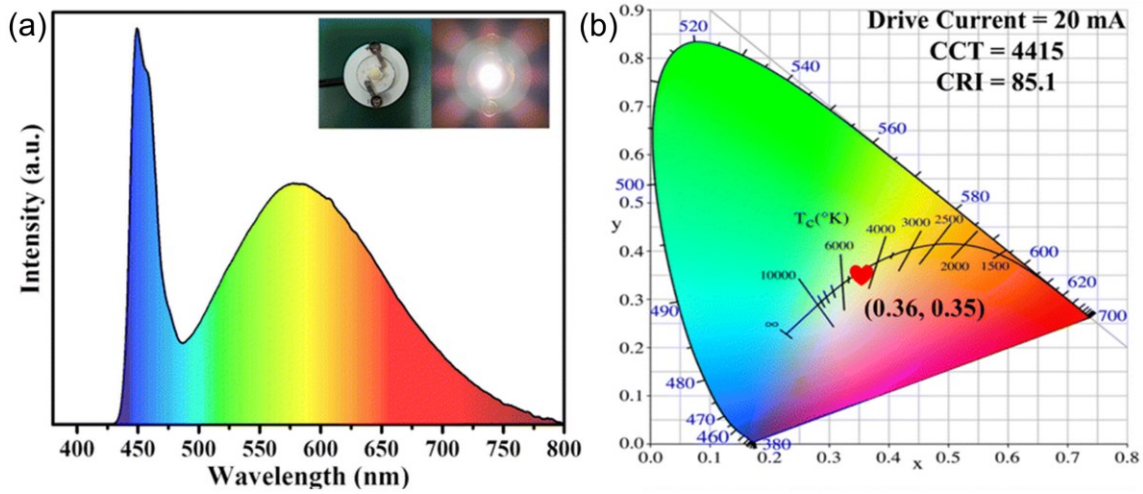

Fig. 19 (a) PL spectra of $DPCu_4I_6$ based pc-WLED device under the excitation of 450 nm LED chip. Inset: Photographs of $DPCu_4I_6$ based pc-WLED under ambient light (left) and under operation conditions (right). (b) CIE coordinate of $DPCu_4I_6$ based pc-WLED. Reproduced from ref 257. Copyright 2023 Royal Society of Chemistry.

Yet, another strategy to achieve high-performance pc-WLED is the utilization of a white-emitting phosphor that covers the full wavelength region of the visible light, onto a commercial LED. For example, Lian *et al*. reported the fabrication of a WLED using a white light emitting $(TBA)CuI_2$ luminescent ink (emission covers 400 nm to 850 nm) on a 275 UV LED chip (Fig. 20a – c). The emission spectra of this pc-WLED exhibits CIE value of (0.28, 0.30), which is very close to the pure white light (0.33, 0.33).[115, 258] The CRI value for this white LED was found to be 78, which is higher than that of the widely used fluorescent lamp (~72).[259] In a separate study, the same research group achieved CIE of (0.31, 0.33), CRI of 91.3 and CCT of 6574 K in a pc-WLED using $(TPA)CuI_2$ as a white phosphor on a 365 nm LED chip.[260]

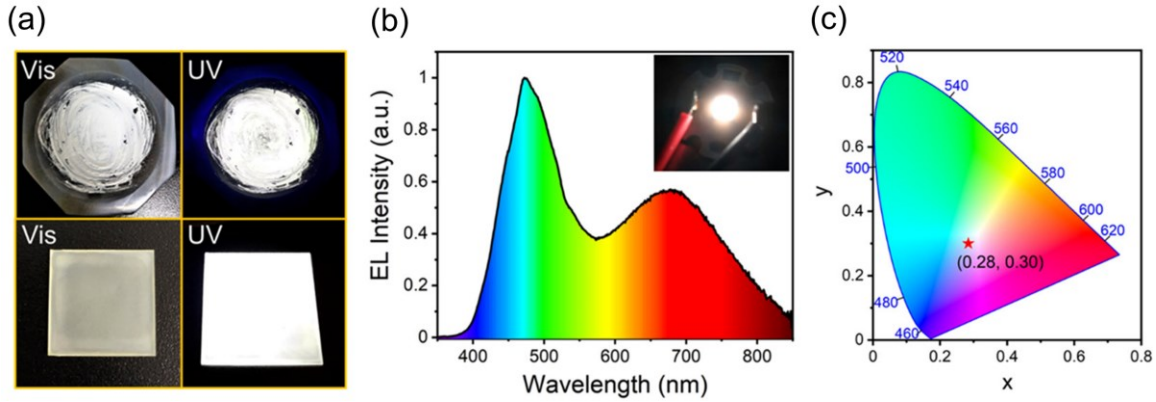

Fig. 20 (a) Photographs of $(TBA)CuI_2$ powder sample under ambient light and 275 nm UV light (top), $(TBA)CuI_2$/PVDF composite film under ambient light and 275 nm UV light (bottom). (b) PL spectra of $(TBA)CuI_2$ based single component pc-WLED. Inset shows the pc-WLED under operation conditions. (c) CIE coordinate of the $(TBA)CuI_2$ based pc-WLED. Reproduced with permission from ref 115. Copyright 2021 American Chemical Society.

The potential of coordination Cu(I) halides for solid-state lighting have also been explored by several research groups.[143, 159, 167, 174, 183] Li and co-workers have reported the use of composites of coordination Cu(I) halides for preparation of white phosphors.[159, 167, 183, 197] For instance, a composite of blue emitting 1D-Cu_2I_2(*tpp*)$_2$(*bpp*) (*tpp* = triphenylphosphine, *bpp* = 1,3-bis(4-pyridyl)propane) and yellow emitting 2D-Cu_4I_4(*dipe*)$_2$ exhibits white light emission with CIE of (0.34, 0.35), CRI of 73.9 and CCT of 4988 K.[183] A prototype LED device was fabricated coating the inner surface of the light cover with this white composite phosphor, where phosphor was not in direct contact with the UV LED (Fig. 21a – b). Another work from the same research group reported a pc-WLED based on yellow emissive [$Cu_4I_4(Ph_3As)_3$] and 390 nm UV light as the excitation light source.[197] This single-component pc-WLED exhibits CIE very close to the pure white light with a CRI of 81 and a CCT of 6000 K.

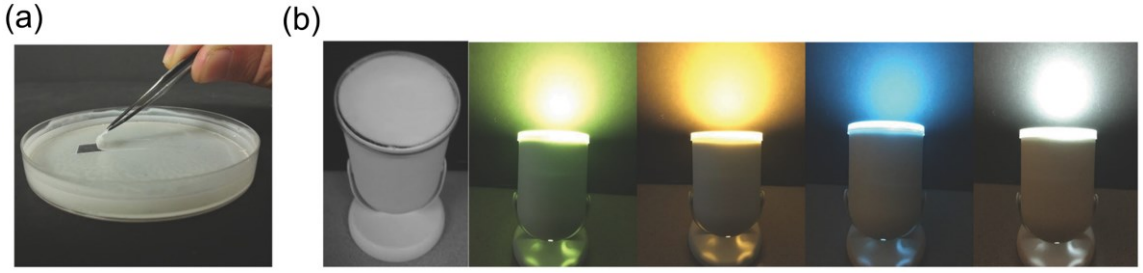

Fig. 21 (a) Photograph of thin coating layer based on 1D-Cu_2I_2(*tpp*)$_2$(*bpp*) and 2D-Cu_4I_4(*dipe*)$_2$ phosphors with binder PolyOx N750. (b) A prototype LED lamp under day light (left) and "on" stage: greenish yellow (3D-Cu_4I_4(*dipe*)$_2$), orange (2D-Cu_4I_4(*dipe*)$_2$), blue (1D-Cu_2I_2(*tpp*)$_2$(*bpp*)), white (1D-Cu_2I_2(*tpp*)$_2$(*bpp*) and 2D-Cu_4I_4(*dipe*)$_2$). Reproduced with permission from ref 183. Copyright 2016 John Wiley and Sons.

Although other blue light excitable (bandgap <2.7 eV) yellow emitting coordination Cu(I) halides such as 2D-Cu_2I_2(4,4′-*dps*)$_2$ (*dps* = dipyridyl sulfide) and 1D-Cu_2I_2(*tpp*)$_2$(4,4′-*bpy*) have been reported in literature, lower decomposition temperature (<160 °C) hinders their suitability for lighting applications.[159] Similarly, 1D-CuI(*py*)$_{1-x}$(*pm*)$_x$ emits white light with a CIE value of (0.31, 0.33), however, it decomposes below 150 °C.[157] Noteworthy, hybrid Cu(I) halides have been tested for solid-state lighting applications in larger numbers in literature compared to the coordination Cu(I) halides. Low thermal stability of coordination Cu(I) halides (generally, ≤200 °C) due to weak metal-organic coordination bonds hinders their use for lighting applications.[59, 159, 183] One advantage of these newly developed AIO compounds over the typical neutral coordination Cu(I) halides is that some of these compounds demonstrate high thermal stability, remaining stable at temperature over 200 °C and, in some cases, exceeding 300 °C (see Table 2).[203] For instance, after being exposed to hot air (100 °C) 0D-Cu_4I_6(*pr-ted*)$_2$ and 0D-Cu_4I_6(*tpp*)$_2$(*bttmm*)$_2$ (where *pr-ted* = 1-propyl-1,4-diazabicyclo[2.2.2]octan-1-ium; *bttmm* = 1-(1*H*-benzo[*d*][1,2,3]triazol-1-yl)-*N*,*N*,*N*-trimethylmethanaminium) maintained 90% of their initial PL quantum yield values.[203] These results suggest the potential of this subclass of compounds (AIO) and highlight the need for their further exploration.

4.2. Information storage, sensing and anticounterfeiting

Counterfeiting and duplicity of important information and documents are critical problems in our individual life and in the world economy. Therefore, the development of effective anti-counterfeiting techniques is important for desirable information storage and security applications. In general, anti-counterfeiting is accomplished by encrypting important information that can only be revealed under especial conditions. Environmentally friendly elemental compositions, high PLQY values, solution processability and ease of their dispersion in polymers, allow the consideration of luminescent hybrid Cu(I) halides for anti-counterfeiting applications. Moreover, the versatility of luminescent inks based on hybrid Cu(I) halides on different substrate surfaces such as colored papers, glass slide, plastic/Teflon sheets, etc., instantiate their multi-purpose usability.[62, 63, 118] Several research groups demonstrated anti-counterfeiting applications by constructing single-component hybrid Cu(I) halide luminescent ink based symbols which are invisible on different types of substrates under daylight and can be decrypted by using UV light.[62, 106, 111, 118] For instance, Chen *et al*. printed the logo of BIT (Beijing Institute of Technology) on a filter paper using the silicon ink of green emissive $(TPP)_2Cu_4I_6{\cdot}2DMSO$.[118] The logo is invisible under daylight but turns green color under 365 nm UV light, decrypting the hidden logo (Fig. 22a). This illustrates that a simple luminescent Cu(I) halide can be used for anti-counterfeiting applications. However, such encrypted pattern/symbol using a single light emitter may not be strong enough for certain anti-counterfeiting due to the ease of its decryption technique and can be easily cloned. Later, An *et al*. demonstrated a two-component materials system for a more effective anti-counterfeiting application, which utilizes the differing PL characteristics of the two Cu(I) halides, cyan emissive $(TPA)CuBr_2$ and orange emissive $(TPA)_2Cu_4Br_6$ (Fig. 22b).[107] The encrypted '8888'-shaped pattern looks inconspicuous under daylight. The cyan '8796' pattern becomes visible under 254 nm UV light, while the orange '0135' pattern stands out under 365 nm UV light. Similar types of information encryption-decryption applications also have been demonstrated by Li *et al*. employing green emissive $(ETPP)CuBr_2$ and yellow emissive $(ETPP)_2Cu_4Br_6$ (ETPP = (ethyl)triphenyl phosphonium).[103] These results suggest that two or multi-component effective digital encryption can be fabricated by arbitrary distribution of hybrid Cu(I) halide-based phosphors.

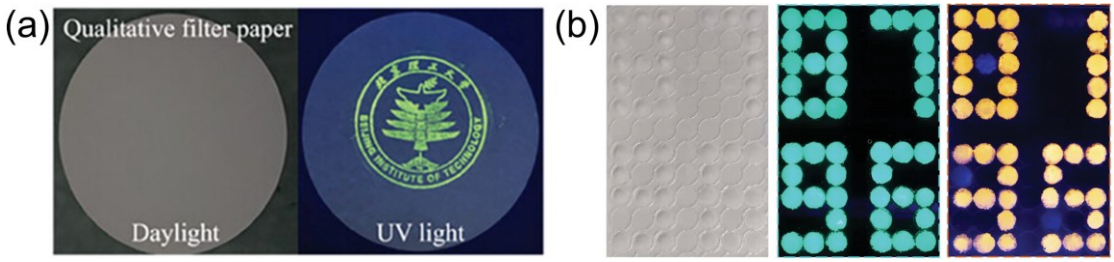

Fig. 22 (a) Photographs of the $(TPP)_2Cu_4I_6{\cdot}2DMSO$ ink-based BIT logo stamp-printed on a filter paper encrypted under daylight (left) and decrypted under 365 nm UV light (right). Reproduced with permission from ref 118. Copyright 2024 John Wiley and Sons. (b) Photographs of encrypted pattern based on cyan emissive $(TPA)CuBr_2$ and orange emissive $(TPA)_2Cu_4Br_6$ inks. From left to right: under daylight, under 254 nm UV light, under 365 nm UV light. Reproduced with permission from ref 107. Copyright 2023 John Wiley and Sons.

Stimuli-responsive Cu(I) halide materials may also offer diversified potential applications in sensing, multi-modal anti-counterfeiting, and information storage.[11, 12, 261] In recent years, stimuli-responsive materials achieved significant attention due to their switchable optical properties (e.g., emission color, intensity) that can be observed by necked eye or by a device (i.e., emission lifetime, intensity, peak position, broadness) (Scheme 2).[15, 262] The switchable optical properties are associated with achieving phase/structural transition by the help of external stimuli such as chemical exposure, temperature, pressure, magnetic field, etc.[62, 83, 263]

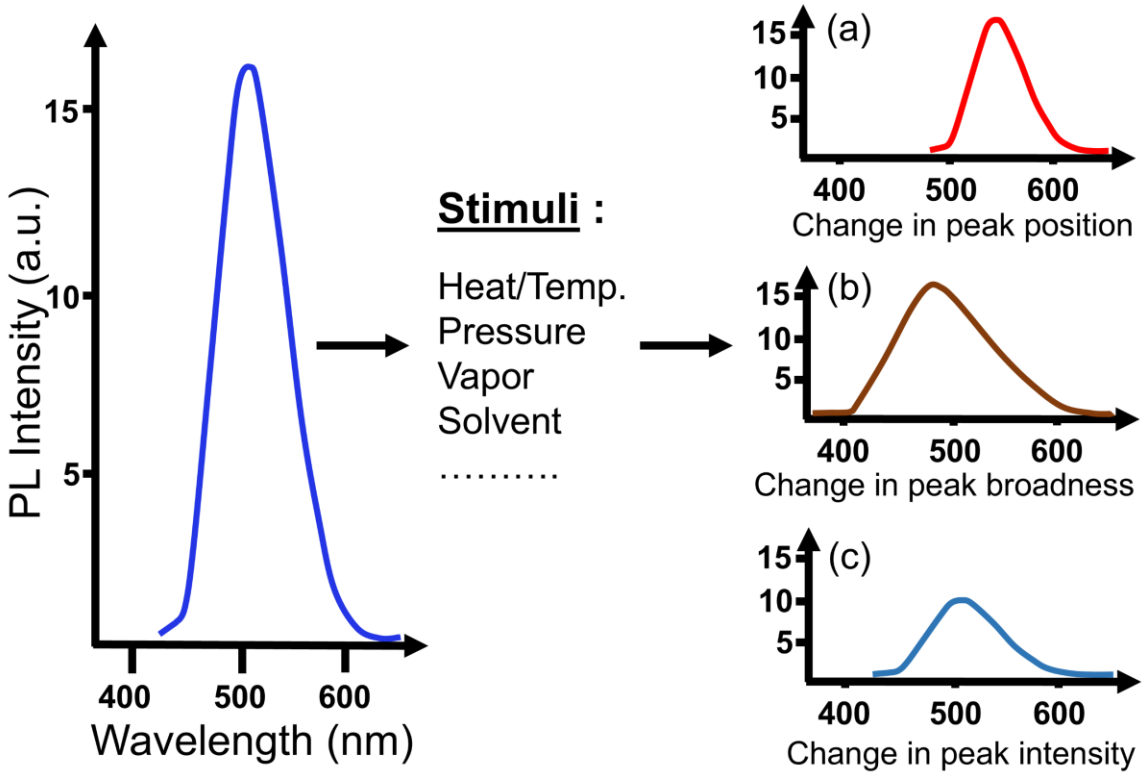

Scheme 2. Conceptual representation of the switchable optical properties of hybrid Cu(I) halides with the help of external stimuli such as heat or temperature, pressure, chemical vapor, solvent, etc. that leads to the change in PL emission (a) peak position, (b) peak broadness, and (c) peak intensity.

An interesting feature of some hybrid Cu(I) halide families is that different hybrids containing the same organic motifs (e.g., $(TEP)_2Cu_2Br_4$ and $(TEP)_2Cu_4Br_6$; $(TPA)CuBr_2$ and $(TPA)_2Cu_4Br_6$; $(ETPP)CuBr_2$ and $(ETPP)_2Cu_4Br_6$; α- and β-$Gua_3Cu_2I_5$) can be interconverted in presence of external stimuli, such as chemical, thermal and/or mechanical stimuli.[62, 82, 83, 97, 103, 107] This enables the use of organic-inorganic Cu(I) halides for sensing, high-level multi-modal anticounterfeiting, information storage applications. For instance, $(TPA)CuBr_2$ converts to $(TPA)_2Cu_4Br_6$ in presence of water accompanied with the PL emission switching from cyan to orange.[82, 107] Utilizing the water-sensitivity, An *et al*. fabricated test-papers based on $(TPA)CuBr_2$ to detect trace water in *iso*-propyl alcohol (IPA).[107] Authors demonstrated that the test-papers were able to detect the presence of ≥10% water in the IPA samples by changing the color from cyan to orange. Separately, Tian *et al*. demonstrated a triple-mode high-security level anti-counterfeiting application potential of $(TPA)CuBr_2$ and $(TPA)_2Cu_4Br_6$, by controlling external stimuli-response under different excitation light sources, water and heat treatment.[82] A pattern of flowerpot and petals has been printed on a

paper in which the flower is composed of $(TPA)CuBr_2$ (top), whereas the flowerpot (flowerpot, plant stem and leaves) is made of $(TPA)_2Cu_4Br_6$ (bottom) (Fig. 23). First, due to the differing optimal excitation wavelengths (PLE_{max}) of $(TPA)CuBr_2$ and $(TPA)_2Cu_4Br_6$, only flowerpot (orange) is visible under 365 nm UV light, while both flowerpot (orange) and flower (cyan) are visible under 254 nm UV light (Fig. 23a – c). Second, due to the water-sensitivity of $(TPA)CuBr_2$, the whole pattern (flowerpot and flower) appears orange under 254 nm UV after water treatment (Fig. 23d). Third, the orange emission of flowerpot and cyan emission of the flower under 254 nm UV light can be recovered after heat treatment (Fig. 23e). Similarly, several other groups, including Tian *et al.*, Popy *et al.*, Li *et al.*, demonstrated the potential of interconvertible luminescent hybrid Cu(I) halides in anti-counterfeiting applications by encrypting information in numeric patterns.[62, 82, 103] These results demonstrate the potential of stimuli-responsive luminescent hybrid Cu(I) halides for high-level encryption following permutation and combination strategy.

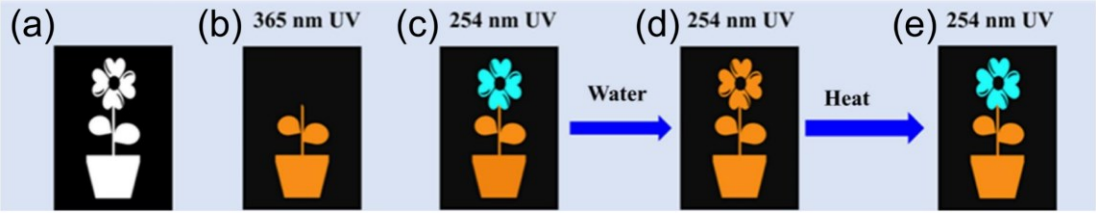

Fig. 23 Demonstration of triple-mode anti-counterfeiting application using interconvertible $(TPA)CuBr_2$ (cyan) and $(TPA)_2Cu_4Br_6$ (orange). The pattern of flowerpot and petals under (a) daylight, (b) 365 nm UV light, (c) 254 nm UV light. (d) Whole pattern appears orange after water treatment, under 254 nm UV light. (e) The cyan emission of $(TPA)CuBr_2$ (flower) has been recovered after heat treatment, under 254 nm UV light. Reproduced with permission from ref 82. Copyright 2023 Elsevier.

Some low-dimensional hybrid Cu(I) halides exhibit low temperature congruent melting, i.e., these materials reversibly melt without decomposition.[62, 107] This suggests that such materials are melt-processible, providing yet another avenue for their preparation and thin film deposition.[264, 265] Often, their melting transitions are linked with their PL emission behaviors, e.g., temperature responsive luminescence 'on-off' behavior has been reported for several families of hybrid Cu(I) halides.[62, 88, 107] In combination, low temperature congruent melting and sensitivity of PL emission upon heating can be useful for anticounterfeiting applications, such as recyclable information encryption-decryption by temperature. An *et al*. demonstrated multi-modal anti-counterfeiting applications of $(TPA)CuBr_2$ (cyan) and $(TPA)_2Cu_4Br_6$ (orange) utilizing their congruent melting at different temperatures.[107] In a separate study, An *et al*. demonstrated that an encrypted symbol based on water stable $(TOA)CuBr_2$ (TOA = tetraoctylammonium) anticounterfeiting ink can be decrypted by using 254 nm UV light even under water (Fig. 24a – d).[88] In warm water heated above 328 K, the luminescence 'off' state of $(TOA)CuBr_2$ is triggered, and the symbol encryption can be recovered. Interestingly, this process of encryption and decryption is reversible by applying hot and cold water. Moreover, the authors also fabricated an erasable PL paper based on $(TOA)CuBr_2$ to display real-time transient information. They employed a NIR (808 nm) light as a pen to write information on the PL paper using its photo-thermal conversion property. In absence

of the NIR light, the paper quickly self-erases the information to become ready for re-writing on the paper.

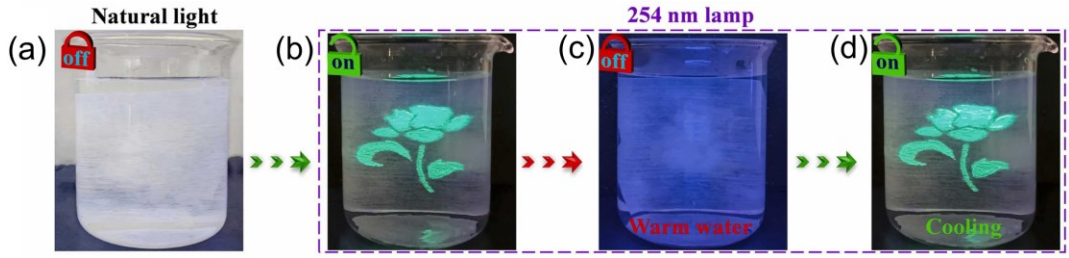

Fig. 24 Photographs of encryption-decryption of a flower symbol based on (TOA)$CuBr_2$ under water. (a) The encrypted symbol is invisible under daylight. (b) the encrypted symbol is decrypted under 254 nm UV light. (c) (TOA)$CuBr_2$ undergoes luminescence 'off' state in warm water and the flower symbol disappeared under 254 nm UV light. (d) The encrypted symbol became visible again under 254 nm UV light upon cooling. Reproduced with permission from ref 88. Copyright 2024 Elsevier.

The melt-processibility of hybrid Cu(I) halides could potentially enable their use in flexible and wearable optoelectronic devices.[266] This also provides a cost-effective and toxic solvent-free alternative approach to the traditional solution processable thin film deposition techniques for metal halides.[264, 265] For instance, Popy *et al*. demonstrated that a good substrate coverage of melt-processed thin films of $(TEP)_2Cu_2Br_4$ and $(TEP)_2Cu_4Br_6$ can be obtained utilizing the congruent melting behavior of these materials (Fig. 25).[62] Although other low melting Cu(I) halides are also known in literature, the work in the area of melt-processing of Cu(I) halide thin films is in its infancy.[88, 107] Further work is necessary to gain an in-depth understanding of the heating and cooling processes and influencing factors on the deposition of the films. Such work can be followed by studies focused on the use of melt processed thin films of hybrid Cu(I) halides in practical applications.

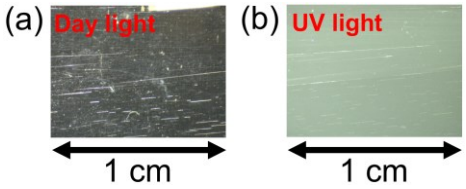

Fig. 25 Photographs of the melt-processed $(TEP)_2Cu_2Br_4$ thin films on microscopic glass slide (a) under day light and (b) under 365 nm UV light. Reproduced from ref 62. Copyright 2024 John Wiley and Sons.

Many coordination Cu(I) halides show thermochromism due to their characteristic temperature dependence of luminescence.[105, 186, 232, 237, 267] A few coordination Cu(I) halides also demonstrate switchable PL emission associated with the structural transition in response to external chemical-stimuli (i.e., $[CuI(4\text{-pic})]_4$ and $[CuI(4\text{-pic})]_\infty$; (pic = methylpyridine)).[155] Given the stimuli-

responsive (i.e., temperature and chemical stimuli) characteristics of coordination Cu(I) halides, there is a distinct lack (as compared to that for hybrid organic-inorganic Cu(I) halides) of demonstrations of these materials for anticounterfeiting and information storage applications in literature.

4.3. Scintillation and X-ray imaging

The high PLQY values and negligible self-absorption due to large Stokes shifted emissions of hybrid Cu(I) halides make them potential candidates for radiation detection applications. Although the X-ray absorption coefficients of organic-inorganic Cu(I) halides are comparatively lower than the typical all-inorganic scintillator materials due to the absence of heavy metals, some organic-inorganic Cu(I) halides are known to demonstrate impressive radioluminescence properties (Table 6). $(TEA)_2Cu_2Br_4$ (also written as $(C_8H_{20}N)_2Cu_2Br_4$) based scintillator demonstrates X-ray detection limit of ~52.1 $nGy_{air}\ s^{-1}$, which is more than hundred times lower than the required dose rate of 5.5 $\mu Gy_{air}\ s^{-1}$ for X-ray medical diagnostics.[75] Another important parameter to evaluate the performance of scintillators is the scintillation light yield. Steady-state X-ray light yield of $(TEA)_2Cu_2Br_4$ single crystals was found to be ~91,300 photons/MeV, which is ~3.65 and 1.69 times higher than that of the commercial scintillators LuAG:Ce (25,000 photons/MeV) and CsI:Tl (54,000 photons/MeV), respectively, and is close to the record high light yield value of all-inorganic Rb_2CuBr_3 (91,056 photons/MeV). Subsequently, Su *et al*. also demonstrated the X-ray imaging ability of $(TEA)_2Cu_2Br_4$ based ceramic wafer scintillator with diameter of ~5 cm and thickness of 0.5 mm. The authors were able to observe contrast images of the target objects such as a metal spring in aluminum specimen and internal circuitry of a microchip under X-ray illumination (Fig. 26a – f). A few other reports are also available in literature, where hybrid Cu(I) halides such as $(TEP)_2Cu_4Br_6$ and $(PTPP)_2Cu_4I_6$ demonstrate potential for gamma-ray detection.[62, 81] For instance, the calculated light yield of $(PTPP)_2Cu_4I_6$ single crystals was obtained 24,240 photons/MeV excited with the γ-rays of ^{137}Cs. This value is 1.01 times than that of the commercial scintillator LYSO:Ce (24,000 photons/MeV) under the same measurement conditions.

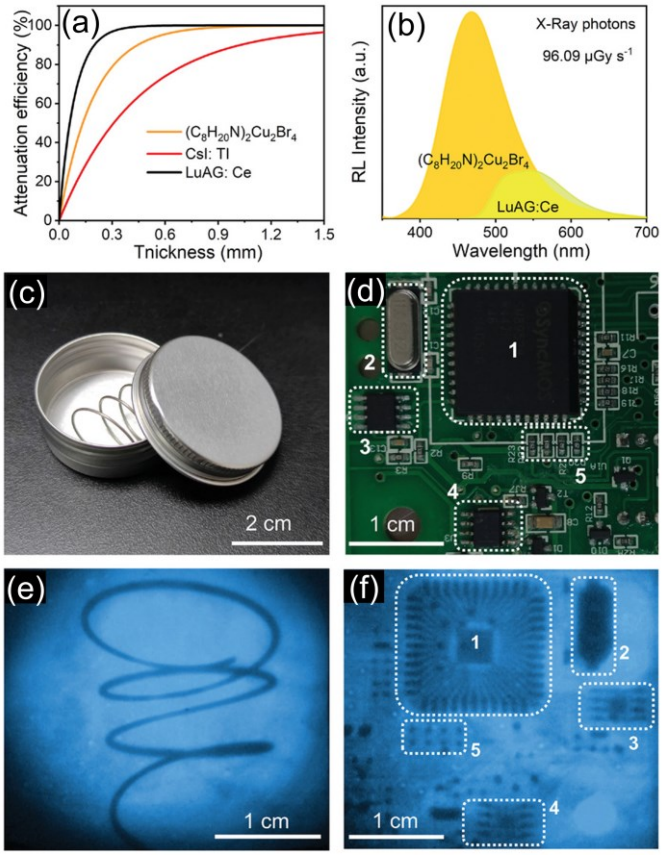

Fig. 26 (a) Attenuation efficiencies of $(TEA)_2Cu_2Br_4$, LuAG:Ce and CsI:Tl scintillators as a function of photon energy of 22 keV. (b) RL spectra of $(TEA)_2Cu_2Br_4$ and LuAG:Ce scintillators (tube voltage: 50 kV; dose rate: 96.09 $\mu Gy_{air}\ s^{-1}$). Photographs of aluminum specimen box with an iron spring (c) and 3.5 nm diameter circuit board (d) under daylight. X-ray images of aluminum specimen box with an iron spring (e) and 3.5 nm diameter circuit board (f) under 8.15 $\mu Gy_{air}\ s^{-1}$ X-ray dose. Reproduced with permission from ref 75. Copyright 2022 John Wiley and Sons.

To date, several studies on the coordination Cu(I) halides have also reported their promising scintillation properties with high light yields (see Table 6). For example, a recent study by Yuan *et al*. reported a series of coordination Cu_2X_2 (X = Cl, Br, I) compounds bearing diphenyl-2-pyridylphosphine (*Dppy*), tri-(4-fluorophenyl)phosphine) (F-*PPh*$_3$) ligands (abbreviated as **Cu_2Cl_2**, **Cu_2Br_2**, **Cu_2I_2**) with excellent scintillation properties.[268] These compounds reach record high scintillation light yield up to 175,000 photons/MeV in their class. Remarkably high PLQY and light yield in these compounds have been attributed to an efficient TADF process due to very low ΔE ($S_1 - T_1$) values of 0.11 eV to 0.05 eV for **Cu_2Cl_2** to **Cu_2I_2**, respectively. Theoretically, TADF process may enable utilization of all excitons for emission, significantly enhancing quantum efficiency and scintillation light yield.[268] Fig. 27g shows that the radioluminescence (RL) responses of **Cu_2Cl_2**, **Cu_2Br_2** and **Cu_2I_2** are 0.86, 0.98 and 2.01-fold, respectively, higher than the scintillation standard LYSO. The mechanochromic luminescence properties of usual TADF materials hinder their processability to construct scintillation screen using currently available

strategies. However, the non-mechanochromic TADF of **Cu_2X_2** allowed the preparation of high-quality scintillation screen using a soft-pressing method. The scintillation screen made of **Cu_2X_2** demonstrates low detection limit with high resolution X-ray imaging with spatial resolution values of 17.4-, 23.2- and 27.6-line pairs per millimeter (lp mm^{-1}) (Fig. 27h – i).

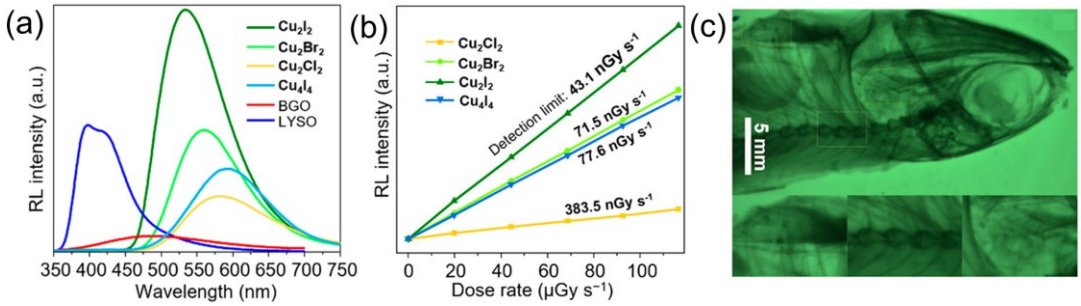

Fig. 27 (a) A comparison of the RL spectra of **Cu_2X_2** crystals, **Cu_4I_4** nanoclusters and commercial scintillators BGO, LYSO. (b) RL detection limits of the scintillation films of **Cu_2X_2** and **Cu_4I_4**. (c) Image of a small fish recorded using **Cu_2I_2** scintillation screen. Reproduced with permission from ref 268. Copyright 2023 American Chemical Society.

4.4. Hybrid *vs* coordination Cu(I) halides (optoelectronic applications)

The reported fundamental properties and practical application demonstrations suggest that both hybrid and coordination of Cu(I) halides have their own advantages and disadvantages. For instance, although PL emission color tunability and high emission efficiency can be achieved in both classes of Cu(I) halides by modifying inorganic structural motifs and/or employing suitable organic motifs, PL emission can be systematically tuned in coordination Cu(I) halides showing M/XLCT type transitions in a more predictable manner via guided HOMO-LUMO engineering of the employed ligands. In contrast, hybrid Cu(I) halides are midgap STE-based emitters and deliberate and predictive tuning of their PL emission is more difficult at present. This leads to two important consequences for potential practical applications: first, full spectral tunability of PL emission is easier to achieve in coordination Cu(I) halides whereas the demonstrated tunability of PL emission in hybrid Cu(I) halides is based on serendipitous materials discovery. Secondly, tuning of the absorption onsets of hybrid Cu(I) halides has proven difficult due to the large Cu-3*d* and Cu-4*s* orbital gaps, and most known members require high energy UV excitation. In contrast, coordination Cu(I) halides with comparatively lower band gaps can be designed following the ligand engineering approach. The blue excitability of coordination Cu(I) halides is a notable advantage of this class especially for solid-state lighting applications. On the other hand, coordination Cu(I) halides showing M/XLCT type transitions tend to have lower PLQYs as compared to the highest PLQYs approaching 100% observed for hybrid Cu(I) halides with STE emissions and coordination Cu(I) halides showing CC emissions. The latter group also shows poor tunability of PL/PLE properties as CC-based emission is essentially another name for localized low energy STE emissions.

Beyond fundamental optical properties, hybrid Cu(I) halides typically possess better thermal stability (up to 300 °C),[62, 82, 114, 184] especially compared to the neutral coordination Cu(I) halides.

However, this advantage is not generalizable, as some hybrid Cu(I) halides are also known for their low temperature melting/decomposition transitions.[269] In addition, recently developed AIO-type compounds also tend to demonstrate better thermal stability, bridging the gap between hybrid and coordination Cu(I) halides. Thermal behavior of Cu(I) halides can be a major parameter to optimize for their prospective use not only in solid-state lighting but also radiation detection applications. Recent work on excellent radiation detection properties of melt grown single crystals of all-inorganic Cu(I) halides such as $Cs_3Cu_2I_5$ shows that congruent melting behavior of luminescent Cu(I) halides can be very important for their use as scintillator materials.[270, 271] In this regard, the demonstration of congruent melting behavior of some of the reported hybrid Cu(I) halides is an important advantage for this subclass.

Important to note, the comparisons presented above are based only on a limited number of hybrid and AIO-type Cu(I) halides, although the number of known neutral coordination Cu(I) halides are greater. As more materials are discovered, individual members of various subclasses may show better potential for certain applications. The select results discussed here suggest the high overall potential of luminescent Cu(I) halides for practical applications and warrant further exploration of their use in these and other applications. For example, more work on engineering and design of creative new WLED device architectures in which Cu(I) halide phosphors are not in direct contact with the hottest spots (i.e., the surface of UV LED) could provide a real boost for the application prospects of both hybrid and coordination Cu(I) halides as inexpensive and earth-abundant phosphors for solid-state lighting applications.

Table 6 Summary of organic-inorganic Cu(I) halide-based scintillators.

Compound	PLQY (%)	Light yield (Photons / MeV)	Detection limit (nGy_{air} / s)	Resolution (lp / mm)	Ref.
$(TBA)CuCl_2$	92.8	23,373	-	-	94
$(TBA)CuBr_2$	80.5	24,134	-	-	94
$(ETPP)CuBr_2$	65.17	57,974	453.6	19.56	103
$(PPh_4)CuBr_2$	1.3	5,000	6730	-	114
$(TEA)_2Cu_2Br_4$	99.7	91,300	52.1	9.54	75
$(TEP)_2Cu_2Br_4$	92	2,800	-	-	62
$(Bmpip)_2Cu_2Br_4$	48.2	16,000	710	-	114
$(BMP)_2Cu_2Br_2I_2$	99.5	25,000	40.4	5.61	189
$(TEP)_2Cu_4Br_6$	98	15,800	-	-	62
$(ETPP)_2Cu_4Br_6$	94.15	53,576	-	-	103
$(ETPA)_2Cu_2I_4$	97.56	19,900	524	5.47	84
$(BzTPP)_2Cu_2I_4$	44.2	27,706	352	4.91	120
$(4\text{-}bzpy)_3Cu_3I_6$	0.3	7,011	-	-	90
$\beta\text{-}(MTP)_2Cu_4I_6$	89	64,000	72.6	20	97
$(PTPP)_2Cu_4I_6$	93.1	24,240	756.3	14.83	81
$(L_1)_2Cu_4I_6$	95.3	32,600	96.4	31	272
$(L_2)_2Cu_4I_6$	92.2	30,500	102.1	30.8	272
$(4\text{-}bzpy)_2Cu_6I_8$	0.1	5,353	-	-	90
$Cu_4I_4(PPh_3)_4$	64	1,971	-	-	197
$Cu_4I_4(AsPh_3)_3$	100	15,000	18.1	-	197
$Cu_4I_4(AsAn_3)_3$ (*EtCN*)	60	8,700	37	-	197
$Cu_4I_4(AsAn_3)_3$ (^iPrCN)	63	11,600	35	-	197
$Cu_4I_4(py)_4$	92.4	20,200	55	20	273
Cu_4I_4(4-*Bn-py*)$_4$	88.2	36,900	102.1	24.3	274
Cu_4I_4(4-^{t}*Bu-py*)$_4$	86.2	30,800	137.2	21.2	274
$Cu_4I_4(DBA)_4$	94.9	12,842	-	5	275
$CuI(PPh_3)_2$ (3-Me-*py*)	93.21	28,400	44	9.8	276
$CuBr(PPh_3)_2$ (3-Me-*py*)	90.24	21,700	144	6.8	276
$CuCl(PPh_3)_2$ (3-Me-*py*)	94.96	5,950	339	-	276
$CuI(PPh_3)_2$ (*py*)	96.61	23,200	51	8.8	276
$CuI(PPh_3)_2$ (3,5-dm-Me-*py*)	91.88	23,500	63	8.3	276
Cu_2I_2(*Dppy*) (F-*PPh*$_3$)	85	175,300	58.2	27.6	268
Cu_2Br_2(*Dppy*) (F-*PPh*$_3$)	76	102,400	82.2	23.2	268
Cu_2Cl_2(*Dppy*) (F-*PPh*$_3$)	38	97,900	418.3	17.4	268

TBA = tetrabutylammonium; ETPP = (ethyl)triphenylphosphonium; PPh_4 = tetraphenylphosphonium; TEA = tetraethylammonium; TEP = tetraethylphosphonium; Bmpip = BMP = 1-butyl-1-methyl-piperidinium; ETPA = ethyltripropylammonium; BzTPP = benzyltriphenylphosphonium; 4-bzpy = 4-benzylpyridine; MTP = methyltriphenylphosphonium; PTPP = pentyltriphenylphosphonium; L_1 = 1-

propyl-1,4-diazabicyclo[2.2.2]octan-1-ium; L_2 = 4-dimethylamino-1-ethylpyridinium; *PPh_3* = triphenylphosphine; *$AsPh_3$* = triphenylarsine; *$AsAn_3$* = (*p*-anisyl)arsine; *py* = pyridine; 4-*Bn-py* = 4-benzylpyridine; 4-*^{t}Bu-py* = 4-tert-butylpyridine; *DBA* = dibenzylamine; *Dppy* = diphenyl-2-pyridylphosphine; F-*PPh_3* = tri-(4-fluorophenyl)phosphine).

5. Conclusion and future outlook

The structural versatility of organic motifs, variable coordination and connection modes of Cu(I) halides offer extreme structural diversity in both hybrid organic-inorganic and coordination Cu(I) compounds. In many cases, the coordination numbers and geometries of the Cu(I) centers (e.g., $[Cu_2X_4]^{2-}$ and $[Cu_4X_6]^{2-}$ in hybrids; Cu_2X_2 and Cu_4X_4 in coordination compounds) can be controlled by using stoichiometric amounts of corresponding organic and inorganic reactants. Moreover, the geometry of the Cu-X units in coordination compounds mostly relies on the size and denticity of the organic ligands. However, the precise influence of the structures of organic cations, including their packing patterns, rigidity and hydrogen bonding ability on the formation of the diversified Cu(I) halide units are still unclear. This is especially true in the case of hybrid Cu(I) halides (e.g., for having $[CuX_2]^-$, $[CuX_3]^{2-}$, $[Cu_2X_4]^{2-}$ and $[Cu_2X_5]^{3-}$ structural units). Literature studies on structure-property relationships of these compounds suggest that their opto-electronic properties are highly dependent on their distinct crystal structures including the packing pattern, coordination and geometries of the metal centers, connectivity mode of the inorganic motifs within themselves (in hybrid and coordination compounds) and with the organic motifs (in coordination compounds). Therefore, very fine control of the crystal structure is needed to prepare a custom design Cu(I) halide-based light emitter. To achieve such precise control over the crystal structures, developing computational and/or machine learning approaches could be beneficial for the guided preparation of targeted Cu(I) halide-based light emitters. In such approaches, the shape, size, symmetry, packing pattern and HOMO-LUMO energies of the organics (cations and ligands), stoichiometry of the reagents, and synthesis methods would need to be considered.

More research is necessary to ascertain a few important fundamental questions, which also have relevance for potential practical applications of luminescent Cu(I) halides. As stated, the very highest efficiency Cu(I) halides are hybrids with STE emission and coordination Cu(I) halides with CC emissions. In both cases, the PL properties remain unpredictable and uncontrollable, which raises important questions on the roles of utilized organics in the deformation of the Cu(I)-halide polyhedra, in the formation of STE and/or CC states, or in deciding the depth of the STE and/or CC states (i.e., emission wavelength). Although the existence of STE (mid-gap) emission in hybrid Cu(I) halides is well justified in literature through various optical measurements including femto-second transient absorption and computational results, the relationships between the STE (or CC) state, structural deformation and electron-phonon coupling need further clarification through additional studies. Moreover, the possibility of midgap defects-based emission in luminescent Cu(I) halides has not been considered strongly in literature. In hybrid Cu(I) halides, the linear dependency of PL emission intensity to excitation power is used to rule out the possibility of defect-based emission. In contrast, to the best of our knowledge, power-dependent PL experiments have not been reported in literature for luminescent coordination Cu(I) halides. This omission needs to be addressed in future studies for a direct comparison between hybrid and coordination Cu(I) halides. Important to note, controversy remains about the maximum excitation power employed in the power-dependent PL measurements, i.e., if the PL saturation for hybrid Cu(I) halides is not observed due to the low excitation power used. The latter is because

researchers often need to limit the experiment to a certain excitation power due to either the instrument limitations or to avoid the material degradation, which is common not only for hybrid and coordination Cu(I) halides but also other hybrid metal halides studied in recent years. These challenges suggest the necessity for alternative avenues in addition to power-dependent PL to probe the possibility of defect-based emission in Cu(I) halides. Here, additional computational studies focusing on defect properties of Cu(I) halides will be very helpful; such computational studies are rarely done due to large and complex crystal structures of Cu(I) halides and associated computational time costs. Nevertheless, mapping of defect properties of various Cu(I) halides is of utmost importance for an in-depth analysis and understanding of the optoelectronic properties of Cu(I) halides.

The low cost, less toxic and earth abundant elemental compositions, solution processability, vast structural diversities and rich optical and electronic properties of hybrid organic-inorganic and coordination Cu(I) halides make them exceptionally promising for diversified practical applications including solid-state lighting, radiation detection, information storage, sensing and anticounterfeiting. Among these, luminescent Cu(I) halides are an exciting new materials class for scintillation radiation detection (Table 6). Recent reports suggest that Cu(I) halides demonstrate excellent scintillation light yield with low detection limit and high spatial resolution. As the next step, these materials should be incorporated into working detector devices for a direct comparison with the current state-of-the-art scintillators, some of which are also air sensitive metal halides such as CsI(Tl). However, for their consideration in long-term applications, the air-, thermal- and photostability of Cu(I) halides need to be improved. Although, some of the stability issues (i.e., stability in air and moisture) can be addressed via engineering approaches, e.g., by coating the material with inert hydrophobic organic or inorganic layers, the main obstacle for their application in solid-state lighting is their poor thermal stability (<300 °C). As is the case for many other metal halide families, Cu(I) halides are easy to make, but are also easy to break. The weak coordination bond between ligands and Cu(I) in coordination compounds, soft lattice and low formation energy of hybrid Cu(I) halides are the reasons for their decomposition under harsher conditions including high temperatures and long-term light exposure. Therefore, much work is needed to ensure their long-term stability under device operation conditions. Such targeted work may involve chemical strategies aimed at strengthening the bonding between organic and inorganic structural components, or a crystal engineering approach to target denser packing of the inorganic structural units with no harm to emission efficiency. Additionally, development of creative device engineering approaches that allow the use of Cu(I) halide phosphors without a direct contact with the LED base may boost their application prospects in solid-state lighting. Yet another challenge for Cu(I) halide-based pc-WLEDs is the necessity for the more expensive UV LED chips. This is particularly true for hybrid Cu(I) halides due to their optimal excitation wavelengths in the UV region. The shift of PLE spectra of Cu(I) halides to blue region will allow the use of the more affordable blue LED chips. Therefore, future work on optimization of the electronic structures and optical absorption profiles of Cu(I) halides is necessary.

From the perspective of synthetic inorganic chemistry, the emergence of AIO-type Cu(I) halides (only briefly mentioned in this review) featuring both ionic and covalent coordination bonds is an important recent development.[68] More work on syntheses and characterizations of new

Cu(I) halides that are in between the typical hybrid organic-inorganic and neutral coordination Cu(I) halides may yield novel materials that combine the advantages of both. Furthermore, a recent work on other metal halides suggests interconvertibility of some hybrid organic-inorganic and coordination metal halides under external stimuli.[277] This is an interesting new research direction, which if successfully demonstrated for Cu(I) halides, will provide another avenue for the control of PL emission and result in the discovery of new families of stimuli responsive luminescent materials. Finally, there is a recent study reporting the possibility of incorporation of Mn(II) and Cu(I) as optical centers in a single material, which resulted in a series of compounds with various anionic $[Cu_xI_y]^{(y-x)-}$ clusters and diphosphine dioxide-chelated $[Mn(O\wedge O)_3]^{2+}$ cations.[133] The resultant dual phosphorescence from the two optical centers can be controlled, providing tunable photoemission with PLQY values up to 100%.[133] Preparation of new families of heterometallic multiband emitters for design and discovery of customized luminescent materials, especially broadband white light emitters is an interesting research direction that may yield important results for single component pc-WLEDs. In addition to the potential practical benefits, such exploratory research is also likely to yield exciting new families of Cu(I) halides with novel crystal and electronic structure types.

Author contributions

Dilruba A. Popy: Data curation, Formal analysis, Writing – Original Draft, Writing – Review & Editing; Bayram Saparov: Funding acquisition, Supervision, Writing – Original Draft; Writing – Review & Editing.

Conflicts of interest

The authors declare no conflicts of interest.

Acknowledgments

This work was supported by the National Science Foundation (NSF DMR-2045490).

References

1. S. Chang, J. H. Koo, J. Yoo, M. S. Kim, M. K. Choi, D.-H. Kim and Y. M. Song, *Chem. Rev.*, 2024, **124**, 768-859.
2. M.-S. Wang and G.-C. Guo, *Chem. Commun.*, 2016, **52**, 13194-13204.
3. B. Saparov, in *Encyclopedia of Inorganic and Bioinorganic Chemistry*, 2023, DOI: https://doi.org/10.1002/9781119951438.eibc2858, pp. 1-13.
4. W. Liu, W. P. Lustig and J. Li, *EnergyChem*, 2019, **1**, 100008.
5. X. Guan, Z. Lei, X. Yu, C.-H. Lin, J.-K. Huang, C.-Y. Huang, L. Hu, F. Li, A. Vinu, J. Yi and T. Wu, *Small*, 2022, **18**, 2203311.
6. P. Rasin, V. Kumar Suresh, K. Malappuram Mahipal and A. Sreekanth, *Curr. Anal. Chem.*, 2023, **19**, 693-703.
7. S. Abhishek Kumar and S. Bheeshma Pratap, in *Luminescence*, ed. P. Sergei, IntechOpen, Rijeka, 2019, DOI: 10.5772/intechopen.82123, p. Ch. 1.
8. X. Yao, T. Li, J. Wang, X. Ma and H. Tian, *Adv. Opt. Mater.*, 2016, **4**, 1322-1349.
9. G. Zhao, H. Dong, Q. Liao, J. Jiang, Y. Luo, H. Fu and W. Hu, *Nat. Commun.*, 2018, **9**, 4790.
10. S.-J. Zou, Y. Shen, F.-M. Xie, J.-D. Chen, Y.-Q. Li and J.-X. Tang, *Mater. Chem. Front.*, 2020, **4**, 788-820.
11. Z. Han, K. Wang, H.-C. Zhou, P. Cheng and W. Shi, *Nat. Protoc.*, 2023, **18**, 1621-1640.
12. C. Sun, S. Su, Z. Gao, H. Liu, H. Wu, X. Shen and W. Bi, *ACS Appl. Mater. Interfaces*, 2019, **11**, 8210-8216.
13. H. Sun, S. Liu, W. Lin, K. Y. Zhang, W. Lv, X. Huang, F. Huo, H. Yang, G. Jenkins, Q. Zhao and W. Huang, *Nat. Commun.*, 2014, **5**, 3601.
14. H. Zhang and H. Zhang, *Light: Sci. Appl.*, 2022, **11**, 260.
15. Y. Yang, P. Su and Y. Tang, *ChemNanoMat*, 2018, **4**, 1097-1120.
16. K. B. Subila, G. Kishore Kumar, S. M. Shivaprasad and K. George Thomas, *J. Phys. Chem. Lett.*, 2013, **4**, 2774-2779.
17. M. Çadırcı, *J. Lumin.*, 2020, **228**, 117551.
18. M. Saleh, K. G. Lynn, L. G. Jacobsohn and J. S. McCloy, *J. Appl. Phys.*, 2019, **125**, 075702.
19. S. Ummartyotin, N. Bunnak, J. Juntaro, M. Sain and H. Manuspiya, *Solid State Sci.*, 2012, **14**, 299-304.
20. J. Gierschner, J. Shi, B. Milián-Medina, D. Roca-Sanjuán, S. Varghese and S. Park, *Adv. Opt. Mater.*, 2021, **9**, 2002251.
21. J. Yang, M. Fang and Z. Li, *Aggregate*, 2020, **1**, 6-18.
22. J. M. Ha, S. H. Hur, A. Pathak, J.-E. Jeong and H. Y. Woo, *NPG Asia Mater.*, 2021, **13**, 53.
23. M. Fang, J. Yang and Z. Li, *Prog. Mater Sci.*, 2022, **125**, 100914.
24. Y. Shoji, Y. Ikabata, Q. Wang, D. Nemoto, A. Sakamoto, N. Tanaka, J. Seino, H. Nakai and T. Fukushima, *J. Am. Chem. Soc*, 2017, **139**, 2728-2733.
25. C. Wang and Z. Li, *Mater. Chem. Front.*, 2017, **1**, 2174-2194.
26. Y. Guo, L. Xu, H. Liu, Y. Li, C.-M. Che and Y. Li, *Adv. Mater.*, 2015, **27**, 985-1013.
27. S. Hirata, K. Totani, J. Zhang, T. Yamashita, H. Kaji, S. R. Marder, T. Watanabe and C. Adachi, *Adv. Funct. Mater.*, 2013, **23**, 3386-3397.
28. C. Zhou, H. Lin, S. Lee, M. Chaaban and B. Ma, *Mater. Res. Lett.*, 2018, **6**, 552-569.
29. B. Saparov and D. B. Mitzi, *Chem. Rev.*, 2016, **116**, 4558-4596.
30. H. Lin, C. Zhou, M. Chaaban, L.-J. Xu, Y. Zhou, J. Neu, M. Worku, E. Berkwits, Q. He, S. Lee, X. Lin, T. Siegrist, M.-H. Du and B. Ma, *ACS Mater. Lett.*, 2019, **1**, 594-598.

31. A. Yangui, R. Roccanova, Y. Wu, M.-H. Du and B. Saparov, *J. Phys. Chem. C*, 2019, **123**, 22470-22477.
32. H. Yuan, F. Massuyeau, N. Gautier, A. B. Kama, E. Faulques, F. Chen, Q. Shen, L. Zhang, M. Paris and R. Gautier, *Angew. Chem. Int. Ed.*, 2020, **59**, 2802-2807.
33. J. Fu, T. Bian, J. Yin, M. Feng, Q. Xu, Y. Wang and T. C. Sum, *Nat. Commun.*, 2024, **15**, 4562.
34. L. Lanzetta, N. Aristidou and S. A. Haque, *J. Phys. Chem. Lett.*, 2020, **11**, 574-585.
35. F. Sani, S. Shafie, H. N. Lim and A. O. Musa, *Materials*, 2018, **11**, 1008.
36. S. F. Hoefler, G. Trimmel and T. Rath, *Monatsh. Chem.*, 2017, **148**, 795-826.
37. G. Zhou, B. Su, J. Huang, Q. Zhang and Z. Xia, *Mater. Sci. Eng. R: Rep.*, 2020, **141**, 100548.
38. D. Banerjee and B. Saparov, *Chem. Mater.*, 2023, **35**, 3364-3385.
39. C. Zhou, H. Lin, Y. Tian, Z. Yuan, R. Clark, B. Chen, L. J. van de Burgt, J. C. Wang, Y. Zhou, K. Hanson, Q. J. Meisner, J. Neu, T. Besara, T. Siegrist, E. Lambers, P. Djurovich and B. Ma, *Chem. Sci.*, 2018, **9**, 586-593.
40. K. M. McCall, C. C. Stoumpos, S. S. Kostina, M. G. Kanatzidis and B. W. Wessels, *Chem. Mater.*, 2017, **29**, 4129-4145.
41. L. Zhou, J.-F. Liao, Z.-G. Huang, J.-H. Wei, X.-D. Wang, W.-G. Li, H.-Y. Chen, D.-B. Kuang and C.-Y. Su, *Angew. Chem. Int. Ed.*, 2019, **58**, 5277-5281.
42. S. Liu, X. Fang, B. Lu and D. Yan, *Nat. Commun.*, 2020, **11**, 4649.
43. Z. Wang, Z. Zhang, L. Tao, N. Shen, B. Hu, L. Gong, J. Li, X. Chen and X. Huang, *Angew. Chem. Int. Ed.*, 2019, **58**, 9974-9978.
44. D. A. Popy, B. N. Evans, J. Jiang, T. D. Creason, D. Banerjee, L. M. Loftus, R. Pachter, D. T. Glatzhofer and B. Saparov, *Mater. Today Chem.*, 2023, **30**, 101502.
45. R. Tan, Z. Zang and S. Zhao, *Chem. Sci.*, 2024, DOI: 10.1039/D4SC04119D.
46. L. R. V. Buizza and L. M. Herz, *Adv. Mater.*, 2021, **33**, 2007057.
47. K. Han, J. Jin, B. Su and Z. Xia, *Trends Chem.*, 2022, **4**, 1034-1044.
48. Y. Qin, P. She, X. Huang, W. Huang and Q. Zhao, *Coord. Chem. Rev.*, 2020, **416**, 213331.
49. R. Peng, M. Li and D. Li, *Coord. Chem. Rev.*, 2010, **254**, 1-18.
50. J. Yin, Q. Lei, Y. Han, O. M. Bakr and O. F. Mohammed, *Phys. Status Solidid RRL*, 2021, **15**, 2100138.
51. E. Cariati, E. Lucenti, C. Botta, U. Giovanella, D. Marinotto and S. Righetto, *Coord. Chem. Rev.*, 2016, **306**, 566-614.
52. L. P. Ravaro, K. P. S. Zanoni and A. S. S. de Camargo, *Energy Rep.*, 2020, **6**, 37-45.
53. F. Dumur, *Org. Electron.*, 2015, **21**, 27-39.
54. Z. Ma, X. Ji, S. Lin, X. Chen, D. Wu, X. Li, Y. Zhang, C. Shan, Z. Shi and X. Fang, *Adv. Mater.*, 2023, **35**, 2300731.
55. A. Y. Baranov, M. I. Rakhmanova, X. Hei, D. G. Samsonenko, D. V. Stass, I. Y. Bagryanskaya, M. R. Ryzhikov, V. P. Fedin, J. Li and A. V. Artem'ev, *Chem. Commun.*, 2023, **59**, 2923-2926.
56. X. Hei, S. J. Teat, M. Li, M. Bonite and J. Li, *J. Mater. Chem. C*, 2023, **11**, 3086-3094.
57. X. Hei, S. J. Teat, M. Li, M. Bonite and J. Li, *Inorg. Chem.*, 2023, **62**, 3660-3668.
58. J. Qu, S. Xu, H. Shao, P. Xia, C. Lu, C. Wang and D. Ban, *J. Mater. Chem. C*, 2023, **11**, 6260-6275.
59. W. Liu, Y. Fang and J. Li, *Adv. Funct. Mater.*, 2018, **28**, 1705593.

60. H. Araki, K. Tsuge, Y. Sasaki, S. Ishizaka and N. Kitamura, *Inorg. Chem.*, 2005, **44**, 9667-9675.
61. A. Mensah, J.-J. Shao, J.-L. Ni, G.-J. Li, F.-M. Wang and L.-Z. Chen, *Front. Chem.*, 2022, **9**.
62. D. A. Popy, Y. Singh, Y. Tratsiak, A. M. Cardoza, J. M. Lane, L. Stand, M. Zhuravleva, N. Rai and B. Saparov, *Aggregate*, 2024, **5**, e602.
63. D. Banerjee, D. A. Popy, B. C. Leininger, T. D. Creason, V. N. Mapara, M. Furis, M. F. Borunda and B. Saparov, *ACS Appl. Mater. Interfaces*, 2023, **15**, 30455-30468.
64. T. Pinky, D. A. Popy, Z. Zhang, J. Jiang, R. Pachter and B. Saparov, *Inorg. Chem.*, 2024, **63**, 2174-2184.
65. H. Li, Y. Lv, Z. Zhou, H. Tong, W. Liu and G. Ouyang, *Angew. Chem. Int. Ed.*, 2022, **61**, e202115225.
66. X. Hei and J. Li, *Mater. Chem. Front.*, 2023, **7**, 4598-4604.
67. K. Zhu, Z. Cheng, S. Rangan, M. Cotlet, J. Du, L. Kasaei, S. J. Teat, W. Liu, Y. Chen, L. C. Feldman, D. M. O'Carroll and J. Li, *ACS Energy Lett.*, 2021, **6**, 2565-2574.
68. X. Hei and J. Li, *Chem. Sci.*, 2021, **12**, 3805-3817.
69. K. Tsuge, Y. Chishina, H. Hashiguchi, Y. Sasaki, M. Kato, S. Ishizaka and N. Kitamura, *Coord. Chem. Rev.*, 2016, **306**, 636-651.
70. P. C. Ford, E. Cariati and J. Bourassa, *Chem. Rev.*, 1999, **99**, 3625-3648.
71. A. Schlachter, K. Tanner and P. D. Harvey, *Coord. Chem. Rev.*, 2021, **448**, 214176.
72. I. U. o. Pure and A. Chemistry, 2019, DOI: 10.1351/goldbook.O04328.
73. in *The Organometallic Chemistry of the Transition Metals*, ed. R. H. Crabtree, 2014, DOI: https://doi.org/10.1002/9781118788301.ch2, pp. 40-68.
74. A. Merker, M. Scholz, M. Morgenroth, T. Lenzer and K. Oum, *J. Phys. Chem. Lett.*, 2021, **12**, 2736-2741.
75. B. Su, J. Jin, K. Han and Z. Xia, *Adv. Funct. Mater.*, 2023, **33**, 2210735.
76. X. Liu, T. Zhang, L. Zhou, M. Li and R. He, *Inorg. Chem.*, 2024, **63**, 5821-5830.
77. S. Jagner and G. Helgesson, in *Adv. Inorg. Chem.*, ed. A. G. Sykes, Academic Press, 1991, vol. 37, pp. 1-45.
78. C. Brink and C. H. MacGillavry, *Acta Crystallogr.*, 1949, **2**, 158-163.
79. K. P. Bigalke, A. Hans and H. Hartl, *Z. Anorg. Allg. Chem.*, 1988, **563**, 96-104.
80. Z. Song, B. Yu, L. Meng, G. Liu and Y. Dang, *Mater. Adv.*, 2022, **3**, 2447-2455.
81. D.-Y. Li, Q. Tan, M.-P. Ren, W.-Q. Wang, B.-L. Zhang, G. Niu, Z. Gong and X.-W. Lei, *Sci. China Mater.*, 2023, **66**, 4764-4772.
82. Y. Tian, H. Peng, Q. Wei, Y. Chen, J. Xia, W. Lin, C. Peng, X. He and B. Zou, *Chem. Eng. J.*, 2023, **458**, 141436.
83. J. Wu, Y. Guo, J.-L. Qi, W.-D. Yao, S.-X. Yu, W. Liu and S.-P. Guo, *Angew. Chem. Int. Ed.*, 2023, **62**, e202301937.
84. Y. Zhan, P. Cai, X. Pu, Q. Ai, J. Si, X. Yao, G. Bai and Z. Liu, *Inorg. Chem. Front.*, 2024, **11**, 579-588.
85. C. Shen, H. Chen, L. Xu, K. Wu, L. Meng, S. Zhang, J. Wang and D. Wang, *Inorg. Chem.*, 2024, **63**, 3173-3180.
86. X. Meng, J. Jiang, X. Yang, H. Zhao, Q. Meng, Y. Bai, Q. Wang, J. Song, C. Katan, J. Even, W. W. Yu and F. Liu, *Angew. Chem. Int. Ed.*, 2024, **n/a**, e202411047.
87. Z. Wang, Y. Du, C. Wang, L. Ma, C. Li, T. Lin, J. Xiao and Z. Yan, *Inorg. Chem.*, 2024, **63**, 13546-13557.

88. R. An, P. Du, Y. Wang, X. Wang, S. Song, J. Feng, H. Sun and H. Zhang, *Nano Today*, 2024, **56**, 102294.
89. K.-H. Song, J.-J. Wang, L.-Z. Feng, F. He, Y.-C. Yin, J.-N. Yang, Y.-H. Song, Q. Zhang, X.-C. Ru, Y.-F. Lan, G. Zhang and H.-B. Yao, *Angew. Chem. Int. Ed.*, 2022, **61**, e202208960.
90. Q. Kong, X. Jiang, Y. Sun, J. Zhu and X. Tao, *Inorg. Chem. Front.*, 2024, **11**, 3028-3035.
91. D. A. Popy, T. D. Creason, Z. Zhang, D. J. Singh and B. Saparov, *J. Solid State Chem.*, 2022, **316**, 123626.
92. Y. Qiu, Z. Ma, Z. Li, H. Sun, G. Dai, X. Fu, H. Jiang and Z. Ma, *Inorg. Chem.*, 2022, **61**, 8320-8327.
93. Z. Cai, X.-N. Hua, M. Liu, J. Chen, Z. Wang, X. Liu, Y. Zhang, X. Zhang, S. Xiao and B. Sun, *J. Mol. Struct.*, 2023, **1288**, 135772.
94. L. Lian, X. Wang, P. Zhang, J. Zhu, X. Zhang, J. Gao, S. Wang, G. Liang, D. Zhang, L. Gao, H. Song, R. Chen, X. Lan, W. Liang, G. Niu, J. Tang and J. Zhang, *J. Phys. Chem. Lett.*, 2021, **12**, 6919-6926.
95. H. Peng, Y. Tian, X. Wang, T. Dong, Z. Yu, Y. Xiao, Z. Zhang, J. Wang and B. Zou, *J. Phys. Chem. C*, 2022, **126**, 8545-8552.
96. H. Peng, Y. Tian, Z. Zhang, X. Wang, T. Huang, T. Dong, Y. Xiao, J. Wang and B. Zou, *J. Phys. Chem. C*, 2021, **125**, 20014-20021.
97. B. Li, J. Jin, X. Liu, M. Yin, X. Zhang, Z. Xia and Y. Xu, *ACS Mater. Lett.*, 2024, **6**, 1542-1548.
98. J.-L. Qi, J. Wu, Y. Guo, Z.-P. Xu, W. Liu and S.-P. Guo, *Inorg. Chem. Front.*, 2023, **10**, 3319-3325.
99. H. Peng, X. Wang, Y. Tian, T. Dong, Y. Xiao, T. Huang, Y. Guo, J. Wang and B. Zou, *J. Phys. Chem. Lett.*, 2021, **12**, 6639-6647.
100. I. W. Gilley, T. D. Creason, T. M. McWhorter and B. Saparov, *Adv. Photonics Res.*, 2022, **3**, 2200172.
101. S. Chen, J. Gao, J. Chang, Y. Li, C. Huangfu, H. Meng, Y. Wang, G. Xia and L. Feng, *ACS Appl. Mater. Interfaces*, 2019, **11**, 17513-17520.
102. H. Peng, S. Yao, Y. Guo, R. Zhi, X. Wang, F. Ge, Y. Tian, J. Wang and B. Zou, *J. Phys. Chem. Lett.*, 2020, **11**, 4703-4710.
103. D.-Y. Li, J.-H. Wu, X.-Y. Wang, X.-Y. Zhang, C.-Y. Yue and X.-W. Lei, *Chem. Mater.*, 2023, **35**, 6598-6611.
104. R. G. Dastidar, T. Okamoto, K. Takahashi, Y. Takano, C. Vijayakumar, C. Subrahmanyam and V. Biju, *Nanoscale*, 2024, **16**, 5107-5114.
105. R. Gautier, C. Latouche, M. Paris and F. Massuyeau, *Sci. Rep.*, 2017, **7**, 45537.
106. X. Liu, F. Yuan, C. Zhu, J. Li, X. Lv, G. Xing, Q. Wei, G. Wang, J. Dai, H. Dong, J. Xu, B. Jiao and Z. Wu, *Nano Energy*, 2022, **91**, 106664.
107. R. An, J. Hao, S. Song, H. Zhang, J. Feng, X. Wang and H. Sun, *Adv. Opt. Mater.*, 2023, **11**, 2202596.
108. X. Meng, S. Ji, Q. Wang, X. Wang, T. Bai, R. Zhang, B. Yang, Y. Li, Z. Shao, J. Jiang, K.-l. Han and F. Liu, *Adv. Sci.*, 2022, **9**, 2203596.
109. Y. Wang, S. Zhang, B. Zou and R. Zeng, *J. Phys. Chem. C*, 2023, **127**, 7380-7388.
110. W. Meng, C. Wang, Y. Li, G. Hu, S. Sui, G. Xu, M. Peng and Z. Deng, *Chem. Eur. J.*, 2023, **29**, e202202675.

111. L. Zhang, R. Shi, H. Qiu, X. Jiang, G. Sun, R. Long and W.-H. Fang, *J. Phys. Chem. Lett.*, 2022, **13**, 11936-11941.
112. H. Peng, X. Wang, Y. Tian, B. Zou, F. Yang, T. Huang, C. Peng, S. Yao, Z. Yu, Q. Yao, G. Rao and J. Wang, *ACS Appl. Mater. Interfaces*, 2021, **13**, 13443-13451.
113. F. Liu, D. Mondal, K. Zhang, Y. Zhang, K. Huang, D. Wang, W. Yang, P. Mahadevan and R. Xie, *Mater. Adv.*, 2021, **2**, 3744-3751.
114. T. Xu, Y. Li, M. Nikl, R. Kucerkova, Z. Zhou, J. Chen, Y.-Y. Sun, G. Niu, J. Tang, Q. Wang, G. Ren and Y. Wu, *ACS Appl. Mater. Interfaces*, 2022, **14**, 14157-14164.
115. L. Lian, P. Zhang, G. Liang, S. Wang, X. Wang, Y. Wang, X. Zhang, J. Gao, D. Zhang, L. Gao, H. Song, R. Chen, X. Lan, W. Liang, G. Niu, J. Tang and J. Zhang, *ACS Appl. Mater. Interfaces*, 2021, **13**, 22749-22756.
116. H. Peng, Y. Xiao, Y. Tian, X. Wang, T. Huang, T. Dong, Y. Zhao, J. Wang and B. Zou, *J. Mater. Chem. C*, 2021, **9**, 16014-16021.
117. W.-T. Zhang, J.-Z. Liu, J.-B. Liu, K.-Y. Song, Y. Li, Z.-R. Chen, H.-H. Li and R. Jiang, *Eur. J. Inorg. Chem.*, 2018, **2018**, 4234-4244.
118. K. Chen, B. Chen, L. Xie, X. Li, X. Chen, N. Lv, K. Zheng, Z. Liu, H. Pi, Z. Lin and A. L. Rogach, *Adv. Funct. Mater.*, 2024, **34**, 2310561.
119. J.-L. Qi, J. Wu, S.-F. Yan, J.-J. Xu, W. Liu and S.-P. Guo, *Inorg. Chem.*, 2023, **62**, 18825-18829.
120. N. Lin, R.-C. Wang, S.-Y. Zhang, Z.-H. Lin, X.-Y. Chen, Z.-N. Li, X.-W. Lei, Y.-Y. Wang and C.-Y. Yue, *Laser Photonics Rev.*, 2023, **17**, 2300427.
121. P. Fu, S. Geng, R. Mi, R. Wu, G. Zheng, B. Su, Z. Xia, G. Niu, J. Tang and Z. Xiao, *Energy Environ. Mater.*, 2024, **7**, e12518.
122. X. Bin, L. Wu, J. Liu, T. Lin and R. Zeng, *Crystals*, 2022, **12**, 1799.
123. R. Zhang, H. Xie, F. Wang, Q. Zhao, L. Meng, Z. Tang, B. Su and H. Liu, *Laser Photonics Rev.*, 2024, **18**, 2400450.
124. N. Lin, X. Wang, H.-Y. Zhang, K.-Q. Sun, L. Xiao, X.-Y. Zhang, C.-Y. Yue, L. Han, Z.-W. Chen and X.-W. Lei, *ACS Appl. Mater. Interfaces*, 2024, **16**, 41165-41175.
125. N. Hassan, S. Nagaraja, S. Saha, K. Tarafder and N. Ballav, *Chem. Sci.*, 2024, **15**, 4075-4085.
126. H. Yin, W. Li, Z. Wang, P. Wang, X. Xu, P. Han, X. Mao, F. Liu, K. Han, J. Chen and R. Zhang, *Chem. Eng. J.*, 2023, **470**, 144353.
127. D. Ma, Y. Lan, D. Zhang, X. Qin, Z. Yang, H. He, X. Dai, Z. Ye and X. Cao, *Mater. Today Chem.*, 2023, **29**, 101408.
128. S. Fang, B. Zhou, H. Li, H. Hu, H. Zhong, H. Li and Y. Shi, *Adv. Opt. Mater.*, 2022, **10**, 2200605.
129. A. V Dev, M. G. Basavarajappa, S. S. Deshpande, P. Mukherjee, A. Ajayakumar, C. Muthu, T. Okamoto, S. Chakraborty, D. D. Sarma, V. Biju and C. Vijayakumar, *Chem. Mater.*, 2024, **36**, 5912–5921.
130. X. Liu, Y. Li, L. Zhou, M. Li, Y. Zhou and R. He, *Adv. Opt. Mater.*, 2022, **10**, 2200944.
131. X. Wang, C. Wang, C. Tao, Z. Kuang, X. Wang, L. Xu, Y. Wei, Q. Peng, W. Huang and J. Wang, *Nano Lett.*, 2023, **23**, 11860-11865.
132. J. A. Rusanova, K. V. Domasevitch, O. Y. Vassilyeva, V. N. Kokozay, E. B. Rusanov, S. G. Nedelko, O. V. Chukova, B. Ahrens and P. R. Raithby, *J. Chem. Soc., Dalton Trans.*, 2000, DOI: 10.1039/B002451L, 2175-2182.

133. A. V. Artem'ev, M. P. Davydova, A. S. Berezin, D. G. Samsonenko, I. Y. Bagryanskaya, V. K. Brel, X. Hei, K. A. Brylev, O. I. Artyushin, L. E. Zelenkov, I. I. Shishkin and J. Li, *ACS Appl. Mater. Interfaces*, 2022, **14**, 31000-31009.
134. T. D. Creason, T. M. McWhorter, Z. Bell, M.-H. Du and B. Saparov, *Chem. Mater.*, 2020, **32**, 6197-6205.
135. T. D. Creason, A. Yangui, R. Roccanova, A. Strom, M.-H. Du and B. Saparov, *Adv. Opt. Mater.*, 2020, **8**, 1901338.
136. H. D. De Ahna and H. D. Hardt, *Z. Anorg. Allg. Chem.*, 1972, **387**, 61-71.
137. H. D. Hardt and H. J. Stoll, *Z. Anorg. Allg. Chem.*, 1981, **480**, 193-198.
138. R. A. Rader, D. R. McMillin, M. T. Buckner, T. G. Matthews, D. J. Casadonte, R. K. Lengel, S. B. Whittaker, L. M. Darmon and F. E. Lytle, *J. Am. Chem. Soc*, 1981, **103**, 5906-5912.
139. H. Bruns, M. Patil, J. Carreras, A. Vázquez, W. Thiel, R. Goddard and M. Alcarazo, *Angew. Chem. Int. Ed.*, 2010, **49**, 3680-3683.
140. L. Lv, S. Wang and W. Liu, *Inorg. Chim. Acta*, 2021, **518**, 120241.
141. N. P. Rath, J. L. Maxwell and E. M. Holt, *J. Chem. Soc., Dalton Trans.*, 1986, DOI: 10.1039/DT9860002449, 2449-2453.
142. C. Xu, Y. Li, L. Lv, F. Lin, F. Lin, Z. Zhang, C. Luo, D. Luo and W. Liu, *Inorg. Chim. Acta*, 2020, **512**, 119893.
143. Y. Lv, J. Yang, H. Li, W. Liu and G. Ouyang, *Mater. Adv.*, 2024, **5**, 1234-1239.
144. C. Hirtenlehner and U. Monkowius, *Inorg. Chem. Commun.*, 2012, **15**, 109-112.
145. A. Tsuboyama, K. Kuge, M. Furugori, S. Okada, M. Hoshino and K. Ueno, *Inorg. Chem.*, 2007, **46**, 1992-2001.
146. M. Wallesch, D. Volz, D. M. Zink, U. Schepers, M. Nieger, T. Baumann and S. Bräse, *Chem. Eur. J.*, 2014, **20**, 6578-6590.
147. D. M. Zink, M. Bächle, T. Baumann, M. Nieger, M. Kühn, C. Wang, W. Klopper, U. Monkowius, T. Hofbeck, H. Yersin and S. Bräse, *Inorg. Chem.*, 2013, **52**, 2292-2305.
148. H. Araki, K. Tsuge, Y. Sasaki, S. Ishizaka and N. Kitamura, *Inorg. Chem.*, 2007, **46**, 10032-10034.
149. K. Hassanein, C. Cappuccino, P. Amo-Ochoa, J. López-Molina, L. Maini, E. Bandini and B. Ventura, *Dalton Trans.*, 2020, **49**, 10545-10553.
150. X.-Q. Liang, R. K. Gupta, Y.-W. Li, H.-Y. Ma, L.-N. Gao, C.-H. Tung and D. Sun, *Inorg. Chem.*, 2020, **59**, 2680-2688.
151. A. Schlachter and P. D. Harvey, *J. Mater. Chem. C*, 2021, **9**, 6648-6685.
152. Y. Chen, H.-X. Li, D. Liu, L.-L. Liu, N.-Y. Li, H.-Y. Ye, Y. Zhang and J.-P. Lang, *Cryst. Growth Des.*, 2008, **8**, 3810-3816.
153. D. Li, W.-J. Shi and L. Hou, *Inorg. Chem.*, 2005, **44**, 3907-3913.
154. J. C. Dyason, P. C. Healy, C. Pakawatchai, V. A. Patrick and A. H. White, *Inorg. Chem.*, 1985, **24**, 1957-1960.
155. E. Cariati, X. Bu and P. C. Ford, *Chem. Mater.*, 2000, **12**, 3385-3391.
156. C.-Y. Yue, N. Lin, L. Gao, Y.-X. Jin, Z.-Y. Liu, Y.-Y. Cao, S.-S. Han, X.-K. Lian, B. Hu and X.-W. Lei, *Dalton Trans.*, 2019, **48**, 10151-10159.
157. X. Zhang, W. Liu, G. Z. Wei, D. Banerjee, Z. Hu and J. Li, *J. Am. Chem. Soc*, 2014, **136**, 14230-14236.
158. A. J. Blake, N. R. Brooks, N. R. Champness, P. A. Cooke, A. M. Deveson, D. Fenske, P. Hubberstey, W.-S. Li and M. Schröder, *J. Chem. Soc., Dalton Trans.*, 1999, DOI: 10.1039/A902290B, 2103-2110.

159. W. Liu, Y. Fang, G. Z. Wei, S. J. Teat, K. Xiong, Z. Hu, W. P. Lustig and J. Li, *J. Am. Chem. Soc*, 2015, **137**, 9400-9408.
160. H. Ohara, A. Kobayashi and M. Kato, *Chem. Lett.*, 2014, **43**, 1324-1326.
161. J. Egly, D. Bissessar, T. Achard, B. Heinrich, P. Steffanut, M. Mauro and S. Bellemin-Laponnaz, *Inorg. Chim. Acta*, 2021, **514**, 119971.
162. H. Ohara, A. Kobayashi and M. Kato, *Dalton Trans.*, 2014, **43**, 17317-17323.
163. J.-C. Li, H.-X. Li, H.-Y. Li, W.-J. Gong and J.-P. Lang, *Cryst. Growth Des.*, 2016, **16**, 1617-1625.
164. O. Bienemann, R. Haase, A. Jesser, T. Beschnitt, A. Döring, D. Kuckling, I. dos Santos Vieira, U. Flörke and S. Herres-Pawlis, *Eur. J. Inorg. Chem.*, 2011, **2011**, 2367-2379.
165. P. C. Healy, C. Pakawatchai and A. H. White, *J. Chem. Soc., Dalton Trans.*, 1983, DOI: 10.1039/DT9830001917, 1917-1927.
166. J.-L. Chen, P. Song, J. Liao, H.-R. Wen, R. Hong, Z.-N. Chen and Y. Chi, *Inorg. Chem. Commun.*, 2010, **13**, 1057-1060.
167. W. Liu, K. Zhu, S. J. Teat, B. J. Deibert, W. Yuan and J. Li, *J. Mater. Chem. C*, 2017, **5**, 5962-5969.
168. P. P. Mazzeo, L. Maini, A. Petrolati, V. Fattori, K. Shankland and D. Braga, *Dalton Trans.*, 2014, **43**, 9448-9455.
169. W. Lu, J.-j. Ma, W.-z. Luo, B. Li and T. Zhang, *Inorg. Chim. Acta*, 2016, **442**, 97-104.
170. E. Cariati, D. Roberto, R. Ugo, P. C. Ford, S. Galli and A. Sironi, *Inorg. Chem.*, 2005, **44**, 4077-4085.
171. A. Bondi, *J. Phys. Chem.*, 1964, **68**, 441-451.
172. K. R. Kyle, C. K. Ryu, P. C. Ford and J. A. DiBenedetto, *J. Am. Chem. Soc*, 1991, **113**, 2954-2965.
173. R.-Z. Li, D. Li, X.-C. Huang, Z.-Y. Qi and X.-M. Chen, *Inorg. Chem. Commun.*, 2003, **6**, 1017-1019.
174. X. Hei, Y. Fang, S. J. Teat, C. Farrington, M. Bonite and J. Li, *Zeitschrift für Naturforschung B*, 2021, **76**, 759-764.
175. N. Kitada and T. Ishida, *CrystEngComm*, 2014, **16**, 8035-8040.
176. X. Chai, S. Zhang, Y. Chen, Y. Sun, H. Zhang and X. Xu, *Inorg. Chem. Commun.*, 2010, **13**, 240-243.
177. J. P. Safko, J. E. Kuperstock, S. M. McCullough, A. M. Noviello, X. Li, J. P. Killarney, C. Murphy, H. H. Patterson, C. A. Bayse and R. D. Pike, *Dalton Trans.*, 2012, **41**, 11663-11674.
178. M. Yu, C. Liu, S. Li, Y. Zhao, J. Lv, Z. Zhuo, F. Jiang, L. Chen, Y. Yu and M. Hong, *Chem. Commun.*, 2020, **56**, 7233-7236.
179. M. P. Davydova, M. I. Rakhmanova, I. Y. Bagryanskaya, K. A. Brylev and A. V. Artem'ev, *J. Struct. Chem.*, 2020, **61**, 894-898.
180. A. V. Artem'ev, A. Y. Baranov, M. I. Rakhmanova, S. F. Malysheva and D. G. Samsonenko, *New J. Chem.*, 2020, **44**, 6916-6922.
181. K. Xu, B.-L. Chen, R. Zhang, L. Liu, X.-X. Zhong, L. Wang, F.-Y. Li, G.-H. Li, K. A. Alamry, F.-B. Li, W.-Y. Wong and H.-M. Qin, *Dalton Trans.*, 2020, **49**, 5859-5868.
182. A. Y. Baranov, A. S. Berezin, D. G. Samsonenko, A. S. Mazur, P. M. Tolstoy, V. F. Plyusnin, I. E. Kolesnikov and A. V. Artem'ev, *Dalton Trans.*, 2020, **49**, 3155-3163.
183. Y. Fang, W. Liu, S. J. Teat, G. Dey, Z. Shen, L. An, D. Yu, L. Wang, D. M. O'Carroll and J. Li, *Adv. Funct. Mater.*, 2017, **27**, 1603444.

184. D. Liang, Z. Sun, S. Lu, J. Zhao, Y. Zhou, K. An and Z. Zang, *Inorg. Chem.*, 2023, **62**, 7296-7303.
185. D. Gust, M. Scholz, K. Oum and T. Lenzer, *Molecules*, 2023, **28**.
186. P. Boden, P. Di Martino-Fumo, J. M. Busch, F. R. Rehak, S. Steiger, O. Fuhr, M. Nieger, D. Volz, W. Klopper, S. Bräse and M. Gerhards, *Chem. Eur. J.*, 2021, **27**, 5439-5452.
187. T. Hofbeck, T. A. Niehaus, M. Fleck, U. Monkowius and H. Yersin, *Molecules*, 2021, **26**, 3415.
188. X. Zhang, H.-J. Yang, Y.-J. Mao, J.-Y. Wang, A. Pang and L.-J. Xu, *J. Mol. Struct.*, 2024, **1318**, 139242.
189. P. Mao, Y. Tang, B. Wang, D. Fan and Y. Wang, *ACS Appl. Mater. Interfaces*, 2022, **14**, 22295-22301.
190. J. a. Lai, C. Li, Z. Wang, L. Guo, Y. Wang, K. An, S. Cao, D. Wu, Z. Liu, Z. Hu, Y. Leng, J. Du, P. He and X. Tang, *Chem. Eng. J.*, 2024, **494**, 153077.
191. J.-L. Qi, Y. Guo, J. Wu, Q.-F. Huang, J.-J. Xu, S.-F. Yan, W. Liu and S.-P. Guo, *Angew. Chem. Int. Ed.*, 2024, **n/a**, e202407074.
192. L. Xie, Z. Liu, H. Yang, K. Chen, N. Lv, H. Pi, X. Chen, X. Li, Z. Liu, S. Li, Z. Wang, Y. Wang and B. Chen, *Adv. Opt. Mater.*, 2024, **n/a**, 2401050.
193. D.-Z. Wang, C.-S. Liu, J.-R. Li, L. Li, Y.-F. Zeng and X.-H. Bu, *CrystEngComm*, 2007, **9**, 289-297.
194. A. V. Artem'ev, E. P. Doronina, M. I. Rakhmanova, X. Hei, D. V. Stass, O. g. A. Tarasova, I. Y. Bagryanskaya, D. G. Samsonenko, A. S. Novikov, N. A. Nedolya and J. Li, *Dalton Trans.*, 2023, **52**, 4017-4027.
195. W. Ki, X. Hei, H. T. Yi, W. Liu, S. J. Teat, M. Li, Y. Fang, V. Podzorov, E. Garfunkel and J. Li, *Chem. Mater.*, 2021, **33**, 5317-5325.
196. Y. Fang, C. A. Sojdak, G. Dey, S. J. Teat, M. Li, M. Cotlet, K. Zhu, W. Liu, L. Wang, D. M. ÓCarroll and J. Li, *Chem. Sci.*, 2019, **10**, 5363-5372.
197. Y. V. Demyanov, Z. Ma, Z. Jia, M. I. Rakhmanova, G. M. Carignan, I. Y. Bagryanskaya, V. S. Sulyaeva, A. A. Globa, V. K. Brel, L. Meng, H. Meng, Q. Lin, J. Li and A. V. Artemev, *Adv. Opt. Mater.*, 2024, **12**, 2302904.
198. D. Sun, S. Yuan, H. Wang, H.-F. Lu, S.-Y. Feng and D.-F. Sun, *Chem. Commun.*, 2013, **49**, 6152-6154.
199. I.-H. Park and S. S. Lee, *CrystEngComm*, 2011, **13**, 6520-6525.
200. T. Li and S.-W. Du, *J. Cluster Sci.*, 2008, **19**, 323-330.
201. Y. Cheng, P. Xu, Y.-B. Ding and Y.-G. Yin, *CrystEngComm*, 2011, **13**, 2644-2648.
202. X. Hei, S. J. Teat, W. Liu and J. Li, *J. Mater. Chem. C*, 2020, **8**, 16790-16797.
203. W. Liu, K. Zhu, S. J. Teat, G. Dey, Z. Shen, L. Wang, D. M. O'Carroll and J. Li, *J. Am. Chem. Soc*, 2017, **139**, 9281-9290.
204. A. V. Artem'ev, E. A. Pritchina, M. I. Rakhmanova, N. P. Gritsan, I. Y. Bagryanskaya, S. F. Malysheva and N. A. Belogorlova, *Dalton Trans.*, 2019, **48**, 2328-2337.
205. A. V. Artem'ev, M. P. Davydova, X. Hei, M. I. Rakhmanova, D. G. Samsonenko, I. Y. Bagryanskaya, K. A. Brylev, V. P. Fedin, J.-S. Chen, M. Cotlet and J. Li, *Chem. Mater.*, 2020, **32**, 10708-10718.
206. X. Hei, W. Liu, K. Zhu, S. J. Teat, S. Jensen, M. Li, D. M. O'Carroll, K. Wei, K. Tan, M. Cotlet, T. Thonhauser and J. Li, *J. Am. Chem. Soc*, 2020, **142**, 4242-4253.
207. R. Roccanova, W. Ming, V. R. Whiteside, M. A. McGuire, I. R. Sellers, M.-H. Du and B. Saparov, *Inorg. Chem.*, 2017, **56**, 13878-13888.

208. C. Zhou, H. Lin, Q. He, L. Xu, M. Worku, M. Chaaban, S. Lee, X. Shi, M.-H. Du and B. Ma, *Mater. Sci. Eng. R: Rep.*, 2019, **137**, 38-65.
209. L. Zhou, J.-F. Liao and D.-B. Kuang, *Adv. Opt. Mater.*, 2021, **9**, 2100544.
210. Y. Han, X. Cheng and B.-B. Cui, *Mater. Adv.*, 2023, **4**, 355-373.
211. J. R. Albani, *Structure and Dynamics of Macromolecules: Absorption and Fluorescence Studies*, Elsevier Science, 2011.
212. S. Zhou, L. Zhou, Y. Chen, W. Shen, M. Li and R. He, *J. Phys. Chem. Lett.*, 2022, **13**, 8717-8724.
213. B. Zhang, X. Wu, S. Zhou, G. Liang and Q. Hu, *Front. Optoelectron.*, 2021, **14**, 459-472.
214. Y. Jing, Y. Liu, M. Li and Z. Xia, *Adv. Opt. Mater.*, 2021, **9**, 2002213.
215. B. Su, J. Jin, Y. Peng, M. S. Molokeev, X. Yang and Z. Xia, *Adv. Opt. Mater.*, 2022, **10**, 2102619.
216. M.-H. Du, *ACS Energy Lett.*, 2020, **5**, 464-469.
217. L. Lian, M. Zheng, P. Zhang, Z. Zheng, K. Du, W. Lei, J. Gao, G. Niu, D. Zhang, T. Zhai, S. Jin, J. Tang, X. Zhang and J. Zhang, *Chem. Mater.*, 2020, **32**, 3462-3468.
218. R. Hoffmann, *Acc. Chem. Res.*, 1971, **4**, 1-9.
219. F. C. De Schryver, D. Declercq, S. Depaemelaere, E. Hermans, A. Onkelinx, J. W. Verhoeven and J. Gelan, *J. Photochem. Photobiol. A*, 1994, **82**, 171-179.
220. A. Batra, G. Kladnik, H. Vázquez, J. S. Meisner, L. Floreano, C. Nuckolls, D. Cvetko, A. Morgante and L. Venkataraman, *Nat. Commun.*, 2012, **3**, 1086.
221. H. Ohtsu, M. Okuyama, T. Nakajima, M. Iwamura, K. Nozaki, D. Hashizume and M. Kawano, *Inorg. Chem.*, 2021, **60**, 9273-9277.
222. B. Zhang, J. Zhang, A. Sun, C. Liu, M. Gu, Y. Chen, B. Wei and C. Du, *New J. Chem.*, 2021, **45**, 8763-8768.
223. J. Kistner-Morris, A. Shi, E. Liu, T. Arp, F. Farahmand, T. Taniguchi, K. Watanabe, V. Aji, C. H. Lui and N. Gabor, *Nat. Commun.*, 2024, **15**, 4075.
224. E. I. Musina, A. V. Shamsieva, I. D. Strelnik, T. P. Gerasimova, D. B. Krivolapov, I. E. Kolesnikov, E. V. Grachova, S. P. Tunik, C. Bannwarth, S. Grimme, S. A. Katsyuba, A. A. Karasik and O. G. Sinyashin, *Dalton Trans.*, 2016, **45**, 2250-2260.
225. A. Neshat, R. B. Aghakhanpour, P. Mastrorilli, S. Todisco, F. Molani and A. Wojtczak, *Polyhedron*, 2018, **154**, 217-228.
226. B. Wang, Y. Fu, Y. Shen, P. Wang, Y. Chen, F. Feng, Z. Xu, W. Huang and D. Wu, *Inorg. Chem.*, 2024, **63**, 8070-8078.
227. G. Blasse, in *Adv. Inorg. Chem.*, ed. A. G. Sykes, Academic Press, 1990, vol. 35, pp. 319-402.
228. J. C. Dyason, P. C. Healy, L. M. Engelhardt, C. Pakawatchai, V. A. Patrick, C. L. Raston and A. H. White, *J. Chem. Soc., Dalton Trans.*, 1985, DOI: 10.1039/DT9850000831, 831-838.
229. Z. Liu, P. I. Djurovich, M. T. Whited and M. E. Thompson, *Inorg. Chem.*, 2012, **51**, 230-236.
230. A. Lapprand, M. Dutartre, N. Khiri, E. Levert, D. Fortin, Y. Rousselin, A. Soldera, S. Jugé and P. D. Harvey, *Inorg. Chem.*, 2013, **52**, 7958-7967.
231. S. Nagaoka, Y. Ozawa, K. Toriumi and M. Abe, *Chem. Lett.*, 2018, **47**, 1101-1104.
232. Q. Benito, X. F. Le Goff, G. Nocton, A. Fargues, A. Garcia, A. Berhault, S. Kahlal, J.-Y. Saillard, C. Martineau, J. Trébosc, T. Gacoin, J.-P. Boilot and S. Perruchas, *Inorg. Chem.*, 2015, **54**, 4483-4494.

233. F. De Angelis, S. Fantacci, A. Sgamellotti, E. Cariati, R. Ugo and P. C. Ford, *Inorg. Chem.*, 2006, **45**, 10576-10584.
234. S. Perruchas, C. Tard, X. F. Le Goff, A. Fargues, A. Garcia, S. Kahlal, J.-Y. Saillard, T. Gacoin and J.-P. Boilot, *Inorg. Chem.*, 2011, **50**, 10682-10692.
235. A. Vogler and H. Kunkely, *J. Am. Chem. Soc*, 1986, **108**, 7211-7212.
236. G. Hu, G. J. Mains and E. M. Holt, *Inorg. Chim. Acta*, 1995, **240**, 559-565.
237. H. D. Hardt and A. Pierre, *Inorg. Chim. Acta*, 1977, **25**, L59-L60.
238. N. P. Rath, E. M. Holt and K. Tanimura, *Inorg. Chem.*, 1985, **24**, 3934-3938.
239. M. Radjaipour and D. Oelkrug, *Berichte der Bunsengesellschaft für physikalische Chemie*, 1978, **82**, 159-163.
240. R. Czerwieniec, M. J. Leitl, H. H. H. Homeier and H. Yersin, *Coord. Chem. Rev.*, 2016, **325**, 2-28.
241. H. Yersin, R. Czerwieniec, M. Z. Shafikov and A. F. Suleymanova, *ChemPhysChem*, 2017, **18**, 3508-3535.
242. C. E. Housecroft and E. C. Constable, *J. Mater. Chem. C*, 2022, **10**, 4456-4482.
243. A. Schinabeck, M. J. Leitl and H. Yersin, *J. Phys. Chem. Lett.*, 2018, **9**, 2848-2856.
244. M. Xie, C. Han, J. Zhang, G. Xie and H. Xu, *Chem. Mater.*, 2017, **29**, 6606-6610.
245. X. Li, J. Zhang, Z. Zhao, X. Yu, P. Li, Y. Yao, Z. Liu, Q. Jin, Z. Bian, Z. Lu and C. Huang, *ACS Appl. Mater. Interfaces*, 2019, **11**, 3262-3270.
246. A. Schinabeck, N. Rau, M. Klein, J. Sundermeyer and H. Yersin, *Dalton Trans.*, 2018, **47**, 17067-17076.
247. J. Wang, H. Chen, S. Xu, Q. Su, F. Zhao and H. He, *J. Photochem. Photobiol. A*, 2020, **387**, 112104.
248. X.-L. Chen, R. Yu, X.-Y. Wu, D. Liang, J.-H. Jia and C.-Z. Lu, *Chem. Commun.*, 2016, **52**, 6288-6291.
249. J. Zhang, C. Duan, C. Han, H. Yang, Y. Wei and H. Xu, *Adv. Mater.*, 2016, **28**, 5975-5979.
250. M. J. Leitl, F.-R. Küchle, H. A. Mayer, L. Wesemann and H. Yersin, *J. Phys. Chem. A*, 2013, **117**, 11823-11836.
251. Y. Zhao, M. Yu, F. Jiang, L. Chen and M. Hong, *Inorg. Chem. Commun.*, 2021, **127**, 108517.
252. G.-Y. Fan, Y.-L. Wang, S.-D. Han, Z.-Z. Xue and J. Pan, *Cryst. Growth Des.*, 2023, **23**, 8735-8744.
253. Q. Benito, I. Maurin, M. Poggi, C. Martineau-Corcos, T. Gacoin, J.-P. Boilot and S. Perruchas, *J. Mater. Chem. C*, 2016, **4**, 11231-11237.
254. Y. Liu, F. Bu, W. Liu, H. Li, R. Li and J. Wang, *J. Phys. Chem. Lett.*, 2024, **15**, 6835-6840.
255. M. Worku, L.-J. Xu, M. Chaaban, A. Ben-Akacha and B. Ma, *APL Mater.*, 2020, **8**, 010902.
256. Q. Guo, X. Zhao, B. Song, J. Luo and J. Tang, *Adv. Mater.*, 2022, **34**, 2201008.
257. S. Zhou, Y. Chen, K. Li, X. Liu, T. Zhang, W. Shen, M. Li, L. Zhou and R. He, *Chem. Sci.*, 2023, **14**, 5415-5424.
258. E. R. Dohner, E. T. Hoke and H. I. Karunadasa, *J. Am. Chem. Soc*, 2014, **136**, 1718-1721.
259. B. W. D'Andrade and S. R. Forrest, *Adv. Mater.*, 2004, **16**, 1585-1595.
260. L. Lian, S. Wang, H. Ding, G. Liang, Y.-B. Zhao, H. Song, X. Lan, J. Gao, R. Chen, D. Zhang and J. Zhang, *Adv. Opt. Mater.*, 2022, **10**, 2101640.
261. L. Chen, J.-W. Ye, H.-P. Wang, M. Pan, S.-Y. Yin, Z.-W. Wei, L.-Y. Zhang, K. Wu, Y.-N. Fan and C.-Y. Su, *Nat. Commun.*, 2017, **8**, 15985.
262. R. Gao, D. Yan and X. Duan, *Cell Rep. Phys. Sci.*, 2021, **2**.

263. Y. Liu, A. Li, S. Xu, W. Xu, Y. Liu, W. Tian and B. Xu, *Angew. Chem. Int. Ed.*, 2020, **59**, 15098-15103.
264. G. Ding, Y. Zheng, X. Xiao, H. Cheng, G. Zhang, Y. Shi and Y. Shao, *J. Mater. Chem. A*, 2022, **10**, 8159-8171.
265. T. Li, A. M. Zeidell, G. Findik, W. A. Dunlap-Shohl, J. Euvrard, K. Gundogdu, O. D. Jurchescu and D. B. Mitzi, *Chem. Mater.*, 2019, **31**, 4267-4274.
266. R. Zhao, Z. Gu, P. Li, Y. Zhang and Y. Song, *Adv. Mater. Technol.*, 2022, **7**, 2101124.
267. A. Kobayashi and M. Kato, *Chem. Lett.*, 2017, **46**, 154-162.
268. P. Yuan, T. He, Y. Zhou, J. Yin, H. Zhang, Y. Zhang, X. Yuan, C. Dong, R. Huang, W. Shao, S. Chen, X. Song, R. Zhou, N. Zheng, M. Abulikemu, M. Eddaoudi, M. Bayindir, O. F. Mohammed and O. M. Bakr, *ACS Energy Lett.*, 2023, **8**, 5088-5097.
269. D. E. Belikova, S. A. Fateev, V. N. Khrustalev, V. Kozhevnikova, A. A. Ordinartsev, A. V. Dzuban, E. A. Goodilin and A. B. Tarasov, *J. Mater. Chem. C*, 2024, **12**, 13537-13544.
270. S. Cheng, M. Nikl, A. Beitlerova, R. Kucerkova, X. Du, G. Niu, Y. Jia, J. Tang, G. Ren and Y. Wu, *Adv. Opt. Mater.*, 2021, **9**, 2100460.
271. S. Cheng, A. Beitlerova, R. Kucerkova, M. Nikl, G. Ren and Y. Wu, *Phys. Status Solidid RRL*, 2020, **14**, 2000374.
272. T. He, Y. Zhou, P. Yuan, J. Yin, L. Gutiérrez-Arzaluz, S. Chen, J.-X. Wang, S. Thomas, H. N. Alshareef, O. M. Bakr and O. F. Mohammed, *ACS Energy Lett.*, 2023, **8**, 1362-1370.
273. W. Zhao, Y. Wang, Y. Guo, Y. D. Suh and X. Liu, *Adv. Sci.*, 2023, **10**, 2205526.
274. Y. Zhou, T. He, P. Yuan, J. Yin, S. Chen, L. Gutiérrez-Arzaluz, L. Wang, O. M. Bakr and O. F. Mohammed, *ACS Mater. Lett.*, 2023, **5**, 2002-2008.
275. Q. Hu, C. Zhang, X. Wu, G. Liang, L. Wang, X. Niu, Z. Wang, W.-D. Si, Y. Han, R. Huang, J. Xiao and D. Sun, *Angew. Chem. Int. Ed.*, 2023, **62**, e202217784.
276. X. Liu, Y. Jiang, F. Li, X. Xu, R. Li, W. Zhu, J. Ni, C. Ding, S. Liu and Q. Zhao, *Adv. Opt. Mater.*, 2023, **11**, 2202169.
277. X. Yang, S. Wang, J. Wu, W. Hu, L. Huang, Q. Ling and Z. Lin, *Adv. Opt. Mater.*, 2024, **12**, 2301661.